
Transport in interacting 1d wires with impurity: RG approach and dephasing

Alois Dirnachner



München 2011

Transport in interacting 1d wires with impurity: RG approach and dephasing

Alois Dirnaichner

Diplomarbeit
an der Physik
der Ludwig-Maximilians-Universität
München

vorgelegt von
Alois Dirnaichner
aus Wasserburg a. Inn

München, den 20. Mai 2011

Erstgutachter: Prof. Dr. Jan von Delft
Zweitgutachter: Prof. Dr. Ulrich Schollwöck

Abstract

We study transport in interacting one-dimensional systems with a scattering object. In particular we are interested in inelastic scattering processes. Very recent theoretical [3] and experimental [54] research points toward a strong influence of incoherent scattering on the low-temperature transport features of one-dimensional systems with extended scatterers.

Furthermore, if inelastic processes are strong a straightforward application of the renormalization group (RG) approach is not possible. In the field of transport in one-dimensional weakly interacting electron systems, this procedure is the state-of-the art method to extend results for weak interaction to the low temperature regime [18, 27, 43, 47, 52, 57, 62, 67, 74]. The underlying assumption, namely that the first-order correction in interaction incorporates all effects of the interaction and reproduces itself in higher orders, is widely accepted as a valid “educated guess” disregarding the fact that inelastic processes, if present, arise in subleading orders.

Indeed, for the simple case of a single impurity in an infinite wire it is common believe that the approach is valid [6, 74]. Having this in mind, systems with a great variety of additional degrees of freedom were treated in the same fashion: Junctions of wires [43] and more complex geometries [18], anti-resonant [47] and resonant [57, 62] scatterers, just to name a few. A careful examination of the interplay between the renormalization and possible inelastic processes or dephasing in these cases is missing.

Our strategy is to calculate the second order in interaction for the single impurity situation, thereby establishing a framework with a real-space diagrammatic technique, and to apply this tool to more complex situations, i.e., a finite interacting region and an additional impurity. The diagrammatic technique enables us to identify specific diagrams where the particle number at a given energy is not conserved or the interaction can lead to dephasing in the system.

In particular, by modelling the compound scatterer by an energy dependent S -matrix of the Breit-Wigner type, we are able to find a fingerprint of weak dephasing which carries some features of its counterpart in disordered Luttinger liquids [32].

Contents

1	Introduction	5
1.1	The Luttinger liquid	6
1.1.1	Landau's Fermi liquid theory and peculiarities in 1D	6
1.1.2	The Tomonaga-Luttinger model	10
1.1.3	A short introduction to bosonization	11
1.1.4	Application to the model	14
1.2	Weak interactions in a Luttinger liquid with impurity	19
1.2.1	Scattering states and chiral fields	21
1.2.2	First order in interaction: Hartree-Fock corrections	22
1.2.3	A simple renormalization group approach	25
1.3	Conductance from transmission	30
1.3.1	Resistance at reflectionless leads	30
1.3.2	Energy dissipation at the scatterer	31
1.3.3	Non-zero temperature	31
1.3.4	Criterions for linear response	32
1.3.5	Resonant tunneling of non-interacting electrons	33
1.3.6	Conductance of strongly interacting electrons in one dimension	33
1.4	Applications and recent research	35
1.4.1	Energy dependent S-matrix	35
1.4.2	A side attached impurity	39
1.4.3	Junctions of one-dimensional wires	40
1.4.4	Incoherent scattering	43
2	Statement of the problem	45
3	Perturbative calculations for the S-matrix	49
3.1	Chiral Green's function of particles	49
3.1.1	Dyson Equations	50
3.1.2	Different types of interaction	52
3.1.3	Feynman and real space diagrammatics	53
3.2	First order in interactions	55
3.2.1	First order corrections to the S-matrix	56
3.2.2	Corrections to the reflection coefficient	59
3.2.3	Summary	60
3.3	Second order in interaction	60
3.3.1	Sub-leading diagrams	60

3.3.2 “Double-Fock”, “rainbow” and “crossed” diagrams	61
3.3.3 Corrections to transmission, reflection and checking of unitarity	67
3.4 A second scale	67
3.4.1 Interaction in a box	67
3.4.2 First order in interaction	68
3.4.3 Second order in interaction for a finite system	69
3.5 Energy dependent scattering matrix	72
3.5.1 Resonant scattering in a one-dimensional system at first order in interaction	72
3.5.2 Relations of the energy scales	73
3.5.3 First order in interactions	74
3.5.4 Second order for a symmetric resonant scatterer	77
4 Conclusions	81
A Details of calculations	83
A.1 The scattering matrix	83
A.1.1 Application to the one-dimensional wire with an arbitrary impurity	83
A.2 Chiral Green’s functions in coordinate and energy representation	84
A.3 Detailed calculation of the S-matrix in second order in interaction	84
A.3.1 1 impurity reflection	85
A.3.2 2 reflections	91
A.3.3 3 reflections	96
A.3.4 4 reflections	98
A.3.5 5 reflections	100
A.4 Second scale calculation using pole integrations methods	100
A.4.1 First order in interaction	101
A.4.2 Second order	102
A.5 Check of the unitarity of the S-matrix in various cases	105
A.5.1 Inside a symmetric resonant level	105
A.5.2 Resonant scatterer with broken spacial symmetry	106
A.6 Example calculations for an energy-dependent S-matrix in second order	107
A.6.1 Rainbow diagram: 1-I-E	108
A.6.2 Diagram with crossed interaction lines: 1-II-B	109

Chapter 1

Introduction

One-dimensional systems were originally recognized by chemists who noticed a strongly anisotropic behavior of many organic crystals [67]. The ratio of parallel to perpendicular conductivities in this structures reaches up to 10^3 . This behavior can be understood partly by rather basic considerations: The building blocks of these crystals are shaped cone-like, thus forming chains in one direction perpendicular to the plane of molecules. Weakly coupled neighboring molecules overlap their outer electron wave functions and allow the electrons to move easily along the chain. Hopping from one chain to another is mainly suppressed due to larger distances.

In physics, the examination of the outstanding features of 1d systems started (on a noticeable scale) in the 80s [67]. It soon became apparent that the magnitudes of some effects, present but negligible in two and more dimensions, disagrees drastically with the picture of the well-known Fermi liquid in one dimension.

In these days, insights on these systems were gained by investigating two classes of quasi-1d materials: mixed-valence complexes and charge-transfer compounds. The former contain an-isotropically oriented orbitals which allow electron proliferation in one dimension.

A famous example is KCP ($K_2Pt(CN)_4Br_{0.3} \cdot 3H_2O$) which is studied intensely for almost half a century [58,75]. The d orbitals of Pt in this complex are responsible for a very large ratio of along-chain conductivity to perpendicular directions.

In organic charge-transfer compounds two different kinds of molecules, donors and acceptors, are separated into spatially disjoint chains. Once charge is transferred along such a chain, other ways of electron transport are effectively suppressed. Because there is a large number of molecules which can be donors, there are many interesting compounds with largely different behavior.

Still in the 80s the first truly one-dimensional “wires” were fabricated by gated 2D electron gases in GaAs inversion layers [53]. The properties of the 2DEG, especially the carrier concentration, could be controlled and it was possible to confine the conducting electrons to one transverse channel.

In 1991, Sumio Iijima first created multi-walled carbon nanotubes in the insoluble material of arc-burned graphite rods and soon it was predicted that a single-walled tube would exhibit outstanding conducting features [8]. The growing interest in the community led to independent discoveries by Bethune at

IBM [9] and Iijima at NEC [34] of single-walled carbon nanotubes and methods to specifically produce them. Besides the exploitation of semi- and super-conducting features of some types of nanotubes they soon got utilized to study 1d transport features [12].

The outstanding feature observed throughout all those measurements was the power-law temperature and bias-voltage dependence of the current [10, 11]. This remarkable result led to intense theoretical investigation of one-dimensional quantum wires in parallel to the experiments.

On the theoretical side it became apparent in the 60s that a theory describing density waves as the basic boson excitations of the system was able to predict the observed behavior [51].

The most popular model of one dimensional systems, the Tomonaga-Luttinger model, could be rewritten in terms of free boson excitations by means of exact operator identities. Among the pioneers in this field, Mattis and Lieb [51], Haldane [33] and Kane and Fisher [37] stand out: The former derived carefully the operator identities, the latter explored the physics in the presence of both very weak and strong structure-less or resonant scatterers.

Albeit thoroughly elegant and successful, the bosonized field-theoretical approach has its share of complications when translational symmetry is broken by a barrier or an impurity which can not be considered as a small perturbation to a transparent or a split wire. This was the motivation to attack the problem with a renormalization group procedure extending perturbation theory for weak interactions to the low-temperature regime; an approach pioneered by Matveev, Yue and Glazman in the 90s [74].

These two theoretical approaches are of fundamental importance for the theory of one-dimensional transport. In the last decade, a great variety of subjects have been investigated in one dimensional wires, e.g., disorder [32], complex geometries [18, 43], the Coulomb blockade [56], phonons [26, 27] or localization [30], just to name a few.

In the following sections, we will introduce basic theoretical concepts and present some of the recent applications in this active field of research.

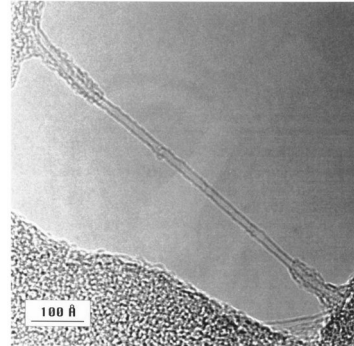


Figure 1.0.1: TEM micrography of a bare section of a single-walled nanotube [9]. The round objects adhering to the tube have diameters corresponding to fullerenes with 60-100 carbons.

1.1 The Luttinger liquid

1.1.1 Landau's Fermi liquid theory and peculiarities in 1D

In solids, the Coulomb interaction is of the same order of magnitude than the kinetic energy. Thus it is not, at least not on a quantitative level, possible to apply

perturbative methods. Yet remarkably, Fermi liquids seem to be very robust against perturbations. The non-interacting model of the Fermi gas reproduces many qualitative features of interacting electrons in metals, such as a well-defined Fermi surface, a linear specific heat capacity, and a temperature-independent paramagnetic susceptibility [17].

In the 50s, Lev Landau related the robustness of the Fermi liquid to the Pauli exclusion principle and the idea of adiabaticity [44]. He realized that a moving fermion can not decay by emitting arbitrary numbers of low-energy particle-hole pairs if it is close to the Fermi level because the phase space for creating particles is narrowed as a direct consequence of the Pauli principle. This leads to the inverse-proportional relation between lifetime and energy of the excitation above the Fermi sea,

$$\tau^{-1}(\epsilon) \propto (\epsilon^2 + \pi^2 T^2),$$

where the particle energy ϵ is measured from the Fermi level. These long-lived excitations were labeled *quasi-particles* by Landau, and the collective physics of quasi-particles is therefore named “Landau Fermi liquid theory”(FL) [66].

Basic elements and results

Landau’s theory is based on the idea of a continuous and one-to-one correspondence between the eigenstates (ground state and excited states) of the free and the interacting system. To check its applicability it is thus essential that the interactions do not lead to a change in the low-energy physics governing long distance correlations, in other words, no phase transition or instability is allowed to occur.

Let us consider a basic excitation of the non-interacting system: We add a particle or a hole with $|k| \gtrsim k_F$ to the ground state. After switching on the interaction, the total momentum will still be conserved but the interaction of the particle with the Fermi sea electrons will change their momentum distribution. The excitation and the interaction-induced response of the background form what is called a Landau quasi-particle. Momentum conservation requires that the quasi-particle still has total momentum k . Furthermore, the continuity hypothesis formulated above demands that $|k| \gtrsim k_F$ and in particular that k_F remains unchanged.

Assuming that the chemical potential is included in the Hamiltonian, the energy of the quasi-particle vanishes on the Fermi surface and can be expanded to first order in the difference $|k - k_F|$ in its vicinity,

$$\epsilon_k^0 = \frac{k_F \hbar}{m^*} (|k - k_F|),$$

wherein m^* is the effective mass. We account for interactions between quasi-particles by a change in energy of

$$\delta E = \sum_k \epsilon_k^0 \delta n(k) + \frac{1}{2\Omega} \sum_{kk'} f(k, k') \delta n(k) \delta n(k'),$$

where $\delta n(k)$ is the change in the quasi-particle occupation number and f is the matrix element describing the interaction. From this starting point one can derive thermodynamic properties: Especially the prediction of a linear specific heat at low temperatures greatly supported the acceptance of FL theory. Since

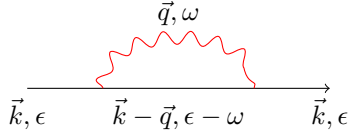


Figure 1.1.1: Self-energy to first order in the interaction for a particle with energy ϵ and momentum \vec{k} .

the theory contains essentially ballistic quasi-particles, it is possible to apply the Landauer-Büttiker formalism which provides a conceptually clear view on transport phenomena. We will provide more details on this issue in section 1.3.

The initial hypothesis of a continuous correspondence is not true in 1d systems. The restriction of the system to one dimension greatly enhances terms that were present but sub-leading in higher dimensions, resulting in a non FL-like structure. We will explain this statement in more detail below.

Applicability of the FL theory

In this section we will briefly outline very general assumptions that have to be made in the derivation of the FL theory. See Ref. [49] for more details. We start with the observation that the imaginary part of the self-energy in the Green's function is inversely proportional to the lifetime of a particle [2],

$$G_R(p, t - t') \sim e^{(-i \operatorname{Re}(\Sigma^R) - \operatorname{Im}(\Sigma^R(p))(t - t'))},$$

and that it is small with respect to the typical quasi-particle energy in the FL theory,

$$\operatorname{Im}(\Sigma^R) \propto \max(\epsilon^2, T^2) \ll \epsilon, T.$$

The $1/\epsilon^2$ dependence of the lifetime is a typical feature of Landau's theory. Let's try to recapitulate this result while making as few assumptions as possible. To this end, we calculate the imaginary part of the self-energy to first order in the interaction at $T = 0, \epsilon = \xi_k$ (see Feynman diagram in figure 1.1.1),

$$\operatorname{Im} \Sigma^R(\epsilon) = -\frac{2}{(2\pi)^{D+1}} \int_0^\epsilon d\omega \int d\vec{q} \operatorname{Im} G^R(\epsilon - \omega, \vec{k} - \vec{q}) \operatorname{Im} V^R(\omega, \vec{q}),$$

where G^R is the retarded free fermion propagator and V^R is a retarded boson field which is real in the coordinate-time representation and therefore an odd function of ω . We replace $V^R = \omega W(\omega, \vec{q})$ to reflect this choice. The energy integration is limited by the Pauli principle. This integration can readily be performed if the result of the \vec{q} integration is ω -independent, namely

$$-\operatorname{Im} \Sigma^R(\epsilon) \sim A \int_0^\epsilon d\omega \omega \sim A\epsilon^2,$$

where we used

$$\operatorname{Im} G^R(\epsilon - \omega, \vec{k} - \vec{q}) \sim \delta(\omega - v_k \vec{q} + q^2/2m).$$

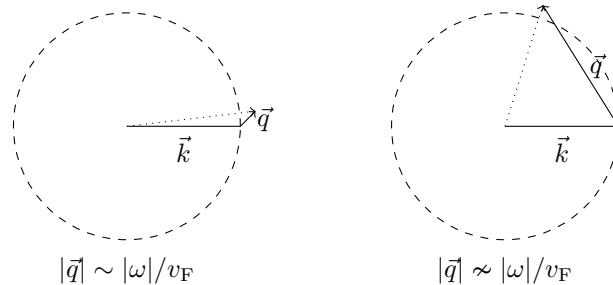


Figure 1.1.2: Small angle scattering event (left) and a process with arbitrary angle. The energy transfer in both processes is of the order of the particle energy ϵ . The momentum transfer q in the small angle process is bound to be of the same order, while q may be large depending on the angle in the second process.

With this assumption, we restore the FL result. We can thus reformulate the requirement for the applicability of the FL theory: Momentum and energy integrals, i.e., transfers, have to be independent. In one dimension, this is clearly violated: Fixing the amount of transferred energy, the momentum transfer is specified (apart from the sign) and vice versa, what is illustrated in figure 1.1.2. If the physical situation only allows forward-scattering¹, the mapping between energy and momentum is exact and we can no longer *expect* the ϵ^2 behavior.

Isotropic scattering is thus a sufficient but not necessary condition for the FL to exist. Consequently, if we confine the scattering of a 3D FL to small angles, we have to expect a departure from the FL comportment. How strong is the violation? Indeed, it can be shown that even for a contact interaction, this modification triggers a logarithmic divergence of the self-energy,

$$\text{Re } \Sigma^R \propto \epsilon^2 \log |\epsilon|,$$

in the vicinity of the Fermi level [49]. The non-analytic input can be traced to a subleading contribution to the specific heat in three dimensions,

$$C(T) = \gamma_3 T + \beta_3 T^3 \log T,$$

a result observed experimentally in He₃ and metals. This effect is even more pronounced in two dimensions. Recent works using Matsubara Green's [16] confirm this result. Efetov et al. [21] report a non-analytic correction

$$\delta C(T) \propto \frac{T}{\log^3(\epsilon_F/T)}$$

using a supersymmetric low energy theory in one dimension.

We can thus conclude that the processes leading to a breakdown of the FL theory in one dimension, namely small-angle scattering processes, are present but subleading in higher dimensions when the scattering is isotropic. The physics we describe in the following sections, summarized under the term ‘‘Luttinger liquid’’, can hence provide insights on 2+ dimensional systems if scattering is restricted to small angles.

¹This assumption is met in the presence of long-range interaction. We will discuss this issue later in more detail.

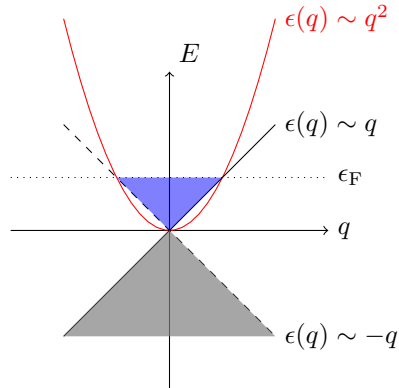


Figure 1.1.3: Dispersion relation in the Luttinger model for right-(solid) and left-moving(dashed) particles compared to the non-linear quadratic dispersion(red). The gray area represents the extended artificial state space of the model.

1.1.2 The Tomonaga-Luttinger model

The first prominent model for electrons in one dimension was the Tomonaga model [69] which intended to describe “sound waves” in a interacting many-fermion problem. The term refers to multi-fermion excitations whose many-body wave function has boson properties. The bosonization procedure, i.e., a procedure based on an identity between fermion and boson operators, can be carried out for this model with the help of some approximations. They are necessary due to the fact that in the Tomonaga model, the spectrum of particles below the Fermi sea is not extending infinitely. Thirteen years after the Tomonaga model was introduced, Luttinger therefore proposed a model with infinite phase space and claimed it “exactly solvable” [48]. It soon turned out that it indeed was, but the results in his pioneering work “fell prey to a subtle paradox inherent in quantum field theory” [51]. A very careful derivation of the operator identities and a discussion of all subtleties was done by Haldane [33].

Notwithstanding, Dzyaloshinskii and Larkin calculated exact propagators for this model in a fermionic language [46] in the 70s. In their pioneering work, the authors found a way to sum up *all* terms of the self-energy expansion using a special Ward identity. For the sake of brevity, we shall not discuss the solution in more detail, but it should be noted that both approaches are fully consistent with each other.

Instead, we present the bosonization solution to the one-dimensional system to pave the way for a review of results obtained by Kane and Fisher [37] in this language for the single-impurity problem. The complete Hamiltonian in the Tomonaga-Luttinger model consists of three parts, namely

$$H = H_0 + V_1 + V_2, \quad (1.1.1)$$

wherein the components read

$$H_0 = \int_{-L/2}^{L/2} \frac{dx}{2\pi} :(\psi_L^\dagger(x)i\partial_x\psi_L(x) + \psi_R^\dagger(x)i\partial_x\psi_R(x)):, \quad (1.1.2)$$

$$V_1 = \int_{-L/2}^{L/2} \frac{dx}{2\pi} g_2 : \rho_L(x)\rho_R(x) :, \quad V_2 = \int_{-L/2}^{L/2} \frac{dx}{2\pi} g_4 : (\rho_L^2(x) + \rho_R^2(x)) :, \quad (1.1.3)$$

In the potentials, $\rho_\eta(x) = : \psi_\eta^\dagger(x)\psi_\eta(x) :$ denotes a normal-ordered pair of fermion operators.² The fermion fields are separated by chirality. Furthermore, we will neglect the spin degrees of freedom and focus on spinless fermions.

V_1 describes interaction between right- and left-moving density fluctuations or particle-hole pairs. The second part V_2 connects electron-hole pairs on the same branches. The strength of the interaction is parameterized by the dimensionless couplings g_2 and g_4 (compare to the descriptive figure 3.1.1). It should be emphasized that this model neglects umklapp or backscattering processes.³ This last assumption means that the interaction potential is short-ranged on the scale of the inverse Fermi momentum, but sufficiently long-ranged that $U(2k_F) \ll U(0)$.⁴ We will come back to this point in section 3.1.2.

The Hilbert space of the Luttinger-Tomonaga model is extended into the whole lower k -space (see figure 1.1.3). This modification does not change the low-energy physics of the system. As long as all energies involved are small with respect to ϵ_F , an excitation of the unphysical high energy states is not possible. The point can be subtle when treating high electric fields or impurity potentials in a Luttinger liquid, therefore we will choose ϵ_F or a smaller energy⁵ as the ultraviolet cutoff. For this Hamiltonian we will present a recipe to identify the fermion fields with boson operators in the next section.

1.1.3 A short introduction to bosonization

The term bosonization refers to the reformulation of a fermionic model in the language of boson operators and fields. Those can be used to calculate the correlation functions. The requirements for this recipe are met by fermions in the vicinity of the Fermi level in one dimension as shown below.

The approach allows one to handle, to a certain extend, strong-interaction problems. The formalism relies on a bosonization procedure, pioneered by Mattis and Lieb [51] and first done discretely by Haldane [33]. The form of the resulting action was proposed earlier by Efetov and Larkin [22]. Instead of introducing the boson fields and showing their correspondence to the fermion operators afterwards, the authors of the former works followed a so-called constructive bosonization approach where a chain of operator identities in Fock space leads

²We recall that a product $:AB:$ is sorted in the way that destruction operators acting on an empty state and creation operators acting on filled states appear to the right.

³These processes are labeled g_1 and g_3 in the literature. We will provide more details in section 3.1.2.

⁴This is not just a convenient choice. The Coulomb potential can be screened for example by mirror charges in a nearby metallic gate [49].

⁵The inverse interaction length v_F/d can play this role.

to the final form of the boson fields. This procedure clarifies the role of the Klein-factors F_η in the relation of the fermion and boson fields $\Psi_\eta \sim F_\eta e^{-i\phi_\eta}$ [70].

This introduction follows a detailed bosonization review by von Delft and Schoeller [70]. Three prerequisites are to be met for the bosonization method to work. The fermion creation and annihilation operators have to fulfill the commutation relations for each species η (η distinguishes different spins or right and left movers, for example),

$$\{c_{k\eta}, c_{k'\eta'}^\dagger\} = \delta_{\eta,\eta'} \delta_{kk'}.$$

Furthermore, the momentum index k should be *unbounded* and take discrete values. Introducing a finite size of the system L , the latter requirement is easily met,

$$k = \frac{2\pi}{L} n_k,$$

where n_k are integers. The vacuum ground state is chosen so that the first empty level above the Fermi sea is denoted $n_k = 1$.

Let us consider free right and left-moving fermions. We immediately realize, that the separation of the species induces lower boundaries for k . Explicitly, for the fermion field Ψ we get

$$\begin{aligned} \Psi(x) &= \sqrt{\frac{2\pi}{L}} \sum_{p=-\infty}^{\infty} e^{ipx} c_p \\ &= \sqrt{\frac{2\pi}{L}} \sum_{k=-k_F}^{\infty} (e^{-i(k_F+k)x} c_{-k-k_F}) + e^{i(k_F+k)x} c_{k+k_F}), \end{aligned} \tag{1.1.4}$$

where the k -space of the fermion fields is not extending infinitely. The question arises, if it is at all necessary to require k to be unbounded for all species. This will be clarified in the following.

To satisfy all three conditions, we introduce two types of fermions with different energy spectra, $\epsilon_k = k v_F$ and $\epsilon_k = -k v_F$ and k ranging from negative to positive infinity. They are shown by the solid and dashed lines in figure 1.1.3. There is an infinite number of each kind of particles in the occupied states below the Fermi level. The artificial part of the spectrum is indicated in the figure by the gray area. The unphysical extension of the spectrum is not expected to alter the physics of a weak interacting system whose energies are bound close to the Fermi level.

The two kinds of fermions in the Luttinger model (denoted $a_{\eta,k,s}$ and $a_{\eta,k,s}^\dagger$) are independent in the sense that the operators commute. Operators of the same species obey the required fermion commutation relation. We are now set to introduce boson particle-hole operators $b_{q,\eta}(p)$ and $b_{q,\eta}^\dagger$,

$$b_{q\eta}^\dagger = \frac{i}{\sqrt{n_q}} \sum_{k=-\infty}^{\infty} c_{k+q,\eta}^\dagger c_{k,\eta} \quad b_{q\eta} = \frac{-i}{\sqrt{n_q}} \sum_{k=-\infty}^{\infty} c_{k-q,\eta}^\dagger c_{k,\eta},$$

with $q = \frac{2\pi}{L} n_q > 0$. The operator $b_{1,q}^\dagger$ annihilates particles in all k -states and creates them in $q+k$ -states. This is possible if $k < 0$ and $k+p > 0$. The sum thus shifts all momenta by q with respect to the state acted upon, thereby

generating particle hole pairs. To see if we create and annihilate “real” bosons, we compute the commutation relations

$$[b_{q\eta}, b_{q'\eta'}^\dagger] = [b_{q\eta}^\dagger, b_{q'\eta'}] = 0, \quad (1.1.5)$$

$$[b_{q\eta}, b_{q'\eta'}^\dagger] = \delta_{\eta\eta'} \sum_k \frac{1}{n_k} \left(:c_{k-q,\eta}^\dagger c_{k-q',\eta}: - :c_{k+q'-q,\eta}^\dagger c_{k,\eta}: \right). \quad (1.1.6)$$

If $q \neq q'$, we can just shift $k \rightarrow k - q'$ in the second term and the normal ordered products cancel out. Note that the subtraction of the sums is only possible due to the normal ordering. It guarantees that no intermediate particle-hole pairs are generated in the infinite sums. For equal momenta q and q' this requirement is not a priori fulfilled. Therefore we normal-order the products according to the definition $:AB := AB - \langle AB \rangle$,

$$\begin{aligned} [b_{q\eta}, b_{q'\eta'}^\dagger] &= \delta_{\eta\eta'} \delta_{qq'} \sum_k \frac{1}{n_q} \left(:c_{k\eta}^\dagger c_{k\eta}: - :c_{k+q,\eta}^\dagger c_{k+q,\eta}: \right. \\ &\quad \left. + \langle c_{k\eta}^\dagger c_{k\eta} \rangle - \langle c_{k+q,\eta}^\dagger c_{k+q,\eta} \rangle \right) \\ &= \delta_{\eta\eta'} \delta_{qq'} \frac{1}{n_q} \left(\sum_{k=-\infty}^0 - \sum_{k=-\infty}^{-n_q} \right) = \delta_{\eta\eta'} \delta_{qq'}. \end{aligned}$$

In the last step, the requirement of an unbounded k -space is used. Note that a sum over the particles in a finite number of states is always finite and equal to the sum over the states shifted by a constant. The difference would thus yield zero.

One can show [33] that the states b^\dagger , acting on the ground state of N particles, span the complete Hilbert space of the N particles. However, we still lack the possibility to add a particle and explore the full Hilbert space of arbitrary particle number. To accomplish this, we introduce operators F_η^\dagger to create electrons of species η in the lowest possible (empty) state. Let $|N\rangle$ be a state with N particles and arbitrary particle-hole excitations, then the completeness ensures that it can be constructed out of the ground state $|N\rangle = f(b^\dagger)|N\rangle_0$. The action of the creation operator is then defined as

$$F_\eta^\dagger |N\rangle = f(b^\dagger) \hat{T}_\eta |N+1\rangle_0,$$

with a phase counting operator \hat{T} used to insert the fermion creation operator at the right place.

We are now in the position to define boson fields ϕ with the aid of the Fourier sums φ_η and φ_η^\dagger over the b 's and b^\dagger 's respectively:

$$\phi_\eta(x) = \varphi_\eta(x) + \varphi_\eta^\dagger(x), \quad \text{where}$$

$$\varphi_\eta(x) = - \sum_{q>0} \frac{1}{\sqrt{n_q}} e^{-iqx} b_{q\eta} e^{-aq/2}, \quad \varphi_\eta^\dagger(x) = - \sum_{q>0} \frac{1}{\sqrt{n_q}} e^{iqx} b_{q\eta}^\dagger e^{-aq/2},$$

and wherein a is introduced to regularize the limit $q \rightarrow \infty$. Intuitively, the boson field can be understood by using its relation to the normal-ordered particle density,

$$\rho_\eta(x) = : \psi_\eta^\dagger(x) \psi_\eta(x) : = \partial_x \phi_\eta(x) + \frac{2\pi}{L} \hat{N}_\eta. \quad (1.1.7)$$

We can identify the second term as the density of a perfect electron crystal $\sim N/L$. Deviations from the crystalline equidistant electron spacing are described by the change of $\phi_\eta(x)$. Integrating the equality over x we see that the boson field accounts for the difference in particle number with respect to the perfect lattice.

To write down the exact bosonization identity relating the fermion and boson operators, we have to express the action of the fermion operator on an arbitrary state in terms of the boson ones. To this end, we note that $\psi_\eta|N\rangle_0$ is an eigenstate of $b_{q\eta}$ with eigenvalue α_q . This allows us to write a coherent-state representation of ψ_η using the field φ_η :

$$\psi_\eta(x)|N\rangle_0 = \exp\left(\sum_{q>0} \alpha_q(x) b_{q\eta}^\dagger\right) F_\eta \lambda_\eta|N\rangle_0 = e^{i\varphi_\eta^\dagger(x)} F_\eta \lambda_\eta(x)|N\rangle_0.$$

The phase operator λ can be identified by comparing expectation values of $F_\eta^\dagger \psi_\eta$ in the representation given above and in its original form.

Finally, the stage is set for the exact operator identity. $\psi_\eta(x)|N\rangle$ can be calculated, and, using the ingredients above, written down in a closed form, namely

$$\psi_\eta(x) = F_\eta \lambda_\eta(x) e^{-i\varphi_\eta^\dagger(x)} e^{i\varphi_\eta(x)} \quad (\text{normal ordered}), \quad (1.1.8)$$

$$= F_\eta a^{-1/2} e^{i\frac{2\pi}{L}(\hat{N}_\eta - \frac{1}{2}\delta_b)x} e^{i\phi_\eta(x)} \quad (\text{not normal ordered}). \quad (1.1.9)$$

In the second line the phase operator is written explicitly and the exponentials are combined using a Hausdorff identity. To achieve the compact representation, we have to add a regularizer in the denominator in front. On the downside, we can no longer guarantee normal ordering of the operators.

1.1.4 Application to the model

We can now use the results of the previous section and write down the Hamiltonian in the boson fields straightforwardly. For the following discussion, it is convenient to adopt the notation used by Kane and Fisher [37] which emerge from a fieldtheoretical approach. The “dual fields” θ_{KF} and ϕ_{KF} shall be defined as difference and sum of left- and right-moving fields ϕ respectively,

$$\theta_{KF}(x) = \frac{1}{2\sqrt{\pi}} \{\phi_L(x) - \phi_R(x)\}, \quad \text{thus} \quad \partial_x \theta_{KF}(x) = \frac{1}{2\sqrt{\pi}} \{\rho_L(x) + \rho_R(x)\}, \quad (1.1.10)$$

$$\phi_{KF}(x) = \frac{1}{2\sqrt{\pi}} \{\phi_L(x) + \phi_R(x)\}, \quad \text{thus} \quad \partial_x \phi_{KF}(x) = \frac{1}{2\sqrt{\pi}} \{\rho_L(x) - \rho_R(x)\}. \quad (1.1.11)$$

We rewrite the Hamiltonian in terms of these boson fields, neglecting the KF-indices:

$$H = v \int_{-L/2}^{L/2} dx : \left[\frac{g}{2} (\nabla \phi)^2 + \frac{1}{2g} (\nabla \theta)^2 \right] :,$$

where the interaction parameters g_2 and g_4 are contained in the sound velocity $v = [(1+g_4)^2 - g_2^2]^{1/2}$ and in the dimensionless interaction parameter

$$g = \sqrt{\frac{1+g_4-g_2}{1+g_4+g_2}},$$

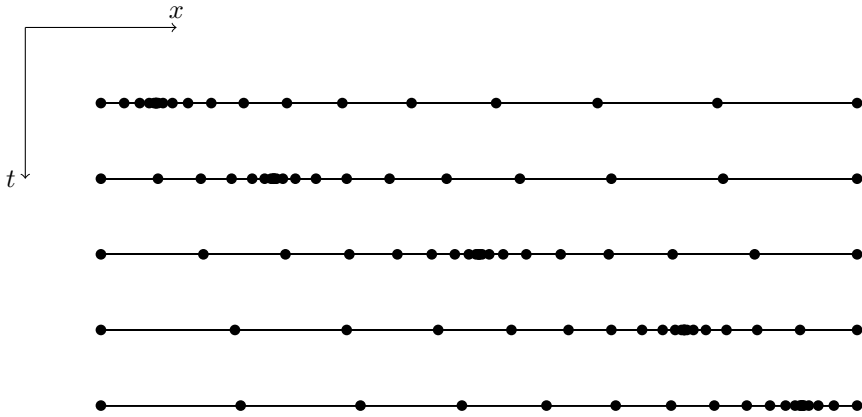


Figure 1.1.4: Phonon propagation in a one-dimensional crystal. The physical picture is in good agreement with collective density fluctuations in the Luttinger liquid.

which is also frequently referred to as Luttinger parameter K . This representation is valid at long wavelengths and short-range interactions (neglecting the momentum dependence of g). It is obviously just the Hamiltonian of an elastic string. The dynamics can be understood by a very simple physical picture: We insert a particle in one end of the wire. Soon it will hit its next neighbor and transfer its momentum. This procedure is repeated at the site of the next neighbor and so on. The resulting motion is a collective one that spreads coherently through the whole system [66], visualized in figure 1.1.4.

Another model with comparable behavior is that of phonons in a one dimensional Wigner crystal [37]. Let $\theta a/\sqrt{\pi}$ be the displacement of the electrons from their lattice positions. The Hamiltonian (1.1.1) then describes the long-wavelength phonon fluctuations. These Goldstone modes destroy the long-ranged crystalline order even at $T = 0$ and lead to algebraic decay of the spatial correlations.

The Landauer conductance in a clean Luttinger liquid is calculated via the current-current correlation function [23],

$$G = \lim_{\omega \rightarrow 0} \frac{1}{\hbar L \omega} \int dx d\tau e^{i\omega\tau} \langle T_\tau J(x, \tau) J(0, 0) \rangle = g \frac{e^2}{h}.$$

We note that g can be understood as a dimensionless measure of conductance of the pure Luttinger liquid. However, the derivation of the Landauer conductance from the transmission amplitudes in the presence of strong interaction is a subtle point. We will discuss the issue in section 1.3.6.

Impurity in a Luttinger Liquid

A Luttinger liquid with an impurity is no longer exactly solvable. In this section, results of Ref. [37] obtained by a perturbative renormalization-group approach are presented. We can approach the problem of scattering in a strongly interacting one-dimensional wire in two limiting cases: A very weak barrier and a weak link or strong barrier.

A weak structureless barrier is represented in real space by a potential $V(x)$ which is nonzero only in the close proximity of $x = 0$. The magnitude is chosen small with respect to the Fermi level. The correction to the Hamiltonian reads

$$\delta H = \int dx V(x) \Psi^\dagger(x) \Psi(x).$$

This equation can be translated to a correction in the action of the boson field where only the most important terms of a gradient expansion around $x = 0$ are kept,

$$\delta S \approx \sum_{n=-\infty}^{\infty} \frac{1}{2} \nu_n \int d\tau e^{i2n\sqrt{\pi}\theta(x=0,\tau)},$$

where the coefficients ν_n are proportional to the backscattering component of the momentum representation of $V(x)$, namely $\nu_n = \tilde{V}(n2k_F)$. n counts the backscattered particles.

One can further compute the effective action of the system. This serves as starting point for a perturbative calculation or a renormalization group transformation. To implement the latter, we introduce a high-frequency cutoff Λ of the order of the Fermi-energy and integrate over energies between Λ and Λ/b with $b > 1$. The final step is the rescaling of the parameter $\tau' = \tau/b$. After this procedure we identify the renormalized coefficients⁶ ν'_n and, by choosing $b = 1 + dl$, extract the differential RG flow

$$\frac{d\nu_n}{dl} = (1 - n^2 g) \nu_n. \quad (1.1.12)$$

From this, we can deduce the following behavior:

- For $g > 1$, renormalization weakens the Fourier component of the backscattering potential for any n .
- If $g = 1$, there is no flow for the $2k_F$ component. A flow parameter with such a behavior is called marginal. The other parameters with $n > 1$ scale to zero.
- A repulsive interaction ($g < 1$) enforces the first Fourier coefficient of the barrier and therefore ν_1 is labeled a relevant flow parameter.

Following this observations we can expect that attractive interactions lead to a vanishing reflection in the limit of energies very close to the Fermi surface. In the opposite case, repulsive interactions strengthen an initially weak barrier and, in the same limit, pin the Luttinger liquid completely.

It is illuminating to integrate the RG flow down to a cut-off energy scale of the order of the temperature, the frequency or the bias (the biggest of these will confine the energy of a particle entering the system from below). Separating variables in equation (1.1.12) and computing the integral yields an effective barrier

$$v_{n,E} \propto v_n E^{n^2 g - 1}.$$

We can relate the barrier strength to the transmission probability and hence to the conductance [23]. Thus we expect $G(T) \propto |\nu_n|^2 T^{n^2 g - 1}$. This result can be

⁶This is the most trivial case. Additional couplings can appear due to the rescaling. The procedure is done more carefully in section 1.2.3.

confirmed by a perturbative calculation in the backscattering potential [37]. To leading order the result reads

$$G(T) = e^2/h \left[g - \sum_{n=1}^{\infty} a_{nT} |\nu_n|^2 T^{2(n^2 g - 1)} \right].$$

Let us repeat the previous discussion for this expression. Attractive interaction yields a positive exponent for the temperature and the correction to the conductance will vanish as we approach zero temperature. On the other hand, choosing the interaction to be repulsive, the second term will diverge in the proximity of zero temperature and we can expect the conductance to vanish. This is a reasonable assumption. However, perturbative calculations do not hold in this region and this statement needs further verification.

Similarly we can treat the conductance at finite frequency. The result is the same apart from the coefficient a_{nV} which replaces the non-universal constant for non-zero temperature a_{nT} : Repulsive interaction leads to a divergence of the correction to the conductance in the low-frequency limit. It should be noted that although the coefficients are not universal, their ratios are [37].

A weak link is built up between two wires in the other limiting case. The unperturbed system is consisting of two separate wires. In the course of perturbation theory a weak link is established between them which allows tunneling into the other wire via a hopping matrix element t . To model this setup in the Hamiltonian, we introduce fields on the left Ψ_L and on the right Ψ_R of the barrier.⁷ The initial Hamiltonian divides into two parts with the left and right fields respectively. The hopping is achieved by an overlap matrix element

$$\delta H \approx -t[\Psi_R^\dagger(x=0)\Psi_L(x=0) + \text{H.c.}].$$

Along the lines of the previous calculation, we can transform to boson fields and apply a perturbative renormalization-group treatment on the effective action. The latter results in a RG flow equation analogue to the case of a weak barrier, namely

$$\frac{dt_n}{dl} = (1 - n^2/g)t_n.$$

This flow equation is the counterpart of the one discussed in the previous paragraph. Remember that we noticed a growing scattering potential for repulsive interaction in the former case. This time the hopping element t is weakened for all values of n ultimately resulting in full decoupling of the wires. Furthermore, fully consistent with the earlier discussion, attractive interaction enforce the matrix element for one single hopping t_1 and thus connects to the former case of a vanishing barrier.

Phase diagram In this paragraph we sum up the results of the energy-shell RG analysis. To this end, we combine the results of the two limiting cases to a single phase diagram in figure 1.1.5. The diagram is divided into a weak barrier (upper) part and a weak link (lower) part. The axis to the right is labeled by the interaction parameter or, equivalently, the dimensionless conductance in the

⁷To be distinguished from right- and left-moving fields.

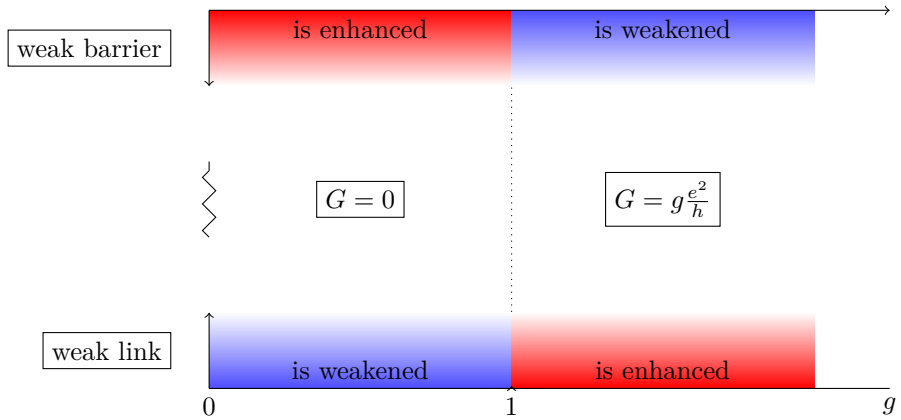


Figure 1.1.5: Phase diagram of the Luttinger liquid in the presence of a weak link or a weak barrier. In the presence of repulsive interactions on the left the barrier is enhanced and suppresses conductance, ultimately disconnecting the wires. Attractive interactions weaken the barrier to the limiting case of a clean wire. The perturbative regimes are colored, the RG technique is used to bridge the white area in-between.

clean Luttinger liquid g . In the direct proximity of the vertical boundaries we can directly apply the results from the perturbative calculations: For repulsive interactions, a small scattering potential ν_1 is enhanced and the hopping matrix element t is downsized. Both compartments reduce the initial conductance G . On the right side of the diagram, attractive interactions weaken the small barrier and grow the link between the wires in their respective regimes. Close to the Fermi surface Kane and Fisher find a conductance close to the value ge^2/h for a clean wire.

It should be noted that the Landauer conductance in the limiting case of a clean wire is subject to ongoing discussion. While approaches in the fermion language predict a ballistic clean conductance of e^2/h in the presence of interaction [6, 50, 60], a characteristic feature of results obtained by bosonization is the aforementioned interaction-dependent conductance. We will, however, postpone this discussion to section 1.3.6 and proceed with the analysis of the phase diagram.

It is a plausible assumption that the connection in the non-perturbative regime in-between is smooth. Indeed it can be shown for the special case $g = 1/2$ that even the smallest obstacle in the wire causes total reflection [37].

Temperature dependence of the conductance Let us stop the renormalization of the impurity at a scale where the temperature is of the order of the momentum cutoff a . This scale is given by [29]

$$e^{l^*} = \frac{v}{aT}.$$

Starting with a weak impurity we can distinguish three regimes for the temperature dependence of the conductance in the case $g < 1$, as can be seen in figure 1.1.6:

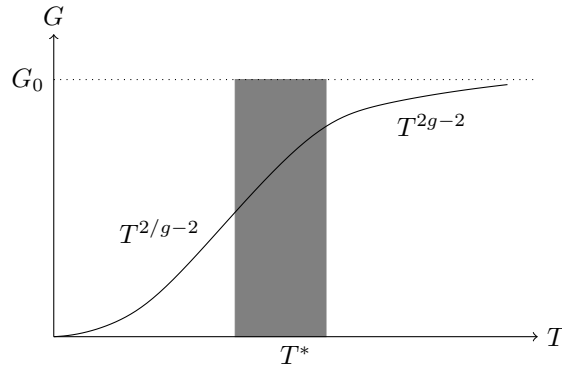


Figure 1.1.6: The temperature dependence of the conductance in the three regimes. The smooth connection in the vicinity of T^* is estimated.

- For high temperatures the conductance is given by a power law with the exponent $2g - 2$. The renormalization of the barrier is initially weak and grows while the temperature is lowered.
- In the intermediate regime the temperature is of the order of the renormalized impurity. The connection in this regime is anticipated to be smooth.
- At low temperatures the weak barrier has grown strong and can be modeled by a weak link between two decoupled wires. The conductance is governed by temperature to the power of $2/g - 2$.

At zero temperature the Luttinger liquid is completely pinned by the initially small impurity.

We thereby provided a qualitative picture of the physics in a one-dimensional system perturbed by a single barrier in two limits. Kane and Fisher continue with an analysis of a resonant structure. We will, however, save this part for later (section 1.4.1) and introduce an approach for weak interactions which is non-perturbative in the impurity strength.

1.2 Weak interactions in a Luttinger liquid with impurity

In the early 90's a new approach to the field of interacting fermions in one dimension was pioneered by Matveev, Glazman and Yue (MGY) [52, 74] and applied more recently to a great variety of problems, e.g., an impurity with resonant level [62] or a Y-junction [43]. The main reasons for the ongoing interest in this approach is the successful qualitative description of effects present also in systems with stronger interaction and the close integration to the Landauer-Büttiker formalism, in contrast to the bosonized theory, as discussed in section 1.3.6. Starting point is the spinless Tomonaga-Luttinger model described in the previous section with a single impurity.

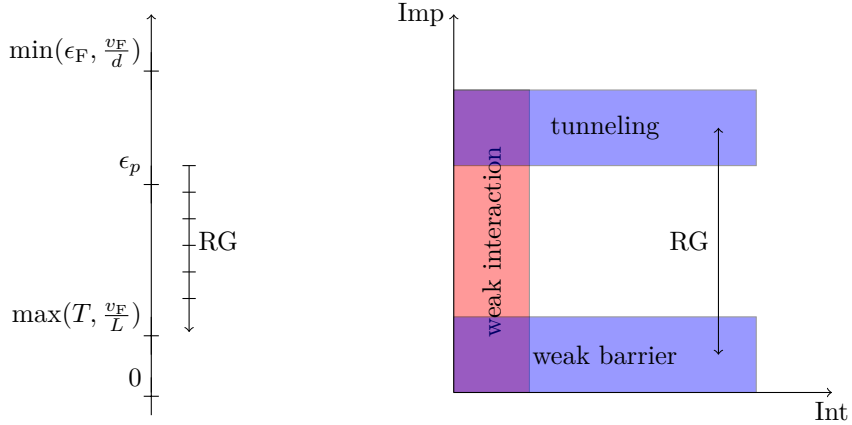


Figure 1.2.1: On the left: energy scales in the weakly perturbed Luttinger liquid. High energy scales in the system are the bandwidth ϵ_F or the energy related to the inverse interaction length v_F/d . On the other end of the scale we find the temperature T and the Thouless energy of the system, related to the system size by v_F/L . ϵ_p denotes the breakdown of perturbation theory in interaction. To the right: scopes of theoretical approaches in the area spanned by strength of impurity(vertical axis) and interaction(horizontal axis). The colored areas are expanded perturbatively towards the center of the figure. In the overlapping regions, the theories are bound to coincide.

Bosonization allows to investigate both the regime of a very strong impurity (weak link) and a small barrier for arbitrary strength of interaction. Since the extrapolation done between these two regimes heavily relies on a perturbative approach, it is a natural question to ask what is happening in between. The idea of MGY is to treat the interaction as a small parameter and explore the physics for arbitrary impurity strength and temperature. As one can see on the map to the right in figure 1.2, the theories are expected to coincide for the strong impurity and the weak link case.

Recent attempts to close the gap were made by Aristov et al. [6]. The group managed to derive universal parts of the RG flow equation valid in the presence of arbitrary interactions.

The assumption of weak repulsive interactions, parameterized by i.e., $\alpha = 1 - g \ll 1$, restricts the applicability of the model. Experimentally, α is found to be close to one in carbon nanotubes [72]. On the other hand, single-mode semiconductor quantum wires reach down to $\alpha \sim 0.2$ to 0.3 [7] and can be screened further by metallic gates. In this regime, the results obtained in this framework should be applicable directly. However, some of the physics of strongly interacting systems can be deduced successfully from the weak interacting regime, e.g., the resonance peak for sequential tunneling through a double barrier is reported to be in good agreement [62].

On the left panel of figure 1.2, we qualitatively compare the important energy scales of the system. As we will see below, even the first order correction to the

scattering amplitudes due to the interaction is logarithmically divergent,

$$\delta S \propto \alpha \log(\Delta/\epsilon) \quad \text{where} \quad \Delta = \min\left(\frac{v_F}{d}, \epsilon_F\right),$$

where α is a measure for the strength of interaction, d is the interaction length and ϵ is the energy of the incoming particles. For a perturbative theory to remain valid we require a small correction δt . If the interaction strength α is fixed the requirement defines an energy scale ϵ_p below which the correction is not small anymore. In order to explore the low- T regime we must find a way to sum up all leading orders of the perturbation theory. We will see in the following that this is possible via a renormalization group approach.

1.2.1 Scattering states and chiral fields

We consider a 1D system of spinless fermions with a scatterer of arbitrary strength located at $x = 0$. Furthermore, far away from the barrier, the electrons do not interact. In a range L around the impurity, the wave-function is altered in a non-trivial way by the interaction: Incoming waves encounter a barrier dressed by density fluctuation. In the following we will send L to infinity.⁸ The *asymptotic* incoming wave-functions far left from the barrier have the form [74]

$$\psi_k(x) = e^{-i(k+k_F)x} + r e^{i(k+k_F)x}. \quad (1.2.1)$$

The wave vector $k \ll k_F$ lies in the vicinity of k_F and the barrier is assumed to be symmetric for simplicity. In the ground state of the non-interacting system we can write the local density as

$$\begin{aligned} \langle \rho(x) \rangle &= \frac{1}{2\pi} \int_{-\infty}^0 dk \psi_k^*(x) \psi_k(x) = \frac{i}{4\pi x} (r^* e^{-i2k_F x} - r e^{i2k_F x}) + \text{const.} \\ &= \frac{1}{2\pi x} |r| \sin(2k_F x + \arg(r)) + \text{const.}, \end{aligned} \quad (1.2.2)$$

where the lower limit is extended to $-\infty$, making use of the extended state space of the Tomonaga-Luttinger model. The density oscillations in equation (1.2.2) (commonly referred to as Friedel oscillations) grow asymptotically in the vicinity of the impurity and decay as $1/x$ away from the origin.⁹ This feature results in the logarithmic divergence of the reflection amplitude at $k \rightarrow k_F$ [74].

We further define field components by separating right- and left-moving field operators (compare equation (1.1.4) in the previous section),

$$\Psi(x) = \Psi_R(x)e^{ik_F x} + \Psi_L(x)e^{-ik_F x}.$$

The fields $\Psi_{R/L}$ are slowly varying on the scale of the inverse Fermi momentum k_F^{-1} .

For the interaction we use the same model as in the previous section, hence the density-density interaction can be written as

$$H_{\text{int}} = \frac{1}{2} \iint dx dy \rho(x) V(x-y) \rho(y), \quad (1.2.3)$$

⁸We will clarify this assumption in the next chapter.

⁹The decay is remarkably slow compared to counterparts in higher dimensions.

where the density at a point x , expressed in terms of the chiral fields, reads

$$\rho(x) = \Psi_R^\dagger \Psi_R + \Psi_L^\dagger \Psi_L + \Psi_R^\dagger \Psi_L e^{-i2k_F x} + \Psi_L^\dagger \Psi_R e^{i2k_F x}. \quad (1.2.4)$$

We combine the two expression and reformulate the interacting part of the Hamiltonian,

$$H_{\text{int}} = g_2 \int_0^\infty dx \Psi_R^\dagger \Psi_R \Psi_L^\dagger \Psi_L, \quad (1.2.5)$$

neglecting the fast oscillating parts and assuming that the interaction range is short (with respect to k_F^{-1}) but finite. Thus we can set the arguments of the density fields, x and y , equal to each other. Furthermore, the interactions between fields of the same chirality g_4 is neglected. This can be justified in a spinless model because the distinction between g_2 and g_4 leads to unphysical current-current interactions [49] (see section 3.1.2 for a detailed discussion of this subject).

1.2.2 First order in interaction: Hartree-Fock corrections

We want to study the influence of the interaction on the reflection and transmission amplitudes of the electrons. To this end, we can either calculate the Green's functions of higher orders or the correction to the wave function. Both can then be compared to the “clean” case to extract the effect of the interactions on the amplitudes. While in the latter of the thesis, the Green's function formalism will be employed, the authors of the seminal paper [74] used the first order Born approximation to calculate the corrected wave function and we shall briefly outline their approach, although not in every detail.

We want to calculate the scattering matrix elements to first order in interaction. To this end, equation (1.2.5) is decomposed in a Hartree and a Fock part. It can be shown, that the Hartree part yields a constant (we show this explicitly in section 3.2.1). We compute the Fock part explicitly:

$$\begin{aligned} H_{\text{int}} &= -g_2 \int_0^\infty dx \left(\langle \Psi_R^\dagger \Psi_L \rangle \Psi_L^\dagger \Psi_R + \langle \Psi_L^\dagger \Psi_R \rangle \Psi_R^\dagger \Psi_L \right) \\ &= -\frac{ig_2}{4\pi} \int_0^\infty \frac{dx}{x} \left(r^* \Psi_L^\dagger \Psi_R + r \Psi_R^\dagger \Psi_L \right). \end{aligned}$$

In the second line we used equation (1.2.2) and equation (1.2.4) to identify the expectation values. Let us further define the incoming and outgoing wavefunctions

$$|i, k\rangle = \begin{cases} e^{i(k+k_F)x} & (x < 0) \\ e^{-i(k+k_F)x} & (x > 0) \end{cases}, \text{ and } |o, k\rangle = \begin{cases} e^{-i(k+k_F)x} & (x < 0) \\ e^{i(k+k_F)x} & (x > 0) \end{cases}.$$

The scattering amplitude from a given incoming wave to an outgoing one to

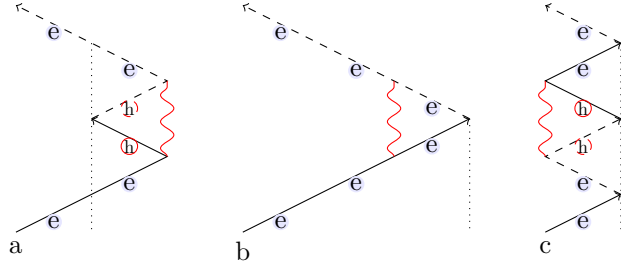


Figure 1.2.2: Real space diagrams (g_2) for reflection. The particle is incident from the bottom left of the diagram, the dotted line represents the impurity.

first order in $e^{-iH_{\text{int}}t}$ reads

$$\begin{aligned} & -i \int \frac{dk}{2\pi} 2\pi \delta(E_k - E_{k'}) |\mathbf{o}, k'\rangle \langle \mathbf{o}, k'| H_{\text{int}} |\mathbf{i}, k\rangle \\ &= \frac{ig_2 r}{4\pi v_F} \int_d^\infty \frac{dx}{x} e^{-i2kx} |\mathbf{o}, k\rangle \\ &= -\frac{\alpha r}{2} \log(kd) |\mathbf{o}, k\rangle. \end{aligned}$$

To compute the first integral, we used the linear dispersion relation $E_k = v_F k$ and neglected fast oscillating parts $\sim \exp(2k_F)$. The second integral is divergent for short distances, therefore we introduce a cutoff d .¹⁰ The result is valid with leading logarithmic accuracy. Analogously, the amplitude for the scattering from an outgoing to an incoming wave (by Friedel oscillations) is given by

$$\frac{\alpha r^*}{2} \log(kd).$$

We are now in the position to compute the first order corrections in interactions. An incident wave that has been reflected by the barrier has undergone one of the following processes in figure 1.2.2:

- The wave was reflected by the barrier (b),
- was reflected by the barrier, scattered back to an incoming wave due to Friedel oscillations and reflected once again by the barrier (c), or
- penetrated the barrier, reflected by the Friedel oscillations on the other side and transmitted back (a).

The sum of these contributions,

$$\delta r = \frac{1}{2} [-\alpha r + \alpha|r|^2 r + \alpha t r^* t] \log(kd) = -\alpha|t|^2 r \log(kd),$$

yields the total first order correction to the reflection amplitude. Performing the summation for the transmission amplitude, we find

$$\delta t = \frac{1}{2} [\alpha t|r|^2 + \alpha|r|^2 t] \log(kd) = \alpha|r|^2 t \log(kd).$$

¹⁰The role of d as a finite range of interaction will become clearer in section 3.2.1

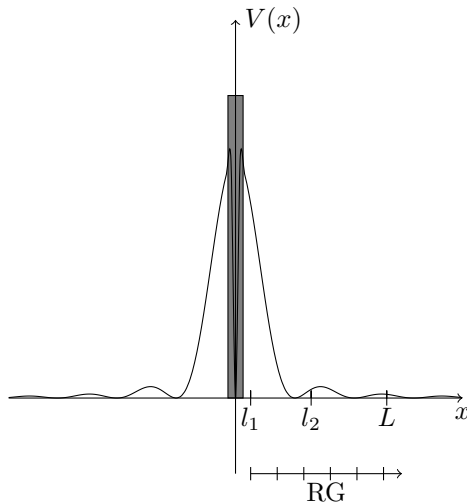


Figure 1.2.3: The impurity potential dressed by Friedel oscillations in a wire of length L . The strength of the effective barrier is measured on the vertical axis. The perturbative result is valid for interaction confined to the region $[-l_1, l_1]$. Interaction in the extended region $[-l_2, l_2]$ requires summation of divergent terms of all orders.

The logarithmic divergence of the first-order result at $k \rightarrow 0$ is a typical infrared divergence in 1D. As long as the correction, namely $\alpha \log(kd)$, is small, this result is a leading correction. However, for smaller energy or momentum, a perturbative calculation is not sufficient: The n th order is expected to diverge as $\alpha^n \log^n$. In this case, it is necessary to sum up the most divergent terms of all orders.

To accomplish this task, we will apply a renormalization group approach in the spirit of MGY. Alternatively, one could apply a parquet summation technique used originally for singularities in X-ray spectra by Abrikosov [1] and Nozières [59].

Real-space interpretation and RG

One way to illustrate the physical meaning of the renormalization group procedure (in real space) is presented in [74]: When we restrict the interaction to the very vicinity of the impurity, e.g., a range $l \sim d$, an electron encounters the slightly modified bare barrier and the first order correction in interaction is leading and proportional to $\alpha \log(l/d)$.

Beyond this scale, the effects of the interaction modify the barrier. It is not sufficient anymore to do perturbation theory with the *bare* impurity. If we choose $l \gg d$ so that $\alpha \log(l/d)$ is not small anymore, an incident particle will be scattered by an order-of-magnitude stronger effective barrier.

The idea of the real-space renormalization group is thus to extend the region of interaction stepwise, ensuring the validity of a perturbative calculation at every step. The essence of this procedure is shown in figure 1.2.3. After the n th

step, the transmission amplitude reads

$$t_{n+1} = t_n - \alpha t_n |r|^2 \log(l/d).$$

Shrinking the step size we can approach the continuous limit and replace this recursive equation by

$$\frac{dt}{d \log(L/d)} = -\alpha t |r|^2. \quad (1.2.6)$$

Finally we can integrate equation (1.2.6) from $L = d$ to $L = 1/(k - k_F)$ with the boundary condition $t|_{L=d} = t_0$ to find the renormalized transmission amplitude [74]

$$t_k = \frac{t_0 |(k - k_F)d|^\alpha}{\sqrt{|r_0|^2 + |t_0|^2 |(k - k_F)d|^{2\alpha}}}. \quad (1.2.7)$$

An equivalent way to sum up the leading terms is given by a scaling procedure in the energy variables. We can rewrite first order corrections in terms of particle energy and UV cutoff,

$$\delta t \sim \log(\Delta/\epsilon),$$

where the ultraviolet cutoff Δ is equivalent to d and of the order of the Fermi energy or the energy associated with the interaction length v_F/d . This procedure is outlined in more detail in the next section, including a more careful derivation of the flow equations on the level of the Hamiltonian.

1.2.3 A simple renormalization group approach

“Poor man” scaling

The result of the perturbative treatment of the single impurity is applicable as long as the corrections remain small, i.e.,

$$\alpha \log\left(\frac{v_F}{d\epsilon}\right) \ll 1.$$

At smaller values of ϵ the corrections of sub-leading order and beyond dominate the transmission as the nth-order correction diverges as $\alpha^n \log^n(v_F/(d\epsilon))$. Thus, to extend the result towards ϵ_F we have to take into account all terms of higher order in α . To achieve this goal, we apply a simple renormalization group approach first applied by Anderson to the Kondo problem [4]. It was successfully adopted to the fermionic 1d problem shortly afterwards in the 70s by Solyom [67].

We noted in the previous section that the bandwidth for the interaction with the Fermi sea electrons Δ is determined by the spatial scale of the interaction, v_F/d . Electrons with energies outside this strip of width $2v_F/d$ will be neglected. Now we transform the problem to one with smaller bandwidth $D = \Delta/\Lambda$ where $\Lambda > 1$. The problem is similar to our problem if we modify the bare transmission to a transmission which accounts for the electrons excluded by this step. Thus we arrive at an effective barrier with renormalized amplitudes r and t . This procedure seems plausible. However, it is not clear whether a perturbative calculation in interaction with leading logarithmic accuracy really captures the correct scaling behavior. Additionally, one has to take into account the renormalization of the interaction parameters.

Energy space RG

Anderson suggested that equivalent problems can be formulated by requiring that the scattering matrix is invariant under the RG transformation. This can be used to calculate both the renormalized transport coefficients and the interaction parameters. It can be shown [67] that for this requirement to be fulfilled, the transformed Hamiltonian has to obey the relation

$$H'_{\text{int}} = P \left[H_{\text{int}} + H_{\text{int}}(1-P) \frac{1}{\omega - H_0} H_{\text{int}} + O(H^3) \right] P, \quad (1.2.8)$$

where the projection operator P is such that a state acted upon contains no particle in the range excluded by the RG. The renormalization of the bare transmission amplitude due to this transformation is found using perturbation theory. Alternatively, this can be done on a microscopic level which includes averaging out the fast modes in the Hamiltonian. This approach is also shown in [74] for the case of electrons with spin. The outline of this procedure is as follows:

- The generic Hamiltonian with interaction is transformed to a basis of scattering wave functions with included barrier potential.
- The requirement equation (1.2.8) is used to calculate a renormalized Hamiltonian with different couplings.
- The new coupling constants are found by comparing H_{int} and H'_{int} .
- Integration over infinitesimal RG steps to a arbitrary cutoff D yields the renormalized couplings.

Starting point is the Hamiltonian of the interacting system

$$H_{\text{int}} = \sum_{k_1, k_2, p} g_1 a_{k_1}^\dagger b_{k_2}^\dagger a_{k_2+2k_F+p} b_{k_1-2k_F-p} \quad (1.2.9)$$

$$+ \sum_{k_1, k_2, p} g_2 a_{k_1}^\dagger b_{k_2}^\dagger b_{k_2+p} a_{k_1-p} \quad (1.2.10)$$

$$+ \frac{1}{2} \sum_{k_1, k_2, p} g_3 a_{k_1}^\dagger a_{k_2}^\dagger b_{k_2-2k_F+p} b_{k_1+2k_F-p-G} \quad (1.2.11)$$

$$+ b_{k_1}^\dagger b_{k_2}^\dagger a_{k_2+2k_F+p} a_{k_1-2k_F-p+G}, \quad (1.2.12)$$

where the coupling constants are, in general, momentum dependent. a_k^\dagger and b_k^\dagger create right- and left-moving electrons with momentum k , respectively. G in the third term is a reciprocal lattice vector (in the half-filled band $G = 4k_F$). g_4 is in the present spinless case not distinguishable from g_2 . Note that we have not excluded backscattering, g_3 , in the Hamiltonian since it will be responsible for the renormalization of the interaction. The basis of free fermion wavefunctions of this Hamiltonian is now transformed by a unitary transformation to incorporate the effect of scattering at the impurity,

$$a_k = \int dq [A_k^q c_q + B_k^q d_q] \quad \text{and} \quad b_k = \int dq [C_k^q d_q + D_k^q c_q], \quad (1.2.13)$$

where A, B, C, D include the reflection and transmission amplitudes (see [74] for details). With these transformations, new non-diagonal quadratic terms appear in H_{int} .

The elimination of the degrees of freedom in the energy range $[D_0 - \delta D_0, D_0]$ is done by replacing *any* product of two fermion operators in H'_{int} that does not belong to the inner band by its average value. So every pair of operators (with same spin) is replaced by $A^\dagger A + \langle A^\dagger A \rangle$ where the average is over $[D_0 - \delta D_0, D_0]$.¹¹

The Hamiltonian of the system after the RG step, H'_{int} , can contain couplings between more than two particles. It is thus necessary to make sure that after infinitely many transformations the number of couplings is still finite or the additional couplings are invariant under scaling or scale to zero (and therefore can be neglected). Applying the transformation to H_{int} , the quadratic part of the full Hamiltonian (which originally consisted of H_0) is replaced by

$$H'_0 = \int dk \epsilon'(k) (c_k^\dagger c_k + d_k^\dagger d_k) - \frac{i}{8\pi} (g_1 - g_2) \int dk dp [(t_k^* r_q' - t_k' r_q^*) c_k^\dagger d_p - \text{H.c.}] \frac{\delta D_0}{D_0 + \epsilon(k) + \epsilon(p)}. \quad (1.2.14)$$

In the next step, the Hamiltonian is diagonalized. This can be done as follows: We take the initial and final states of the bare Hamiltonian

$$|i\rangle = a_k^\dagger |0\rangle \quad \text{and} \quad |f\rangle = a_k^\dagger |0\rangle,$$

and transform them to scattering states with equation (1.2.13). Comparing the matrix element $\langle i | H'_0 | f \rangle$ with $\langle i | H_0 | f \rangle$, the corrections $t - t_0 = \delta t$ can be identified. In the case of the correction to the transmission $t(\epsilon)$ the algebra yields

$$\delta t_\epsilon = \left[\frac{g_2 - 2g_1}{2\pi v_F} t |r|^2 \right] \frac{\delta D_0}{D_0 + \epsilon}. \quad (1.2.15)$$

The second term in equation (1.2.8) generates the renormalization of the interaction constants. For the clean case (without impurity), they are calculated in [67]:

$$g_1(\xi) = \frac{V(2k_F)}{1 + \frac{V(2k_F)}{\pi v_F}} \quad (1.2.16)$$

$$g_2(\xi) = V(0) - \frac{1}{2} V(2k_F) + \frac{1}{2} \frac{V(2k_F)}{1 + \frac{V(2k_F)}{\pi v_F}}, \quad (1.2.17)$$

wherein $\xi = \log(\frac{D_0}{D})$. Corrections due to the impurity are considered small as $1/L$ and can therefore be neglected in the limit of a long wire [74]. We note further, that the solution includes the renormalization of the interaction constants caused by backscattering. Note that since we can neglect backscattering if $V(2k_F) \ll V(0)$, this result allows us to keep the interaction parameters constant in the course of renormalization.

Plugging the interaction constants in equation (1.2.15) and applying a differential form yields

¹¹Details of this rather lengthy calculation can be found in [74].

$$\frac{dt}{d\xi} = -\frac{g_2(\xi) - 2g_1(\xi)}{2\pi v_F} t(1 - |t|^2). \quad (1.2.18)$$

Non-renormalized interaction

If we neglect the cutoff dependence of g_1 and g_2 and apply the RG equation $D \rightarrow D/\Lambda$ repeatedly we can reduce the bandwidth until we arrive at a value of the order of the incoming particle energy ϵ . Beyond this energy scale, the corrections due to interactions are not logarithmic. Each step of this procedure affects the transmission amplitude in the way given above.

Integrating this equation from $D = D_0$ to $D = |\epsilon|$ using the boundary condition $t(\epsilon)|_{D=\Delta} = t_0$ we obtain

$$t_\epsilon = \frac{t_0 | \frac{d\epsilon}{v_F} |^\alpha}{\sqrt{|r_0|^2 + |t_0|^2 | \frac{d\epsilon}{v_F} |^{2\alpha}}}, \quad (1.2.19)$$

where

$$\alpha = \frac{g_2 - 2g_1}{2\pi v_F}.$$

Perturbative expansion of this expression to second order in α yields

$$t(\epsilon) = \frac{t}{\sqrt{|r|^2 + |t|^2}} - \frac{\alpha t |r|^2 \log(\frac{d\epsilon}{v_F})}{2(|r|^2 + |t|^2)^{3/2}} + \frac{\alpha^2 t |r|^2 [|r|^2 - 2|t|^2] \log^2(\frac{d\epsilon}{v_F})}{2(r^2 + t^2)^{5/2}} + O(\alpha^3) \quad (1.2.20)$$

For the sake of completeness we do the same expansion for the reflection coefficient which is calculated from the transmission simply by using the unitary condition $r = \sqrt{1 - |t|^2}$,

$$r(\epsilon) = \frac{r}{\sqrt{|r|^2 + |t|^2}} + \frac{\alpha r |t|^2 \log(\frac{d\epsilon}{v_F})}{2(|r|^2 + |t|^2)^{3/2}} + \frac{\alpha^2 r |t|^2 [|t|^2 - 2|r|^2] \log^2(\frac{d\epsilon}{v_F})}{2(r^2 + t^2)^{5/2}} + O(\alpha^3). \quad (1.2.21)$$

We will show in section 3.3 that these expressions are identical to those calculated with perturbation theory up to the second order. Indeed, a Taylor expansion of this result *has to coincide* with perturbative calculations of all orders. We arrived thus at the point to formulate one of the aims of the project for the first time: The consistency of the RG approach with perturbative calculations to subleading order was never checked carefully for systems of finite size or with a energy-dependent S-matrix. To clarify this point further, we will consistently connect the perturbative approach with the scaling form of the S-matrix elements in the next section.

Check of validity for the RG approach

The test of the RG can be done by comparing the Taylor expansion in α to the perturbative expansion. A mismatch in the coefficients of the logarithms tells us that the theory is non-renormalizable in the S-matrix language, i.e., the notion of a S-matrix becomes invalid when unitarity is broken.

In this section we present a self-consistent way to check the validity of the “Poor-man” scaling without knowing the explicit differential form of the RG equations for perturbative next-to leading order calculations. The technique was presented recently in the context of random matrices to the community [40, 41]. We assume the energy dependence of the S-matrix of the system is governed by a power law

$$r(\epsilon) = A \left(\frac{\epsilon}{\Delta} \right)^\alpha, \quad (1.2.22)$$

where Δ is the ultraviolet cutoff, A and α are constants.¹² If we take the logarithms of both sides and derive with respect to $\log(\epsilon/\Delta)$ we get for α

$$\alpha = \frac{\partial}{\partial \log(\epsilon/\Delta)} \log(r(\epsilon)). \quad (1.2.23)$$

Now let us assume we computed perturbative corrections to the S-matrix in interaction. We sort the corrections in powers of logarithms, namely

$$r^{(n)}(\epsilon) = r_0(\epsilon) + \delta r_1(\epsilon) + \cdots + \delta r_n(\epsilon).$$

This expansion can be substituted into equation (1.2.23) and we find, factoring out r_0 ,

$$\alpha = \frac{\partial}{\partial \log(\epsilon/\Delta)} \left(\log(r_0) + \log \left(1 + \frac{\delta r_1}{r_0} + \cdots + \frac{\delta r_n}{r_0} \right) \right).$$

We are now in the position to Taylor-expand the logarithm,

$$\alpha = \frac{\partial}{\partial \log(\epsilon/\Delta)} \left[\left(\frac{\delta r_1}{r_0} + \frac{\delta r_2}{r_0} + \dots \right) - \frac{1}{2} \left(\frac{\delta r_1}{r_0} + \frac{\delta r_2}{r_0} + \dots \right)^2 + \dots \right]. \quad (1.2.24)$$

From this equation, exploiting the fact that α is constant, we can deduce the following requirements for the perturbative corrections:

$$\alpha = \frac{\delta r_1}{r_0}, \quad (1.2.25)$$

$$0 = \frac{\delta r_2}{r_0} - \frac{1}{2} \left(\frac{\delta r_1}{r_0} \right)^2, \quad (1.2.26)$$

$$0 = \frac{\delta r_3}{r_0} - \left(\frac{\delta r_1 \delta r_2}{r_0^2} \right) + \frac{\delta r_1^3}{3}. \quad (1.2.27)$$

Note that we used no additional assumptions. If these requirements are not met, the ansatz in equation (1.2.22) is not valid.

¹²We can identify the parameters with the known coefficients (bandwidth, interaction strength), but for the sake of the argument this is not necessary.

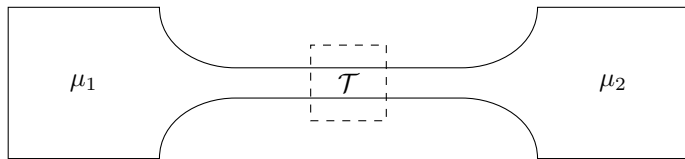


Figure 1.3.1: Simple model of a mesoscopic setup with a wire connecting leads. A scattering black box (dashed rectangle) is transcended by a fraction \mathcal{T} of the electrons following a chemical.

We conclude that, first, our simple perturbative scaling method outlined in the previous section is equal to a more careful derivation on a Hamiltonian level and, second, that it can be validated by comparing higher orders of the Taylor expansion in the weak interaction parameter α to perturbative results. The latter point should be kept in mind during section 1.4, where the procedure shall be applied to resonant levels and Y-junctions.

1.3 Conductance from transmission

The transmission coefficients, subject to the discussion in the last two sections, cannot be probed directly. Instead, one has to deploy transport measurements and measure the conductance or conductivity. An approach to calculate the conductivity from the transmission probability in mesoscopic systems is the Landauer-Büttiker formalism. Preceding the Landauer formalism, the conventional quantum theory of electrical transport employed current-current correlation functions to calculate the conductance. The framework, called Kubo formalism, allows to study linear response of the current to an applied uniform electric field. This view stands in contrast to the Landauer approach using *static* scattering properties and quantum mechanics to derive the transmission probabilities of incident electrons in a mesoscopic system. It thereby appoints the “flux incident on the boundaries of a conductor as the causative agent” [45].

To introduce basic concepts, we consider two reservoirs with chemical potentials μ_i connected by a conductor (see figure 1.3.1). From the reservoirs, electrons diffuse into the wire following a chemical potential difference and encounter a scattering “black-box” with a transmission probability \mathcal{T} .

The notion of an asymptotically free incident electron wave requires a coherent propagation through the device. At finite temperature, inelastic scattering processes are unavoidable. We can, however, neglect them, if the inelastic scattering length is by far larger than the thermal length v_F/T , which is guaranteed for weak interaction [32]. We will come back to the issue of applicability later in this chapter.

1.3.1 Resistance at reflectionless leads

The electrons in the reservoirs are considered free, whereas in the conductor, the spacial confinements restrict the wave functions to quantum mechanical levels. We construct the tube narrow enough so that only M transverse states in the wire are below the Fermi level, thereby constraining the electrons to these transverse modes. For the contacts, we choose a geometry to reduce backscattering of

the single mode into the wire. In the picture, this requirement is reflected by adiabatic contacts.¹³

The electrons originate from reservoirs where they can occupy infinitely many transverse modes. Following the potential difference, the electrons move into the wire where they are only allowed to exist in M transverse modes. Since the Pauli-principle restricts the occupation number, a finite conductance (at zero temperature) of [19]

$$G_c = \frac{Ie}{\mu_1 - \mu_2} = \frac{Me^2}{\pi}$$

is found. It can be seen from this equation that the conductance is proportional to the number of modes in the wire. If we further introduce a “black box” inside the conductor with a transmission probability of \mathcal{T} we arrive at the Landauer conductance formula for zero temperature and bias,

$$G = \frac{Me^2}{\pi} \mathcal{T}.$$

1.3.2 Energy dissipation at the scatterer

Following Landauer’s argumentation, the observed resistance is a result of *elastic* scattering at the “black box” [45]. However, this statement was revised by a result which identified inelastic processes as sources for a finite resistance at an impurity [28]. A phenomenological view is presented by Datta [19]: Clearly there is a potential drop at a scatterer in a conductor of the order I/G_s where G_s^{-1} is the scatterer’s resistance. If we construct a simple scatterer with no internal degrees of freedom the energy has to be dissipated somewhere in the wire. This can be achieved via inelastic electron-phonon scattering for example, and we can associate a energy relaxation range D_{ER} over which we expect this to happen.

The possible sources of the dissipation are still subject to discussion. Later in this thesis, we will test the conservation of probability at a finite wire with a resonant scatterer by perturbation theory for weak interaction. We will examine if higher(second) order processes can lead to a violation of unitarity and thus to possible energy dissipation.

Inelastic processes *inside* a scatterer with finite size can enhance transmission significantly. An electron, incident from the left, that looses its phase memory inside a symmetric resonant structure escapes with a total probability $\mathcal{T}/2$ to the right instead of \mathcal{T}^2 [45].

1.3.3 Non-zero temperature

At zero temperature the sharp energy distributions in contacts on both sides of the scatterer effectively restricts transport to one direction (from the contact with higher chemical potential to the lower one) and only along the channels below the Fermi level. With increasing temperature, however, the distributions flatten and transport takes place through multiple channels in the energy range

$$\mu_1 + a > E > \mu_2 - b,$$

¹³Acoustic horns serve as non-reflecting contacts over a wide range of wave-lengths.

where a and b are of the order of a few $k_B T$ and each channel can have a different transmission probability \mathcal{T} . The influx of electrons per unit energy from the left contact into the left lead (assuming reflection-less contacts) is given by

$$j_l^+(E) = \frac{2e}{h} M f_l(E),$$

and a similar expression for the right contact. The outflux from the left lead into the contact consists of transmitted electrons from the right contact and reflected ones from the left,

$$j_l^-(E) = \frac{2e}{h} (\mathcal{T} f_r(E) + (1 - \mathcal{T}) f_l(E)),$$

assuming that the transmission probabilities on both sides are equal. This is the case when the scatterer is symmetric and no inelastic processes occur. The total flux reads

$$I = \int dE j(E) \text{ where } j(E) = j_l^+ + j_l^- = \frac{2e}{h} \mathcal{T}(E)(f_l(E) - f_r(E)).$$

If the reaction of the system to the perturbation is linear, the current is proportional to the difference of the chemical potentials in the contacts, namely

$$\delta I = \frac{2e}{h} \int dE \mathcal{T}(E)[\mu_l - \mu_r] \left(-\frac{\partial f_0(E)}{\partial E} \right).$$

The assumption of linearity is discussed in the next section in more detail. From this the linear response coefficient, the conductance,

$$G = e \frac{\delta I}{\mu_l - \mu_r} = \frac{2e^2}{h} \int dE \mathcal{T}(E) \left(-\frac{\partial f_0(E)}{\partial E} \right), \quad (1.3.1)$$

can be derived.

We see that the applicability of the Landauer-Büttiker formula relies on the knowledge of the energy distribution of the incoming particles [45]. At low temperatures, the requirement is met: Electrons are bound to the vicinity of the Fermi surface (points, in one dimension). We formulated *basic* assumptions that have to be made to relate transmission and conductance. It remains to be shown that we can connect them linearly as in equation (1.3.1).

1.3.4 Criterions for linear response

From the formulas above one criterion can immediately be deduced: If the applied bias is much smaller than $k_B T$ the Taylor expansion in equation (1.3.1) is a valid approximation. The transmission probability in the coherent regime may vary rapidly due to interference effects at low temperatures, but if we increase temperature, the thermal broadening of the transmission peaks leads to a smooth conductance as a function of the bias in the region of interest $\mu_l < E < \mu_r \ll k_B T$.

On the other hand, if the transmission probability itself varies smoothly over the conducting energy range, thermal broadening is not needed to justify a linear approximation. This is the case for the single structureless impurity in the clean

one-dimensional wire. Indeed, the Landauer conductance formula is applied frequently in this regime to connect theoretical results to experiments [43, 57, 62].

The applicability of the Landauer-Büttiker formalism is limited by the breakdown of phase coherence in the wires. Collisions with phonons and with electrons with enough energy to reach a free state destroy the phase relations between electrons in solids. The scattering with phonons is governed by a scattering length L_{ph} . Therefore, we assume $L_{\text{ph}} \gg v_F/T$. In this regime, phase coherence allows the use of scattering states, wave functions which extend over the system into the strongly coupled contacts.

1.3.5 Resonant tunneling of non-interacting electrons

The most prominent example of resonant tunneling is a single-particle transition through a double barrier. Given that the two barriers separated by a distance L have transparencies $D_i \ll 1$, the electron states in the quantum form a discrete set of broadened levels $E_n = \epsilon_n - i\bar{\Gamma}$. The width of the levels for rectangular barriers reads

$$\bar{\Gamma} = \Gamma_L + \Gamma_R = 2\hbar \frac{L}{v(\epsilon_R)} (D_L + D_R),$$

where $v(\epsilon_R)$ is the electron velocity at the resonant level [42]. The transmission probability can then be approximated by a Breit-Wigner formula,

$$\mathcal{T} = \frac{\Gamma_L \Gamma_R}{(\epsilon - \epsilon_R)^2 + (\bar{\Gamma}/2)^2}.$$

If the level width is energy-independent, equation (1.3.1) can be evaluated exactly. However, we are only interested in the asymptotics of the peak conductance: In experimental setups, the gate voltage is used to tune the energy of the resonance $\epsilon_R(V_g)$ to the energy of the incoming particles.

From equation (1.3.1) we find [42]

$$G_p(T) = \begin{cases} 4G_0 \frac{\Gamma}{\bar{\Gamma}}, & T \ll \bar{\Gamma}, \\ \frac{\pi}{2} G_0 \frac{\Gamma}{T}, & T > \bar{\Gamma} \end{cases},$$

where $\Gamma = \frac{\Gamma_L \Gamma_R}{\bar{\Gamma}}$. We can see from these expressions that the resonance is either of Lorentzian shape with a T -independent height at low temperatures or the peak conductance varies linearly with T^{-1} in the high-temperature regime.

1.3.6 Conductance of strongly interacting electrons in one dimension

The problem in the presence of interaction is much more complicated. We recall the results from section 1.1.4: The conductance in the limiting case of a clean wire is found to depend on the strength of interaction [5, 37],

$$G_0 = K \frac{e^2}{h},$$

where the dimensionless parameter K describes interactions. However, this assumption contradicted with early experiments by Tarucha et al. [68], where

the authors found a non-renormalized conduction of e^2/h in the presence of interaction.

Following the experimental results, a prediction for the non-renormalized version was made by Maslov and Stone [50] using the Kubo formula. Irrespectively, further experiments reported a great variety of results: In Ref. [71], significant deviations from the quantized value were measured in GaAs-AlGaAs quantum wires, more recent experiments on nanotubes by Kong et al. [39] observed the quantized value in the low-T regime and Kasumov et al. [38] reported saturation at 1/4 of the non-interacting conductance.

The variety of results presented a puzzle to the community. Pham et al. [61], e.g., question the validity of the Landauer-Büttiker formalism in the presence of strong interactions. It is argued that a single electron is no longer a valid excitation and a new framework to determine the transport of the system is outlined. We will present another attempt to explain the different results: We relate them to variable boundary conditions constituted by the experimental setup following Ref. [49]. This view was also adopted more recently by Imura et al. [35].

First of all, we note that in a ballistic wire *without* leads, the motion of charges in an electric field can not depend on the interaction between the charges as required by Galilean invariance. This can be confirmed by applying the continuity equation to the density in terms of the boson fields (equation (1.1.7)). We add reflectionless leads and recall that a finite quantized resistance originates from the contacts. The scattering processes at the contacts (back into the reservoirs) are independent of interactions in the wire, even if they are strongly inhomogeneous [49]. However, in experiments at low temperatures, the effect of impurities is pronounced and dominates over the resistance at the leads. Since the source of the scattering is now situated in the wire, the strength of interaction will affect the conductance.

The one-dimensional wire with a small but finite barrier is correctly described by Kane and Fisher and related approaches [25, 37], while the limiting case of a *clean* wire is not. The problem inherent in the description via bosons is the connection to asymptotically free states, as required by the Landauer-Büttiker formalism.

Alternatively, Maslov [49] suggests to measure the heat dissipation at an external resistor connected to a one dimensional (contactless) wire of length L . An AC field over a range L_E is applied parallel to the wire, driven at a frequency $u/L \ll \omega \ll u/L_E$. Under these condition, the author expects a renormalized conductance, omitting the subtle question of connecting Fermi-liquid reservoirs to Luttinger-liquid wires.

To our knowledge, this question is not solved yet. For weak interactions in a wire of finite length L , however, the notion of asymptotically free states is *a priori* well-defined. Therefore, at least on a perturbative level¹⁴, we can safely assume that the language of the S-matrix, i.e., the Landauer-Büttiker formalism, remains valid [18, 32, 74].

¹⁴The validity of the RG approach for finite interacting regions is subject to calculations later in the thesis.

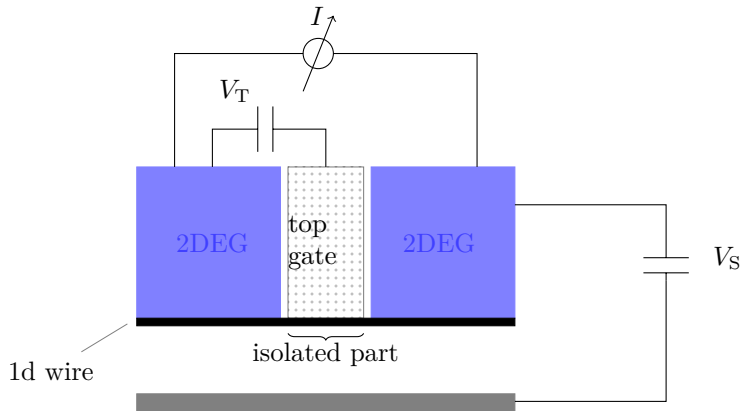


Figure 1.4.1: Top view layout of a cleaved-edge quantum wire. The 2DEG is confined to the surface states at the edge by the bias V_S . By tuning the top gate voltage V_T the part below the gate can be depleted.

1.4 Applications and recent research

1.4.1 Energy dependent S-matrix

A structureless impurity of arbitrary strength is the simplest case of a scatterer in the one-dimensional wire. The energy dependence of the scattering matrix in this case is supposed to be analytic and slowly varying on the scale of the Fermi energy. This allows us to neglect the energy dependence in perturbative calculations.

As soon as we consider a second impurity, quantum levels form between them and allow for resonant transmission or reflection (if all reachable levels are occupied). This case is rather generic. The ends of single-wall carbon nanotubes, e.g., can also serve as barriers. Therefore, the analysis of such scatterers is a nearby generalization of the structureless impurity.

Experimental results were obtained for instance from measurements on single-wall carbon nanotubes (SWNT) with kinks [63] or in GaAs quantum wires with gating [7] to model the resonance. Each of the experimental realizations has its share of complications: Carbon nanotubes have a high contact resistance which renders measurements insensitive to small obstacles in the wire. Measurements on quantum wires on the other hand are always influenced by the adjacent 2DEG and the other close-by 1d energy sub-bands [42].

The resonant level in the GaAs wire is realized by a high negative voltage at a gate which pinches-off the wire. A simplified layout of such a setup is drawn in figure 1.4.1. Nevertheless, one can observe conductance peaks attributed to the formation of small 1d islands under the gate where electrons can tunnel to and from [42] if they can overcome the Coulomb blockade due to charges on the island. Furthermore, Carbon nanotubes can be deformed with the aid of an electronic force microscope. A double-kink structure is used to define pairs of quantum wells in the wire [14].

On theoretical grounds, resonant structures can be analyzed qualitatively in the bosonized language. One can obtain the RG flow for different barrier strength

and interaction [37]. Pushing forward to quantitative agreement was one of the goals of recent theoretical work. Namely, researchers wanted to account for the exponent found in the experiments for the power law governing the temperature dependence of the height $G_p \sim \Gamma/T$ and the width $\Gamma \propto T^{\alpha_e}$ of the conductance peak in different regimes.

Using a four channel Luttinger liquid model for the Carbon nanotube(CNT), the exponent can be related to the interaction strength via [36]

$$\alpha_{\text{bulk}} = (g^{-1} + g - 2)/8 \quad \text{and} \quad \alpha_{\text{edge}} = (g^{-1} - 1)/4$$

for tunneling into the bulk and the edge of a long tube respectively. These exponents are found to be in good qualitative agreement with the experiment [73]. Measurements on carbon nanotube junctions showed Luttinger liquid behavior e.g., by Yao et al., who observed an exponent for the temperature dependence of $\alpha_{\text{end-to-end}} = 2\alpha_{\text{end}} = 2.2$ at junctions of CNTs, slightly above the predicted value of 1.8 for strong interaction in CNTs ($g \sim 0.2$). In quantum wires, LL behavior with a power-law scaling of the resonance width ($g = 0.6 - 0.8$) [7] completed the picture.

Notwithstanding, very recent measurements reported a non-monotonic dependence of the conductance in the low-temperature regime [13]. The unexpected experimental results may reflect the fact that even the “clean” ballistic case is not fully understood in the presence of strong interaction (in Carbon nanotubes $g \sim 0.2 - 0.3$) as discussed in section 1.3.6. A recent attempt to account for the strong temperature dependence includes the concept of correlated sequential tunneling [20].

Other attempts to theoretically examine the features of resonant tunneling and side attached impurities in fermionic one dimensional transport were made for example in the works by Nazarov and Glazman (NG) [57] and Polyakov and Gornyi (PG) [62] on resonant scattering, by Lerner, Yudson and Yurkevich [47] on anti-resonant levels attached to a 1d wire, and, very recently by Altland et al. [3] on incoherent scattering. In the following sections we want to give a short review about this contributions to the research in this field.¹⁵

Electron transport through a double barrier

The formation of a resonant scatterer formed by two barriers of arbitrary strength inside a one-dimensional wire is subject to a study conducted by Polyakov/Gornyi (PG) and Nazarov/Glazman (NG) in parallel. The issue was discussed earlier in a bosonized language by Furusaki [25] and we will compare the results whenever it seems plausible.

We study a system with a one-dimensional wire and two impurities at separated by distance x_0 . The barriers are strong enough to form a system of well defined resonant quantum-levels separated by an energy $\Delta = \pi v_F/x_0$. The basic ideas are taken from the work by MGY: A free electron gas is perturbed by weak interaction and the result is extended to the low temperature regime by means of a renormalization group procedure. The amplitudes of the waves inside the resonant structure are renormalized together with the S-matrix elements.

¹⁵Of course, this choice is by no means complete but one to prepare the grounds for the motivation of the thesis.

Scale	Description
ϵ	Particle energy, of the order of $\max(T, V)$, where V is the bias.
Δ	Level spacing of the scatterer.
D, D_0	The running/initial energy scale of the RG. The bandwidth D_0 is of the order of $\min(\epsilon_F, v_F/d)$.
D_p	For energies above this scale, first order corrections in interaction are supposed to be leading: $\log(D_p/D_0) = -1/\alpha$
D_r	Above this scale, an initially weak barrier remains weak.
$D_{r_{\min}}$	The minimal D_r scale of the two barriers. If they are different, there is an intermediate regime with one weak and one strong barrier.
D_S	The width of the resonant level when the running cutoff is of the same order as the width, $D_S = \Gamma(D_S)$
D_-	A measure for the symmetry of the double barrier. $D_- \sim \frac{\Gamma_1 - \Gamma_2}{\Gamma_1 + \Gamma_2}$.

Table 1.1: Important energy scales in the discussion of 1d transport through a resonant structure as introduced by PG.

The boundary conditions for the energy space RG used by PG are given by the bare amplitudes

$$t_0 = \frac{t_1 t_2}{S(\epsilon)} \quad \text{and} \quad r_{L0}(\epsilon) = r_1 + \frac{r_1 t_1^2}{S(\epsilon)} e^{2\pi i \epsilon / \Delta},$$

where $S(\epsilon) = 1 - r_2 r'_1 e^{2\pi i \epsilon / \Delta}$, and $r_i(r'_i)$ are the reflection amplitudes for barrier i from the left (right). These amplitudes allow multiple resonant levels. Close to a resonance with large level spacing Δ , the amplitudes stated above reduce to a Breit-Wigner type resonance for a single level (as the one used by NG),

$$t(\epsilon) = \frac{i\sqrt{\Gamma_L \Gamma_R}}{(\Gamma_L + \Gamma_R)/2 - i(\epsilon - \Delta)}, \quad r_L(\epsilon) = \frac{(\Gamma_R - \Gamma_L)/2 - (\epsilon - \Delta)}{(\Gamma_L + \Gamma_R)/2 - i(\epsilon - \Delta)}.$$

The analysis of the corrections is based on different relations of the energy scales of the system. To this end, additional scales are defined to mark the breakdown of perturbative corrections. To provide a clearer view, we present all important energy scales introduced by PG in table 1.1, together with a short summary of the PG analysis below.

Separate renormalization of two impurities: $D \gg \Delta$. In this limit, the fine structure of the resonances is not resolved by the renormalization. In the language of the real-space RG, we only account for interacting regions around the scatterer which do not overlap. The complexity of the PG calculation is enhanced by a renormalization of the amplitudes between the two barriers.

In the most trivial case, $D \gg D_{r_{\min}}$, the scatterer consists of one strong and one weak or two weak barriers and the flow equations for each barrier coincide with the single-impurity situation with separately renormalized resonance widths,

$$\Gamma_{R,L}(\epsilon) = \Gamma_{R,L}(\epsilon/D_0)^\alpha.$$

This result is confirmed by both PG and NG. If $\Delta \ll D \ll D_{r_{\min}}$, both barriers are strongly reflecting and the integration turns into a sum over resonance poles.

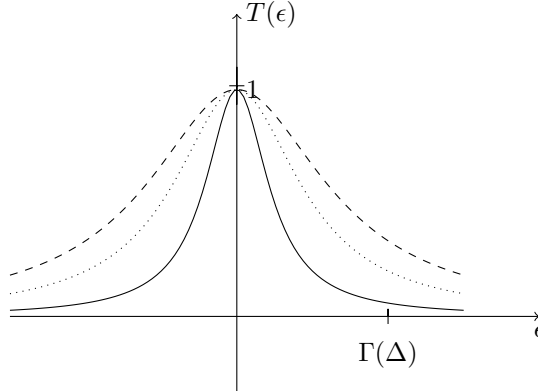


Figure 1.4.2: Transmission for different temperatures in the regime $D_S \ll T \ll \Delta$ (a single symmetric resonance) [62]. Lower temperature (solid line) leads to a reduction of the peak width. The height remains unchanged.

PG find a different scaling exponent, $\alpha/2$, in this case. Since NG only consider one resonant level, this result can not be found in their analysis.

A single resonance: $D \ll \Delta$. In the opposite case, the amplitudes inside the wells are not renormalized. The double-barrier structure is replaced by a single scatterer with an energy dependent S-matrix. The boundary conditions are chosen $D = \Delta$ instead of $D = D_0$ and the position of the resonance level is $\epsilon_R = 0$. If both amplitudes are strong initially or get strong in course of the renormalization and the initial resonance width is small, $D \gg \Gamma(\Delta)$, both PG and NG find an energy dependent resonance width,

$$\Gamma(T) = (\Gamma_1(\Delta) + \Gamma_2(\Delta))(T/\Delta)^\alpha,$$

while the peak transmission does not renormalize (see figure 1.4.2). These findings are in agreement with earlier results [37]. In this limit, the approximation of a single resonant level is valid, additional resonances just give a irrelevant perturbative correction.

Furthermore, inside a resonant energy level, $D \ll D_S$, the result are equal to those obtained for a structure-less single scatterer, with the replacement of the lower cutoff ϵ by D_S . The lineshape in the symmetric case is then given by a Breit-Wigner formula. In the strongly asymmetric case, $D_- \gg T$, the transmission function adopts a double-peak structure, yielding zero transmission at $\epsilon = 0$. This feature remains if $\epsilon_R \neq 0$, additionally developing an interesting asymmetric double peak structure for $\mathcal{T}(\epsilon)$.

Weak barriers Previously, the barriers were always either initially strong, or they got enhanced by renormalization in the regime $D \sim \Delta$. It is possible though, that one or both barriers remain weak during this procedure. The reflection of two symmetric barriers with this feature is small ($\epsilon_R = 0$),

$$R(\epsilon, \Delta) = 2[1 - \cos(2\pi\epsilon/\Delta)](D_r/D)^{2\alpha},$$

and remains small. The oscillating behavior stems from a renormalization of the amplitudes inside the “dot”. Like in the previous setup, an asymmetric barrier leads to a dip in the transmission at $\epsilon = 0$. As soon as we shift ϵ_R away from zero, the situation is reversed: A symmetric barrier leads to a dip, while in the asymmetric case the transmission is not affected by the renormalization (apart from weak oscillations).

Linear conductance To connect the results for the transmission and reflection probabilities in Ref. [62] to the experiment, the authors relate them to the linear conductance in the Landauer-Büttiker formalism. The issue was discussed earlier in section 1.3. In this section, we confine ourselves to results for the case of symmetric, strong barriers. The transmission amplitudes can be related to the conductance using the formula

$$G(\epsilon_0, \mathcal{T}) = \int d\epsilon \mathcal{T}(\epsilon) (-\partial n_F / \partial \epsilon),$$

if both temperature and bias are small enough to assume a linear response.

In the temperature range $\epsilon_F \gg T \sim \Delta \gg \Gamma$, sequential tunneling dominates the physical picture and the temperature dependence of the peak conductance,

$$G_p \sim \mathcal{T}^{\alpha-1},$$

is smoothly connected to the peak conductance of non-interacting electrons (see section 1.3.5). The peak width, on the other hand, is renormalized due to interactions in contrast to the non-interacting situation, $w(T) \sim T$. The scaling of G_p is thereby governed by the single-particle density of states in the contacts at the edge of the Luttinger liquid. Note that this behavior smoothly connects to the non-interacting picture.

For smaller temperatures the lineshape of the conductance as a function of bias is altered significantly. While the peak height saturates at $G_p = 1$ at an intermediate temperature, the width behaves as

$$w \sim T^\alpha,$$

narrowing the peak to a finite value cut by D_S for zero temperature. The estimated scaling of the conductance peak width and height is seen to agree with Furusaki’s [25] for symmetric barriers. To complete the picture, it should be noted that the asymmetric barriers lead to a reduction of the saturated maximum peak height in both PG’s and NG’s work.

Conclusion The authors thoroughly examined the scattering at a structure with resonant transmission for energies far from and inside the resonance. To this end, they calculated the RG equations from the first order perturbation theory. This is only sufficient if unitarity and thus renormalizability is proven to hold for subsequent orders of perturbation theory. We will discuss this point in more detail in chapter 3.

1.4.2 A side attached impurity

The transmission of a discrete localized level with a small capacitance is dominated by the Coulomb repulsion if all reachable levels are occupied as long as no

bias is applied to lift the energy of the electron in the leads. This effect is called *Coulomb-blockade* and leads to an anti-resonant structure of the transmission coefficient. Lerner, Yudson and Yurkevich [47] examined this situation, assuming one level to be close to the Fermi level and a large level-spacing $\delta \gg \Gamma_0, T$.

Like in the previous section, the authors used functional bosonization and the Keldysh technique to extract the corrections leading in a high-energy limit $\epsilon \sim \Gamma_0$ and extend them to the low-energy regime by means of a RG procedure. The renormalization in this case broadens the Breit-Wigner form of the reflection coefficient,

$$\Gamma(\epsilon) = \Gamma_0 \frac{\sqrt{\Gamma_0^2 + \epsilon_0^2}}{|\epsilon|^\alpha},$$

starting from Γ_0 at $\max(\epsilon_0, \Gamma_0)$. The divergence is cut by temperature.

In a weakly interacting wire, the local density of states follows the resonance width for $|\epsilon - \epsilon_0| \gg \Gamma(\epsilon)$, while in the opposite limit it vanishes. The authors argue that the behavior can be mapped to a potential impurity in this regime, triggering the depletion of the wire at the Fermi level. This stands in contrast to the low-energy behavior in the strongly interacting regime, where the characteristic effective interaction α is of the order one. In this range, the transmission is not affected by the hybridization with the impurity [50].

1.4.3 Junctions of one-dimensional wires

Another interesting problem arising in the context of one-dimensional wires is the physics of more complicated geometrical structures consisting of single junctions or networks of such. The question was addressed in the presence of a spin at the junction in a Kondo-model related setup [55] and later by Lal et al. [18, 43] in the framework developed by MGY and presented earlier in section 1.2.1.

The authors of Ref. [43] assume that the electrons in the wire interact weakly by a short-range density-density interaction and scatter at the junction in one of the three available wires. Instead of right- and left-moving electrons, they discern in- and outgoing single particle wave functions with a label for the wire $\psi_{I/O,i}$. Then a three-by-three matrix S can be defined by

$$\psi_O(0) = S\psi_I(0).$$

This matrix is unitary if no inelastic scattering is present. The wires are constructed on a lattice with position indices ranging from 1 to ∞ .¹⁶ The hopping constants at the junction are real numbers $-u_i$ which are related to the S-matrix elements

$$r_{ii} = \frac{2u_i^2}{P} - 1 \quad (\text{on the diagonal}), \quad t_{ij} = \frac{2u_i u_j}{P} \quad (\text{off diagonal}),$$

where

$$P = \sum_{k=1}^3 u_k^2 + i\lambda,$$

and λ denotes the potential at the junction. The details of the perturbative calculation are given in section 1.2.2. The amplitude to first order perturbation

¹⁶The lattice is used in Ref. [43] to simulate the junction.

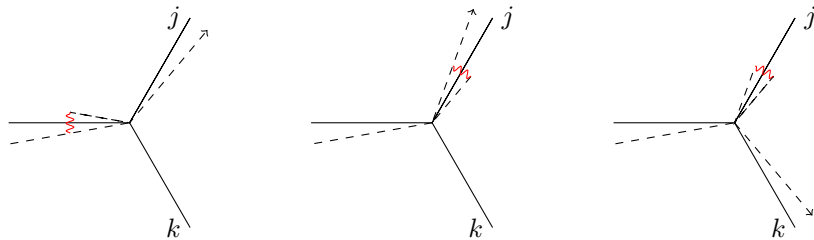


Figure 1.4.3: Possible scattering processes at a junction of three wires to first order in interaction. Additional diagrams can be constructed by permuting the wires.

theory in interaction for the scattering from an incoming to an outgoing wave and vice versa is given by

$$-\frac{\alpha r}{2} \log(kd), \quad \text{and} \quad \frac{\alpha r^*}{2} \log(kd).$$

With these building blocks we can construct all possible first-order scattering events. A transmitted wave (from wire i to j) has one of the following histories (see figure 1.4.3):

- It was reflected from the barrier into the same wire, reflected back by Friedel oscillations and transmitted into wire j ,
- transmitted into wire j , reflected back by a Friedel oscillation and eventually reflected back or
- transmitted into wire j where it was reflected by a Friedel oscillation and transmitted into wire k .

The authors then collect these contributions into a matrix A ,

$$\delta t_{ji} = -A_{ji} \log(kd),$$

whose off-diagonal elements are defined as

$$A_{ji} = -\frac{1}{2} \left[-\alpha_i |r_{ii}|^2 t_{ji} + \alpha_j |r_{jj}|^2 t_{ji} + \sum_{k \neq i,j} \alpha_k t_{jk} r_{kk}^* t_{ki} \right] \log(kd).$$

Analogously, the correction to the reflection in first order in interaction is derived:

$$\delta r_{ii} = -A_{ii} \log(kd), \tag{1.4.1}$$

where

$$A_{ii} = -\frac{1}{2} \left[-\alpha_i r_{ii} + \alpha_i |r_{ii}|^2 r_i + \sum_{j \neq i} \alpha_j t_{ij} r_{jj}^* t_{ji} \right] \log(kd).$$

This form is convenient to write down the real-space flow equations for an interacting region of width L centered around the junction,

$$\frac{dr_{ii}}{d \log(L/d)} = A_{ii} \quad \text{and} \quad \frac{dt_{ij}}{d \log(L/d)} = A_{ij}.$$

Label	Fixed point description	stable with respect to	unstable with respect to
I	The junction is fully reflecting	all	none
II-IV	One wire is cut off the others	V-VII	I
V-VI	The junction is transparent	none	all
VII	The junction has equal reflection at each wire	V-VI	I-IV

Table 1.2: Fixed points and stabilities for the RG flow of a three-wire junction

Lal et al. have rewritten the RG equations using

$$F_{ii} = -\frac{1}{2}\alpha_i r_{ii}$$

as follows:

$$\frac{dS}{d \log(L/d)} = SF^\dagger S - F. \quad (1.4.2)$$

This general result (the choice of dimensionality of the matrix is arbitrary) is used to analyze the fixed points of the RG flow.

Results The fixed points and their stability can be derived in a rigorous fashion by analyzing the flow of a matrix in the close vicinity of a fixed point. This analysis is done in detail in [43]. It turns out, however, that the phase diagram can be drawn from the knowledge of the trivial case of a two-wire junction. In table 1.4.3 we present the fixed points and their flow as well as the label used in the paper.

We know from our previous considerations in section 1.2.2 that for repulsive interaction the renormalization tends to enhance the obstacle in a wire. Therefore, if we modify the reflection of one wire at an otherwise fully transparent junction, the renormalization will drive the barrier towards complete reflection. It follows immediately that case I with a fully reflecting junction is the most stable fixed point while case V-VI is unstable towards all deviations. All other fixed points can be treated in the same manner.

Conductance From the S-matrix, the conductance in the linear response regime can be obtained by the Landauer-Büttiker formalism described in section 1.3. Scattering at the contacts between wires and leads are neglected (“reflection-less contacts”) and the resistance at the interface is taken to be e^2/h . The discussion is restricted to one transverse channel in the wire, the net current in the absence of applied voltage is zero. With these assumptions, we obtain the net current out of wire i via the linear relationship [15]

$$I_i = \frac{e^2}{h} \sum_{j=1}^3 T_{ij} V_j.$$

To derive the conductance, the authors single out a potential probe, e.g., $I_3 = 0$, and compute the three-terminal conductance,

$$G_{12,13} = \frac{I_1}{V_1 - V_3} = \frac{e^2}{h} \left[\mathcal{T}_{12} + \mathcal{T}_{13} + \frac{\mathcal{T}_{12}\mathcal{T}_{13}}{\mathcal{T}_{32}} \right],$$

where the first pair of indices denotes the direction of the current flow, between wire label three and four we apply the voltage. $G_{12,23}$ is derived in the same way.

With these results, temperature and conductance can be related. We stop the RG flow of, say VII to I, at the scale of the temperature $L_T = v_F/T$. If the deviation from the fixed point is not too large, the correction with respect to the fixed point can be written as an Taylor expansion. We end up with an approximation for the exponent of the power-law dependence of the conductance on temperature,

$$G_{12,13}^{\text{VII}} = \frac{e^2}{h} \left[\frac{4}{3} - 27c_1 T^{-2\alpha} \right],$$

where c_1 is a constant. We will stop the discussion here. Additional results and more details are provided in [43]. The generalization to the case of four wires meeting at a junction is straightforward.

1.4.4 Incoherent scattering

In a recent work, Altland et al. [3] examine the transport through a scattering “black box” connected to two incoming and two outgoing leads. Both coherent and incoherent transport is allowed through the structure. The authors argue that “low-dimensional electronic systems containing spatially extended scattering regions rather generically support both coherent and incoherent transport channels.” [3] The statement is supported by experimental measurements on quantum dots [64] and along graphene pn-junctions [54], where the interplay between mode interaction and single-particle scattering can lead to incoherence.

The “black box” can be understood in terms of a quantum dot with general features, namely a finite electrostatic capacitance, coherent scattering at the dot and a non-vanishing incoherent transmission probability. In such a setup (shown in figure 1.4.4), the authors find low energy properties significantly different from those obtained by Kane and Fisher [37]. While the temperature scaling of the conductance,

$$G \propto T^{2/g-2},$$

coincides with the KF approach, the incoherent feature supports a gapless excitation at zero temperature leading to an even split of the current at the scatterer. The result is obtained using Keldysh technique on the bosonized action of the system. It is shown that the gapless mode is not affected by non-thermal noise in the system. The low-energy mode is seen to be a result of symmetries present in the system.

From the asymptotic behavior of the system at low temperatures, a new paradigmatic picture of the Luttinger liquid with impurity is derived, alternative to the Kane-Fisher picture.

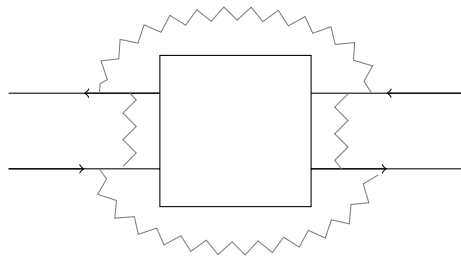


Figure 1.4.4: Two incoming and two outgoing half-infinite chiral leads connected to each side of a scattering “black box”. Both coherent (rectangle) and incoherent (“zigzag”-lines) scattering is allowed between the channels.

Chapter 2

Statement of the problem

In the thesis we study transport in interacting one-dimensional systems with a single scatterer. We consider a setup which is similar to a source-drain setup at equilibrium. A single (spinless) electron with an energy ϵ above the Fermi level is injected into the equilibrium wire.

We are interested in *inelastic processes* in the system, i.e., in processes where the electron leaves the system at another energy or with a modified phase. The problem attracted our attention due to various reasons. The transport through extended structures at low temperatures has been shown to be dominated by incoherent scattering in very recent works by Altland et al. [3](see section 1.4.4).¹ On the experimental side, incoherent scattering in one-dimensional transport was reported very recently in a Graphene quantum point-contact in a quantum Hall regime [54].

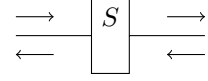
Previous results suggest that there is neither inelastic channel nor dephasing in the leading contribution to the RG in the case of a pointlike scatterer [6]. However, these effects can appear in the case of a compound scatterer. This prediction can be obtained based on an analogy with dephasing in disordered Luttinger liquids: A Cooperon is not effected by dephasing if clean plasmon propagators are used. Nevertheless, accounting for disorder in the plasmon propagator,i.e., taking into account “additional” impurities beyond the ladder diagrams, one arrives at a finite dephasing time [31, 32]. Therefore an interesting problem is to investigate the effect of an “additional impurity” on the dephasing or the inelastic channel in the low-temperature regime. We consider strong impurities and model the resulting resonant structure by a Breit-Wigner scatterer.

The renormalization group approach is only valid in the absence of inelastic processes. This approach has been applied frequently in the last two decades to examine systems with a great variety of degrees of freedom, e.g., junctions of wires [43] and more complex geometries [18], anti-resonant [47] and resonant [57, 62] scattering. It is common believe that the procedure is valid for a single pointlike impurity but its validity was never checked carefully in more complex cases. Ab initio, inelastic processes can not be recognized by this approach since it is based on first order perturbative expansion in interaction.

¹They consider a scattering black box with very general features.

Setup

The electrons are non-interacting in the far distance from the scatterer. Since the system size is extending infinitely this statement needs further examination. We shall explain this point below. Inside the wire, we introduce right- and left-moving particles and describe reflection and transmission in the two channels in terms of a two-by-two scattering matrix S .



The S-matrix is a unitary matrix that relates in- and outgoing states. More specifically, in our case it relates the asymptotically free propagators of different chirality:

$$\begin{pmatrix} G_0^+(x, x_f \rightarrow +\infty, \epsilon) \\ G_0^-(x, x_f \rightarrow -\infty, \epsilon) \end{pmatrix} = \begin{pmatrix} t_{lr}(\epsilon) & r_{ll}(\epsilon) \\ r_{rr}(\epsilon) & t_{rl}(\epsilon) \end{pmatrix} \begin{pmatrix} G_0^+(x_i \rightarrow -\infty, x, \epsilon) \\ G_0^-(x_i \rightarrow +\infty, x, \epsilon) \end{pmatrix}, \quad S^\dagger S = 1$$

where x_i and x_f are the initial and final scattering states. The unitarity requirement can be rewritten as two equations, namely

$$|t_{lr}|^2 + |r_{ll}|^2 = |t_{rl}|^2 + |r_{rr}|^2 = 1 \quad \text{and} \quad t_{lr}r_{rr}^* + r_{ll}t_{rl}^* = r_{rr}t_{lr}^* + t_{rl}r_{ll}^* = 0. \quad (2.0.1)$$

The first expression is related to the conservation of the particle number at energy ϵ , the second equation is sensitive to coherence.

The interaction in the system is considered repulsive and short-ranged with respect to the system size but sufficiently long-ranged so that forward scattering dominates over backscattering. We consider spin-less fermions, only g_2 and g_4 interactions are present in the system. We will neglect g_4 processes, because the phase space for this type of interaction is small and we can expect only sub-leading corrections.

Ansatz

The problem can be treated by bosonization for arbitrary interactions. A weak barrier or a weak link between two half-wires can be treated perturbatively in this language and the two limiting cases can be connected with an renormalization-group approach [37]. Alternatively, one can treat the interaction as a perturbative parameter and include barriers of arbitrary size in the system [74]. We will apply the second ansatz. The first-order correction in interaction to the scattering amplitudes diverges as

$$\delta t/r \sim \alpha \log\left(\frac{\Delta}{\epsilon}\right),$$

for a point-like scatterer, where $\Delta = \min(\epsilon_F, v_F/d)$, $\epsilon \gtrsim T$ and α measures the weak repulsive interaction. For very high energies, $\epsilon \sim \epsilon_F$, the transport through the system will be almost ballistic and the energy dependence of the scattering amplitudes is logarithmic in leading order.

When the temperature is lowered, higher order corrections, of the order $\alpha^n \log^n(\Delta/\epsilon)$, will dominate the perturbative expansion. It is thus necessary to sum up such contributions of *all* orders.

The renormalization group procedure is the most common way to accomplish this task.² We pick an energy Λ , so that $\alpha \log(\Delta/\Lambda) \ll 1$ and calculate the corrected reflection and transmission amplitudes. In the next step, we replace the cutoff Δ by Λ and the original S-matrix elements by the corrected versions. This procedure is repeated until the desired energy scale, e.g., the temperature in an experiment, is reached. It is clear from this summary that the first order correction has to reproduce in higher orders. If it does, the theory is renormalizable.

For our analysis, we calculate the second order in interaction using a real-space diagrammatic technique suggested by Polyakov and Gornyi.

We chose this approach because, in principle, there is no possibility for inelastic or incoherent processes to arise in the first order (which the RG approach is based on) since there is only one intermediate energy state. On the contrary, starting from the second order we have to account for complex diagrams containing electron hole pairs. The interplay of the different energy scales of the system in these diagrams can not be determined a priori and can cause problems for the RG scheme.

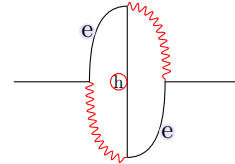
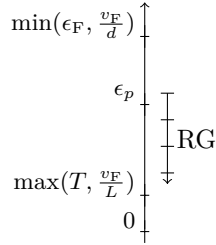
Besides, we can identify these deviations from unitarity with specific scattering processes with the help of the diagrammatic technique.

With the results of this approach we are able to distinguish two possible unitarity-violating processes using equation (2.0.1), namely

- the conservation of a particle at a given energy may be violated. In that case we need to account for additional physical processes to restore the energy conservation in the system.
- A deviation from the second requirement in equation (2.0.1) is a sign for dephasing in the system.

Steps of calculations

We will first calculate the second order correction for the simple system with an infinitely extended wire and a single structureless impurity as considered by Matveev and Glazman to illustrate our method and to check its usability. With the results for the trivial case at hand, the generalization to more complex cases can be done.



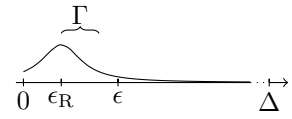
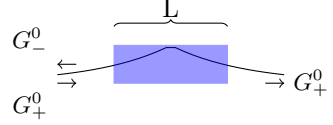
²We omitted the parquet summation technique here. This more careful approach is applied less frequently. See Ref. [59] for details.

The confinement of the interaction to a finite length L is necessary to cleanly define asymptotic scattering states. The constraint is accompanied by a new scale, the Thouless energy of the system, $E_{\text{th}} = v_F/L$. It is known that in the first order in interaction, the infrared cutoff ϵ is replaced by $\max(\epsilon, E_{\text{th}})$, whereas in the second order, the complexity in the interplay of the energy scales is increased and both scales might appear simultaneously in a diagram. We will prove that E_{th} plays the same role in the second order.

A resonant structure brings two more energy scales, namely the position of the resonant level, ϵ_R , and its width Γ . Therefore, we have to deal with too many scales to determine the energy cutoffs a priori. As already mentioned in the beginning of this section, an extended structure can provide dephasing. A resonant structure formed by two barriers is the simplest case of such a structure. In the weak localization regime, the addition of an impurity to the wire triggers dephasing [32]. Furthermore, there is considerable interest in system with resonant scattering [24, 26, 37, 47, 57, 62], and the RG approach outlined above has been applied frequently without verification [47, 57, 62]. We are going to analyze both the limiting on- and off-resonant cases as well as the intermediate regime.

Outline

In the next section, we will introduce chiral scattering Green's functions, present the pictorial representation of the leading logarithmic diagrams in real-space and give some example calculations. The results for the first and second order for a setup with a featureless impurity are presented briefly. To complete the results for the simple case, we prove the unitarity of the S-matrix. In the remaining two sections, we will apply the obtained framework to the non-trivial cases of a finite region of interaction and a resonant scatter of the Breit-Wigner type.



Chapter 3

Perturbative calculations for the S-matrix

3.1 Chiral Green's function of particles

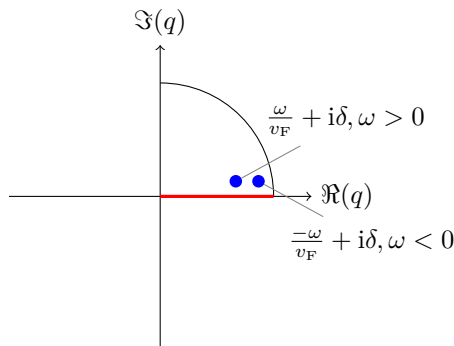
We separate the right- and left moving fields and extend the phase space below the Fermi level to infinity. The free chiral propagators can then be written as

$$G_\alpha(q, \omega) = \frac{1}{\omega - \alpha v_F q + \alpha i \delta \operatorname{sgn}(q)}; \quad \alpha = \pm 1, \delta \rightarrow +0,$$

where the chirality index α labels right(left) moving particles. Energy and momentum are measured from the Fermi level. As a first step, we Fourier-transform from momentum to coordinate representation:

$$\begin{aligned} G_+(x, \omega) &= \int_{-\infty}^{\infty} \frac{dq}{2\pi} \frac{e^{iqx}}{\omega - v_F q + i\delta \operatorname{sgn}(q)} \\ &= \int_0^{\infty} \frac{dq}{2\pi} \frac{e^{iqx}}{\omega - v_F q + i\delta} + \int_0^{\infty} \frac{dq}{2\pi} \frac{e^{-iqx}}{\omega + v_F q - i\delta} \end{aligned}$$

We can close the two contours over the upper right half-planes,



and the integration along the contour yields zero. We are left with

$$\begin{aligned}
G_+(x, \omega) &= \Theta(x)\Theta(\omega)i \operatorname{Res}\left(\frac{e^{iqx}}{\omega - v_F q + i\delta}\right) - \int_{i\infty}^0 dq \frac{e^{iqx}}{\omega - v_F q} \\
&\quad + \Theta(-x)\Theta(-\omega)i \operatorname{Res}\left(\frac{e^{-iqx}}{\omega + v_F q - i\delta}\right) - \int_{i\infty}^0 dq \frac{e^{-iqx}}{\omega + v_F q} \\
&= \Theta(x)\Theta(\omega)i \operatorname{Res}\left(\frac{e^{iqx}}{\omega - v_F q + i\delta}\right) - \int_{i\infty}^0 dq \frac{e^{iqx}}{\omega - v_F q} \\
&= \Theta(x)\Theta(\omega) \frac{1}{iv_F} e^{i(\frac{\omega}{v_F} + i\delta)x} + \Theta(-x)\Theta(-\omega) \frac{-1}{iv_F} e^{-i(\frac{-\omega}{v_F} + i\delta)x}.
\end{aligned}$$

The remaining vertical parts cancel out, since the regularizer is much smaller than the involved energy. A similar calculation yields the left-moving Green's function and we can summarize:

$$G_\alpha(x, \omega) = \Theta(\alpha x \omega) \frac{\operatorname{sgn}(\omega)}{iv_F} e^{i(|\omega| + i\eta)|x|/v_F}. \quad (3.1.1)$$

3.1.1 Dyson Equations

We write down the Dyson Equations for scattering at an impurity of size $d \ll L$ (L is the system size) located at the origin. For such a case, the impurity can be modelled in terms of a external perturbation of the form $V(x) = \gamma_i \delta(x)$. The index i distinguishes the different sides of the impurity. Later we will assume a symmetric barrier and let $\gamma_1 = \gamma_2$. We denote electrons moving to the right ($\omega > 0, x > 0$) and left ($\omega > 0, x < 0$) by indices + and -, respectively. For example, ++ can stand either for free propagation ($xx' > 0$) or for transmission ($xx' < 0$), -+ labels a reflection. The Dyson equation for the electrons ($x < 0 < y$) read

$$G_{++}(x, y) = G_+^0(y - x) + G_+^0(-x)\gamma_1(G_{++}(0, y) + G_{-+}(0, y)), \quad (3.1.2)$$

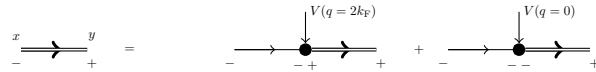
$$G_{++}(0, y) = G_+^0(y) + G_+^0(0)\gamma_1(G_{++}(0, y) + G_{-+}(0, y)), \quad (3.1.3)$$



and

$$G_{-+}(x, y) = G_-^0(-x)\gamma_2 G_{++}(0, y) + G_-^0(-x)\gamma_2 G_{-+}(0, y), \quad (3.1.4)$$

$$G_{-+}(0, y) = G_-^0(0)\gamma_2 G_{++}(0, y) + G_-^0(0)\gamma_2 G_{-+}(0, y). \quad (3.1.5)$$



Solving equation 3.1.3 and 3.1.5, we find

$$G_{-+}(0, y) = \frac{G_+^0(y)\gamma_2 G_-^0(0)}{1 - G_+^0(0)\gamma_1 - G_-^0(0)\gamma_2}, \quad (3.1.6)$$

$$G_{++}(0, y) = \frac{G_+^0(y)(1 - \gamma_2 G_-^0(0))}{1 - G_+^0(0)\gamma_1 - G_-^0(0)\gamma_2}. \quad (3.1.7)$$

Inserting equation (3.1.6) and equation (3.1.7) in equation (3.1.2) and equation (3.1.4) yields the full propagators,

$$G_{++}(x, y) = G_+^0(y - x) + \frac{G_+^0(-x)\gamma_1 G_+^0(y)}{1 - G_+^0(0)\gamma_1 - G_-^0(0)\gamma_2}, \quad (3.1.8)$$

$$G_{-+}(x, y) = \frac{G_-^0(-x)\gamma_2 G_+^0(y)}{1 - G_+^0(0)\gamma_1 - G_-^0(0)\gamma_2}. \quad (3.1.9)$$

These equations can be written in a more compact form for further calculations. To this end we introduce electron reflection and transmission amplitudes:

$$\begin{aligned} r_R^e &= \frac{\gamma_2}{iv_F[1 - G_+^0(0)\gamma_1 - G_-^0(0)\gamma_2]} = \frac{\gamma_2}{iv_F - (\gamma_1 + \gamma_2)/2} \\ t_L^e &= 1 + \frac{\gamma_1}{iv_F - (\gamma_1 + \gamma_2)/2} \end{aligned}$$

The remaining amplitudes for electrons, namely G_{--} and G_{+-} , can be calculated straightforwardly. Also, we don't have to repeat this exercise for holes ($\epsilon < 0$). As can be seen in equation (3.1.1), holes move always in the opposite direction as electrons with the same chiral indices. Thus, instead of G_{++} and G_{-+} for electrons, one writes the same set of equations for holes in terms of operators of the opposite chirality: G_{--} and G_{+-} . Furthermore, we can identify $r_R^h = (r_R^e)^*$. For the remainder this substitution will always be made rendering e and h superfluous.

We end up with a set of Green's functions which include the scattering at a single impurity. Including the Green's functions we did not calculate explicitly, the formulas can be cast in a shorter form. We consider a symmetric barrier, i.e., $r_L = r_R$ and write:

$$G_{\alpha\alpha}^0(x, y, \epsilon) = \begin{cases} \text{sgn}(\epsilon) \frac{t_\epsilon}{iv_F} \exp\{ip_\epsilon|y - x|\} & xy < 0 \wedge \text{sgn}(\epsilon) \text{sgn}(y) = \alpha \\ \text{sgn}(\epsilon) \frac{1}{iv_F} \exp\{ip_\epsilon|y - x|\} & xy > 0 \wedge \text{sgn}(\epsilon) \text{sgn}(y - x) = \alpha \end{cases}, \quad (3.1.10)$$

$$G_{-\alpha\alpha}^0(x, y, \epsilon) = \begin{cases} \text{sgn}(\epsilon) \frac{r_\epsilon}{iv_F} \exp\{ip_\epsilon(x + y)\} & x, y > 0 \wedge \text{sgn}(\epsilon) = \alpha \\ \text{sgn}(\epsilon) \frac{r_\epsilon}{iv_F} \exp\{-ip_\epsilon(x + y)\} & x, y < 0 \wedge \text{sgn}(\epsilon) = -\alpha \end{cases}, \quad (3.1.11)$$

where

$$t_\epsilon = \begin{cases} t & \epsilon > 0 \\ t^* & \epsilon < 0 \end{cases} \quad \text{and} \quad p_\epsilon = \frac{|\epsilon|}{v_F} + i\eta.$$

For a detailed list of all cases, please refer to section A.2. We have thus obtained a set of propagators in energy and real-space representation which include scattering at the impurity.

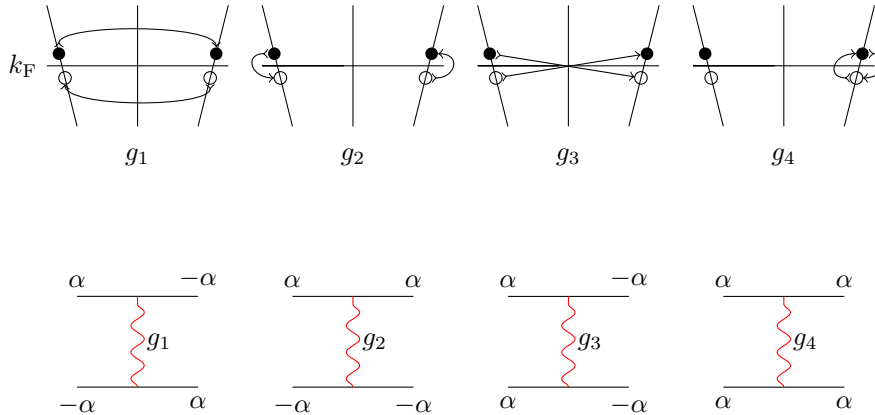


Figure 3.1.1: Different types of interaction in one-dimensional systems. Above, the effect of the interaction is presented with the help of points in the linear dispersion relations, for right-moving particles on the right and left-moving particles on the left, close to the Fermi points. Black dots above the Fermi points represent electrons, white dots stand for holes. The arrow points from the state prior to the interaction to the point after the scattering. The same processes are shown below where α denotes the chirality.

3.1.2 Different types of interaction

In the next section we calculate leading logarithmic corrections due to the first order in interaction in the $T = 0$ Green's function formalism. This is justified provided that $T \ll \epsilon$. This is (to first order) equivalent to the approach by Matveev and Glazman discussed in section 1.2. To list the terms appearing in the perturbation theory we use standard notation and label the processes according to the interactions taking place (see e.g., [67] chapter 2). The different types (see 3.1.1) are:

- forward scattering
 - electrons or holes with the same chirality interact and chirality is conserved: This process is labeled g_4
 - electrons or holes interact with particles of opposite chirality and the chirality is conserved: g_2
- backscattering
 - interaction between particles and holes of same chirality, the interaction inverses the chirality: g_3 . For momentum conservation, a wave vector $4k_F$ is required.
 - particles or holes interact with those of opposite chirality and are backscattered: g_1

In the following we focus on g_2 , arguing that the other types of interactions are either negligible or bound to be of the same magnitude. Namely,

- g_3 processes are Umklapp processes whose contribution is only important in a half filled band, where $4k_F$ is a reciprocal lattice vector [67].



Figure 3.1.2: build-blocks: electron moving to the right, hole moving to the right, electron moving to the left, hole moving to the left

- For short ranged interaction, g_1 and g_2 should be of equal magnitude and opposite sign, since the Pauli principle requires exact cancellation for a point-like interaction [74]. If the interaction is long-ranged, one can argue that $U(2k_F) \ll U(0)$ and neglect backscattering.
- The interaction between particles of same chirality g_4 and g_2 are considered to be of the same magnitude. This is a correct assumption if the original Hamiltonian only contains density-density interaction [49]. In the spin-less (or spin-polarized) case g_2 scattering can not be distinguished from the g_4 -type.¹ However, there are physical situations where $g_2 \neq g_4$.² The phase space for g_4 interaction is small compared to g_2 and we expect only subleading corrections from this type of interaction. It will therefore be neglected in the following.

The formulation of the problem with only interaction of type (g_2) significantly reduces the number of diagrams especially in the second order in interaction.

3.1.3 Feynman and real space diagrammatics

It is convenient to construct a pictorial language representing different terms in perturbation theory. Standard recipes to construct the Feynman-diagrams are found in most text books on quantum field theory, e.g., the classic by Abrikosov, Gorkov and Dzyaloshinski [2].

In the thesis, aside Feynman diagrams, we use a real space representation originally suggested by Polyakov and Gornyi from Karlsruhe. The real space diagrams provide a tool to discern the different possibilities to represent a Feynman diagram as a scattering process in real space. The possible build-blocks that form a typical scattering event are shown in figure 3.1.2. Each line with arrows represents a Green's function in coordinate (right and left arrows to indicate positive or negative direction of motion) and energy representation.³

We present examples of both diagram types (the classical Feynman diagram above, real space representation below) together with the labels in figure 3.1.3. Note that in the Feynman or skeleton diagram, solid and dashed lines connecting the vertices represent right- and left-moving particles respectively. The second picture is a representation in real space. It depicts the path of the electron, the arrow indicating the direction in space: The electron in the picture above is incident from the left (solid line in the left lower corner with label e), interacts (wavy line) and thereby loses enough energy to turn to a right moving hole (label h below the line), gains energy through a second interaction. The particle is

¹The situations both before and after the scattering event in the different channels can not be told apart.

²At the edges of a finite-width Hall bar, electrons of the same chirality are situated on the same edge, while those of different chirality are separated.

³a particle is described by a Green's function with positive energy, a hole's energy level is negative with respect to the Fermi energy

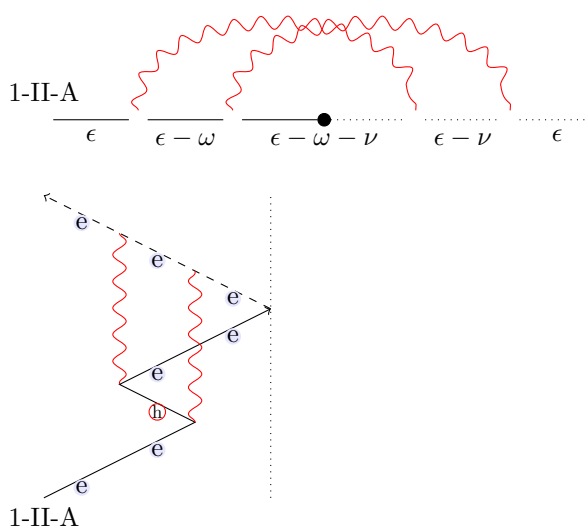


Figure 3.1.3: Feynman (skeleton) diagram (above) and real-space diagram. Both diagrams describe the same process, but multiple real-space diagrams can be drawn for a single skeleton diagram. In the Feynman diagram, the vertices are connected either by right-moving propagators (solid line) or left-moving propagators (dotted line) with the energy given below the line. A black dot labels a reflection at the impurity. In the real-space diagram, electrons(e) and holes(h) can be told apart. Solid and dashed lines stand for right and left movers. The dotted line represents the barrier.

reflected by the impurity. Finally it collects both energies on the way out to the left (dashed line indicates a left moving particle or hole). This pictorial representation can be compared to the formula (for simplicity we omit constant prefactors)

$$\int_{-\Delta}^0 d\nu \int_{\epsilon}^{\epsilon-\nu} d\omega \int dx_i G_{++}^0(x, x_1, \epsilon) G_{++}^0(x_1, x_2, \epsilon - \omega) G_{+-}^0(x_2, x_3, \epsilon - \omega - \nu) \\ G_{--}^0(x_3, x_4, \epsilon - \nu) G_{--}^0(x_4, y, \epsilon) V(x_1 - x_3) V(x_2 - x_4).$$

The choice of the integral limits in that case is non-trivial and depends on the energy conservation at the vertices. Again, the coordinates increase in the direction on the arrow from 1 to 2 in the first or 4 in the second order. The labels for these diagrams are constructed as follows:

1. The first number accounts for the number of impurity reflections.
 2. The second (roman) number denotes one of the different skeleton diagrams. In the first order in interaction this number is not important. In the second order there are three different skeleton diagrams.
- 
- We can call them
- (I) “Rainbow” diagrams
 - (II) Diagrams with crossed interaction lines
 - (III) “Double Fock” diagrams
3. The big letters distinguish the different real space diagrams which are possible for the given structure.

Additionally, we apply the following rules to construct diagrams:

- The interaction does not connect points on different sides of the impurity because short ranged interaction cannot yield logs in this case (the phase space is too small).
- As we will see, the Hartree diagram for g_2 is not of logarithmic order and can therefore be neglected in higher order calculations, as well as all combinations of Hartree-type diagrams.⁴

3.2 First order in interactions

We calculate the first order corrections in interaction and thereby show that first order in g_2 is correctly reproduced by our approach. All results are accurate with respect to the leading logarithmic terms.

⁴Diagrams with a Hartree “bubble” in second order are at most single logarithmic and therefore sub-leading.

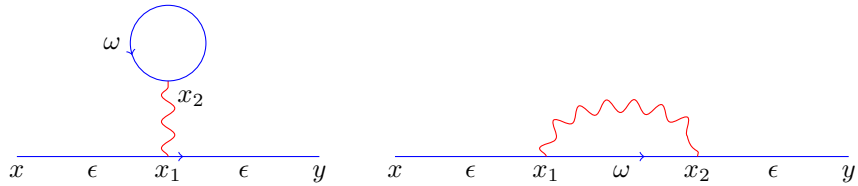


Figure 3.2.1: Hartree and Fock diagrams

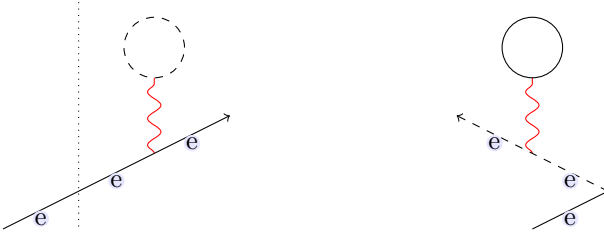


Figure 3.2.2: First order real-space diagrams for the Hartree correction. The “bubble” represents the local electron or hole density.

3.2.1 First order corrections to the S-matrix

The diagrams of first order in interaction are shown in figure figure 3.2.1. There are two different Feynman diagrams in first order, the Hartree diagram to the left in figure 3.2.1 and the Fock diagram. We will see in the following that the contribution due to the former is not logarithmic and can therefore be neglected within our accuracy.

Hartree diagram

Diagrams containing a “bubble” like the one shown in figure 3.2.1 on the left are always sub-leading corrections. Let us illustrate this property. We can draw two real-space diagrams of the Hartree type shown in figure 3.2.2. To calculate the contribution of the Hartree diagrams in g_2 it turns out that it is sufficient to focus on the “bubble”, e.g., in figure 3.2.2 to the right. The interaction in our case does not depend on the energy difference (it is instantaneous) and the integral over ω contains only the Green’s function, namely

$$\begin{aligned} \lim_{x \rightarrow x'} \int_{-\Delta}^{\Delta} d\omega G_{++}^0(x, x', \omega) &= \lim_{x' \rightarrow x+0} \int_0^{\Delta} d\omega \frac{e^{ip_\omega(x'-x)}}{iv_F} - \lim_{x' \rightarrow x-0} \int_{-\Delta}^0 d\omega \frac{e^{ip_\omega(x-x')}}{iv_F} \\ &= \lim_{\delta \rightarrow +0} \int_0^{\Delta} d\omega \frac{e^{ip_\omega \delta} - e^{-ip_\omega \delta}}{iv_F} \\ &= \int_0^{\Delta} d\omega \lim_{\delta \rightarrow +0} \frac{\sin(\omega \delta / v_F)}{iv_F} = 0. \end{aligned}$$

Note that we introduced a finite bandwidth Δ from the beginning to regularize the integral. The calculation for the second diagram is equivalent. We conclude

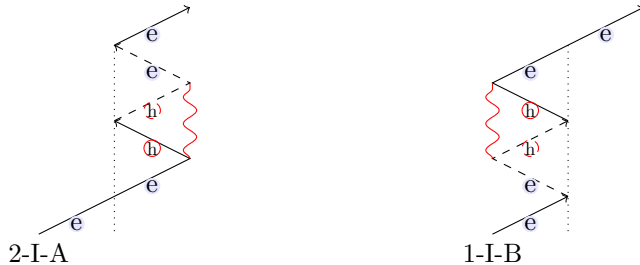


Figure 3.2.3: First order Fock corrections (in g_2) to the transmission coefficient drawn in real space.

that diagrams of the Hartree type are not of logarithmic order in g_2 .

(Fock-)Corrections to the transmission

What remains in the first order, are the so-called Fock diagrams. We start with all processes that result in a transmission of the particle. The interaction $V(x)$ used in the following calculations will be a decaying exponential with a given interaction radius d ,

$$V(x) = \frac{V_0}{2d} e^{-|x|/d}.$$

The simple case of a pointlike interaction leads to cancellation of first order Hartree and Fock terms as requested by the Pauli principle. This can easily be seen following a pictographic argument: If one collapses the wavy lines in both diagrams to a point, they cancel due to the different signs.⁵ In our calculations, we also use the momentum representation with a smooth Lorentzian type function $V(q)$

$$V(x) = \int_{-\infty}^{\infty} dq \frac{V(q)}{2\pi} e^{iqx},$$

where

$$V(q) = \frac{V_0}{(qd + i)(qd - i)}.$$

We make the observation, that in the momentum representation we don't have to decide on the sign of the coordinate difference.⁶ We can write

$$V(x) = V(-x) \Rightarrow \int_{-\infty}^{\infty} dq \frac{V(q)}{2\pi} e^{iqx} = \int_{-\infty}^{\infty} dq \frac{V(q)}{2\pi} e^{-iqx}.$$

Thus, the momentum representation exploits the symmetry in the interaction and simplifies calculus. Figure 3.2.3 shows the processes which are responsible for the logarithmic first order correction in g_2 to the transmission. We calculate these diagrams below.

⁵The minus stems from the “bubble”.

⁶The correct sign is chosen by pole integration

2-I-A The following expression is equivalent to the left picture in figure 3.2.3:

$$\begin{aligned}
G_{++}^{(1)}(x, y, \epsilon) &= i \int_0^\infty dx_1 \int_0^\infty dx_2 \int_{-\infty}^\infty dq \int_{-\Delta}^0 d\omega G_{++}^0(x, x_1, \epsilon) G_{+-}^0(x_1, x_2, \omega) \\
&\quad \times G_{-+}^0(x_2, y, \epsilon) \frac{V(q)e^{iq(x_1-x_2)}}{2\pi} \\
&= -i\left(\frac{1}{-v_F^2}\right) tr^* r \frac{e^{ip_\epsilon(y-x)}}{iv_F} \int_0^\infty dx_1 \int_0^\infty dx_2 \int_{-\infty}^\infty dq \int_{-\Delta}^0 d\omega \\
&\quad \times \exp[i(p_\epsilon + p_\omega + q)x_1 + i(p_\omega + p_\epsilon - q)x_2]
\end{aligned}$$

In most of the calculations, the prefactor of the integral is always calculated separately and prior to the integrals to keep track of the signs and the S-matrix elements t and r (compare equation (A.2.1)). Together with a global i in front we get

$$-itr^* r = -it|r|^2.$$

Additionally, we define

$$A(x, y, \epsilon) = \frac{V_0}{v_F} \frac{1}{iv_F} e^{ip_\epsilon(y-x)}, \quad (3.2.1)$$

and

$$\begin{aligned}
I(\epsilon, d) &= \int_0^\infty dx_1 \int_0^\infty dx_2 \int_{-\infty}^\infty d\omega \int_{-\infty}^\infty dq \\
&\quad \times \Theta(-\omega) \frac{V(q)}{2\pi} \exp[i(p_\epsilon + p_\omega + q)x_1 + i(p_\omega + p_\epsilon - q)x_2]
\end{aligned}$$

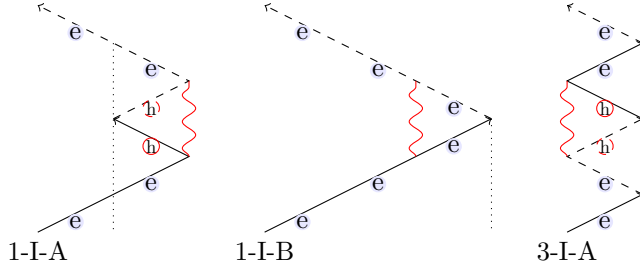
We have to calculate the coordinate, Fourier and interaction energy integrals. Keeping the prefactors aside, the coordinate integrals yields

$$I(\epsilon, d) = - \int_{-\infty}^\infty d\omega \int_{-\infty}^\infty dq \Theta(-\omega) \frac{V(q)}{2\pi} \frac{1}{(p_\epsilon + p_\omega + q)(p_\omega + p_\epsilon - q)}$$

Note that for the coordinate integrals to converge the sign of the regularizer plays a crucial role. This necessity arises due to the infinite system size. In the present case, the regularizer in $p_\epsilon + p_\omega$ has a positive sign and $e^{-\eta x}$, ($x \rightarrow \infty$) is zero. We can use the Sokhotsky-Weierstrass theorem or do contour integration to arrive at⁷

$$I(\epsilon, d) = -V_0 \int_0^\Delta d\omega \frac{1}{2(p_\epsilon + p_\omega)} \frac{1}{[(dp_\epsilon + dp_\omega)^2 + 1]}, \quad (3.2.2)$$

⁷convergence is guaranteed by $V(q)$

Figure 3.2.4: Real-space Fock diagrams (g_2) for reflection.

where Δ denotes a ultraviolet bandwidth cutoff of the order of the Fermi energy. Now we change variables to $\frac{d(\omega+\epsilon)}{v_F}$ and we get

$$I(\epsilon, d) = -v_F^2 V_0 \int_{\frac{d\epsilon}{v_F}}^{\frac{d\Delta}{v_F}} d\Omega \frac{1}{2\Omega(\Omega^2 + 1)}.$$

The logarithmic ultraviolet divergence in this expression is cut by $\min(v_F/d, \epsilon_F)$ and the result reads

$$I(\epsilon, d) = -v_F^2 V_0 \frac{1}{2} \log\left(\frac{v_F}{d\epsilon}\right).$$

Note how the maximum energy transfer in a scattering event is determined by the spacial scale of the interaction [52] or the Fermi energy. In the following, we will simply use $\Delta = \min(v_F/d, \epsilon_F)$ for the cutoff. We reinsert the prefactor and we find

$$\begin{aligned} G_{++}^{(1)}(x, y, \epsilon)_{2-I-A} &= i\left(\frac{1}{-v_F}\right)t(-r^*)r \frac{e^{ip_\epsilon(y-x)}}{iv_F} \times iV_0 \frac{1}{2} \log\left(\frac{v_F}{d\epsilon}\right) \\ &= -A(x, y, \epsilon) \frac{1}{2}t|r|^2 \log\left(\frac{v_F}{d\epsilon}\right). \end{aligned} \quad (3.2.3)$$

2-I-B The second diagram is of the same structure and it can easily be seen that it leads to the same equation so the total contribution simply doubles. The transmission coefficient in first order in interaction reads

$$t^{(1)} = t - \frac{V_0}{v_F}t|r|^2 \log\left(\frac{v_F}{d\epsilon}\right). \quad (3.2.4)$$

3.2.2 Corrections to the reflection coefficient

The processes responsible for a correction to the reflection r are evaluated in the same fashion. We start with the prefactor of the process 1-I-A in figure 3.2.4,

$$it(-r^*)t = i|t|^2 r,$$

where we used the unitarity condition for bare S-matrix elements, $tr^* = -rt^*$. We define further

$$B(x, y, \epsilon) = \frac{V_0}{v_F} \frac{1}{iv_F} e^{-ip_\epsilon(y+x)}.$$

We realize, that the arguments in the exponentials are the same as in 2-I-A and the integrals have the same limits. Thus, there is no need to calculate again, we just have to account for the change in the prefactor. The result reads

$$\begin{aligned} G_{++}^{(1)}(x, y, \epsilon)_{1-\text{I}-\text{A}} &= -i\left(\frac{1}{v_F^2}\right)|t|^2 r \frac{e^{-ip_\epsilon(y+x)}}{iv_F} \times iv_F \frac{1}{2} \log\left(\frac{v_F}{d\epsilon}\right) \\ &= B(x, y, \epsilon) \frac{1}{2} |t|^2 r \log\left(\frac{v_F}{d\epsilon}\right). \end{aligned} \quad (3.2.5)$$

Diagrams 1-I-B and 3-I-A can be calculated similar to 1-I-A, so we proceed and sum up all first order contributions.

3.2.3 Summary

We calculated the first order correction to the reflection

$$r^{(1)} = r \left[1 + \frac{V_0}{v_F} |t|^2 \log\left(\frac{v_F}{d\epsilon}\right) \right], \quad (3.2.6)$$

and the transmission coefficient

$$t^{(1)} = t - \frac{V_0}{v_F} t |r|^2 \log\left(\frac{v_F}{d\epsilon}\right). \quad (3.2.7)$$

The results agree with those in the literature [43, 47, 62, 74] presented in section 1.2.2. It can easily be verified that the first order corrections satisfy the unitarity condition for the S-matrix, namely

$$|r|^2 + |t|^2 = 1 \quad \text{and} \quad tr^* + rt^* = 0. \quad (3.2.8)$$

The first order correction is leading if $\log(\Delta/\epsilon) \ll 1$. When the energy of the incoming particle ϵ approaches the Fermi level, the result is logarithmically divergent and sub-leading orders are even stronger divergent. If we are able to confirm the unitarity of the S-matrix in the second order calculations, we can sum up the perturbative corrections in the RG procedure shown earlier in section 1.2.3.

3.3 Second order in interaction

To calculate the second-order correction we have to account for ten nonequivalent, connected Feynman diagrams shown in figure 3.3.1.

3.3.1 Sub-leading diagrams

Diagrams (a) and (c) to (g) all contain a Hartree “bubble” and can therefore only lead to a logarithm to the power of one or none at all. Diagram (j) is also not double logarithmic. To see this, it is sufficient to analyze the available phase space for the interaction. Given that the propagator between x_1 and x_3 in figure 3.3.2 propagates an electron, we can decide on all signs of the energies in the remaining propagators. Namely,

$$\nu > 0 \wedge \epsilon - \omega > 0 \wedge \nu - \omega < 0 \Rightarrow \nu < \omega < \epsilon \wedge \nu > 0.$$

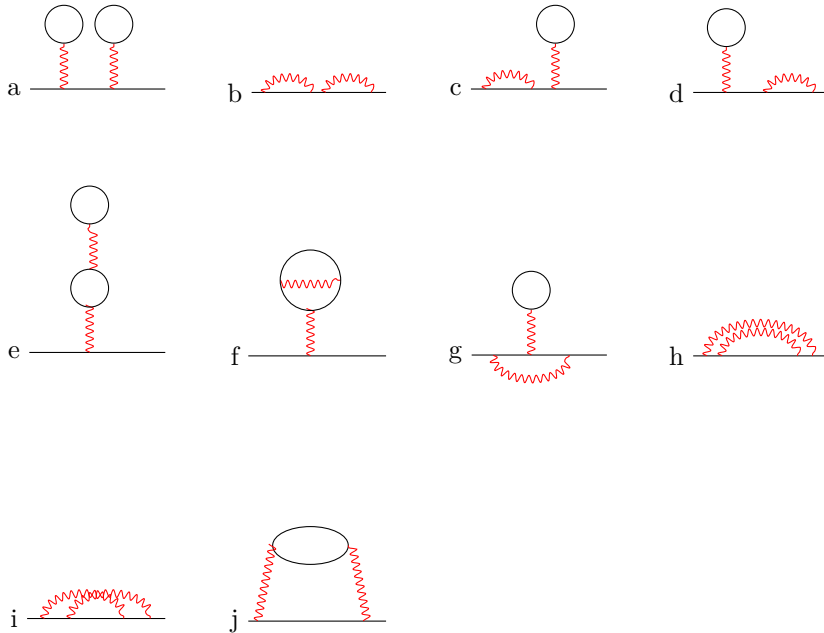


Figure 3.3.1: Second order Feynman diagrams [2].

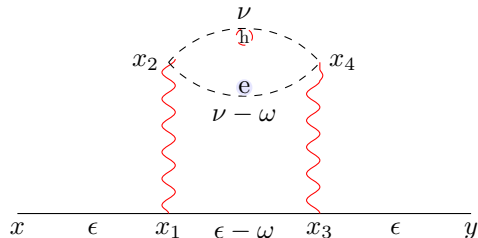


Figure 3.3.2: Energy transfer in diagram (j). Solid lines represent right moving particles, dashed lines stand for left-movers.

We note that the range for ω is limited from above by the particle energy ϵ which is a small parameter and below from $\nu > 0$. A single logarithmic contribution containing the upper cutoff Δ can thus only be provided by the integral over ν . This contribution is bound to be subleading with respect to the diagrams (b), (h) and (i), being of the order $\log^2(\Delta/\epsilon)$ as we will see below.

3.3.2 “Double-Fock”, “rainbow” and “crossed” diagrams

The remaining terms (b) (“double-Fock”), (h) (“rainbow”) and (i) (“crossed”) are subject of this section. Due to the broken translational symmetry, a lot of different diagrams can be drawn in real space. Sorting the processes according to the number of reflections at the impurity is a plausible way to organize the calculation, exploiting the reuseability of some parts of the calculation. For details about the labels, please refer to section 3.1.3.

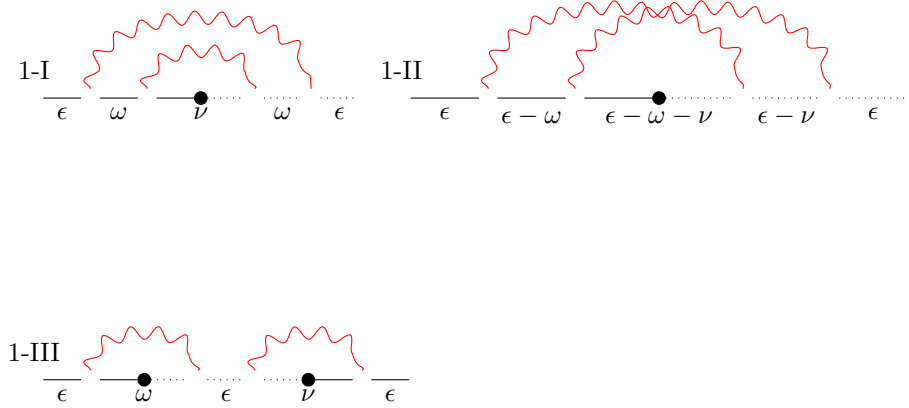


Figure 3.3.3: Skeleton diagrams for “rainbow” (I), “crossed lines” (II) and “double Fock” (III) diagrams.

Example calculations

For the sake of brevity, we present one example calculation for each of the three skeleton diagrams. All other diagrams can be calculated analogously.

Double Fock diagram 2-III-A In the first example diagrams below in figure 3.3.2 (skeleton diagram) and left in figure 3.3.4 (real space diagram) the situation is trivial: The diagram is made up of two parts P and Q ,

$$G_{++}^{(2)}(x, y, \epsilon)_{\text{2-III-A}} = PQ,$$

which can be taken directly from the first order (see section 3.2.2 for the detailed calculations). The first building block is evaluated as follows:

$$\begin{aligned} P &= - \int_0^\infty dx_1 \int_0^\infty dx_2 \int_{-\infty}^0 d\omega \int_{-\infty}^\infty dq G_{++}^0(x, x_1, \epsilon) G_{+-}^0(x_1, x_2, \omega) \\ &\quad \times \frac{t}{iv_F} e^{ip_\epsilon x_2} V(q) e^{iq(x_1 - x_2)} \\ &= - \frac{r|t|^2}{v_F^2} \frac{1}{iv_F} e^{-ip_\epsilon x} \int_0^\infty dx_1 \int_0^\infty dx_2 \int_{-\infty}^\infty d\omega \int_{-\infty}^\infty dq \\ &\quad \times \exp[i p_\epsilon(x_1 + x_2) + i p_\omega(x_1 + x_2) + i q(x_1 - x_2)] \frac{V(q)}{2\pi} \\ &= -i \frac{V_0}{v_F} r|t|^2 \frac{1}{2} \log\left(\frac{v_F}{d\epsilon}\right) \frac{e^{-ip_\epsilon x}}{iv_F}. \end{aligned}$$

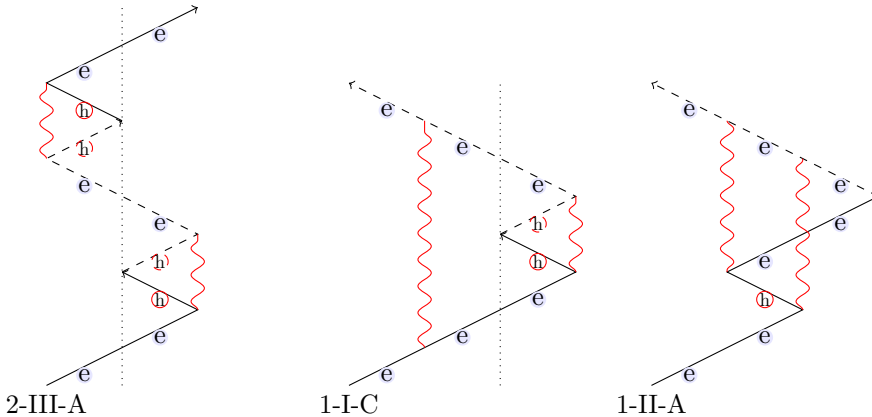


Figure 3.3.4: Real space representations of specific double Fock, rainbow and crossed line diagrams.

In the same fashion we compute the second part,

$$\begin{aligned} Q &= \int_{-\infty}^0 dx_3 \int_{-\infty}^0 dx_4 \int_{-\infty}^0 d\nu \int_{-\infty}^{\infty} dq G_{-+}^0(x_3, x_4, \nu) G_{++}^0(x_4, y, \epsilon) \\ &\quad \times e^{-ip_\epsilon x_3} V(q) e^{iq(x_1 - x_2)} \\ &= -i \frac{V_0}{v_F} r^* t \frac{1}{2} \log\left(\frac{v_F}{d\epsilon}\right) e^{ip_\epsilon y}. \end{aligned}$$

Finally, both parts are combined and yield

$$G_{++}^{(2)}(x, y, \epsilon)_{2-III-A} = -\frac{1}{4} t |t|^2 |r|^2 \frac{V_0^2}{v_F^2} \frac{e^{ip_\epsilon(y-x)}}{iv_F} \log^2\left(\frac{v_F}{d\epsilon}\right).$$

Rainbow diagram 1-I-C We proceed to the next class of diagrams. The expression we need to evaluate reads

$$\begin{aligned} &\int_0^\infty d\omega \int_{-\infty}^0 d\nu \int_{-\infty}^0 dx_1 \int_0^\infty dx_2 \int_0^\infty dx_3 \int_{-\infty}^0 dx_4 G_{++}^0(x, x_1, \epsilon) G_{++}^0(x_1, x_2, \omega) \\ &\quad \times G_{+-}^0(x_2, x_3, \nu) G_{--}^0(x_3, x_4, \omega) G_{--}^0(x_4, y, \epsilon) V(x_1 - x_4) V(x_2 - x_3). \end{aligned}$$

It is convenient to separate the S-matrix elements and the global minus sign from the rest,

$$-t(-r^*)t = -r|t|^2.$$

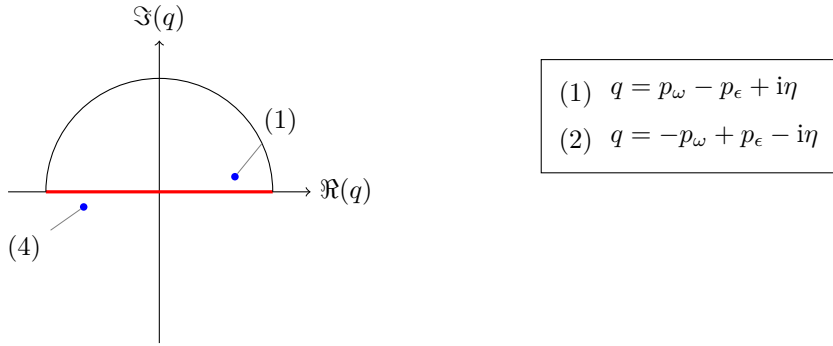
In the next step, we focus on the integrals,

$$\begin{aligned} I(\epsilon, d) := &\int d[\dots] \exp[i(p_\epsilon - p_\omega + q)x_1 + i(p_\omega + p_\nu + Q)x_2] \\ &\times \exp[i(p_\nu + p_\omega - Q)x_3 + i(p_\epsilon - p_\omega - q)x_4]. \end{aligned}$$

We first compute the coordinate integrals. The regularizers have to cut the infinities ($\text{Im}(p_\epsilon - p_\omega) = -\eta$ and $\text{Im}(p_\omega + p_\nu) = \eta$).⁸ Thus the coordinate integrals can be evaluated safely. The result of the integration (neglecting the energy-integrals for a second) reads

$$I(\epsilon, d) = \int_{-\infty}^{\infty} dq \int_{-\infty}^{\infty} dQ \frac{V(q)V(Q)}{(p_\epsilon - p_\omega + q)(p_\epsilon - p_\omega - q)(p_\nu + p_\omega + Q)(p_\nu + p_\omega - Q)},$$

where the integrand has one pole in each half-plane for both q and Q .



We close both contours in the upper half-plane (the integration along the contours yields zero due to V) and end up with the remaining two energy integrals,

$$I(\epsilon, d) = \frac{V_0^2}{4} \int_0^\infty d\omega \int_{-\infty}^0 d\nu \frac{V((\epsilon - \omega)/v_F)V((\omega + \nu)/v_F)}{(p_\epsilon - p_\omega)(p_\omega + p_\nu)}.$$

The two fractions both contain ω , so we choose to integrate over ν first and we end up with

$$\begin{aligned} I(\epsilon, d) &= \frac{V_0^2}{4} \int_0^\Delta d\omega \frac{1}{(\omega - \epsilon)} \log\left(\frac{\omega}{\omega + \Delta}\right) = \frac{1}{4} \int_\epsilon^\Delta d\omega' \frac{1}{\omega'} \log\left(\frac{\omega'}{\Delta}\right) \\ &= \frac{V_0^2}{4} \left[\frac{1}{2} \log^2\left(\frac{\Delta}{\epsilon}\right) - \log(\Delta) \log\left(\frac{\Delta}{\epsilon}\right) \right] \\ &= -\frac{V_0^2}{8} \log^2\left(\frac{\Delta}{\epsilon}\right). \end{aligned}$$

The interaction potentials V provide a possible finite cutoff $\max(\epsilon_F, v_F/d) = \Delta$. Collecting all prefactors, we find the result

$$G_{+-}^{(2)}(x, y, \epsilon)_{1\text{-I-C}} = \frac{1}{8} r|t|^2 \left[\frac{V_0^2 e^{-ip_\epsilon(x+y)}}{v_F^2 - iv_F} \right] \log^2\left(\frac{\Delta}{\epsilon}\right). \quad (3.3.1)$$

Diagram with crossed interaction lines 1-II-A When we look at the structure in figure 3.3.2 we can identify a diagram containing both *a particle*

⁸Note that the regularizer in this calculation is necessary to mimic a finite system size.

and a hole with an entangled energy structure. If we expect a breakdown of the unitarity conditions in second order in interaction, it is supposed to stem from this type of diagrams. The corresponding equation reads

$$\begin{aligned} G_{+-}^{(2)}(x, y, \epsilon)_{\text{I-II-A}} = & \int_{-\infty}^0 d\nu \int_{\epsilon}^{\epsilon-\nu} d\omega \int_{-\infty}^0 dx_2 \int_{x_2}^0 dx_1 \int_{-\infty}^0 dx_4 \int_{x_4}^0 dx_3 G_{++}^0(x, x_1, \epsilon) \\ & \times G_{++}^0(x_1, x_2, \epsilon - \omega) G_{+-}^0(x_2, x_3, \epsilon - \omega - \nu) \\ & \times G_{--}^0(x_3, x_4, \epsilon - \nu) G_{--}^0(x_4, y, \epsilon) V(x_1 - x_3) V(x_2 - x_4), \end{aligned}$$

where the limits for the energy integrals are derived from the relations

$$\begin{aligned} \epsilon - \omega < 0 \wedge \epsilon - \omega - \nu > 0 &\implies \epsilon < \omega < \epsilon - \nu \\ \epsilon - \nu > 0 &\implies \epsilon > 0 > \nu, \end{aligned}$$

which reflects the particle or hole nature of the propagators.⁹ Again, we separate the S-matrix elements and the external variables first,

$$r,$$

wherein we note one minus due to the single hole propagating Green which cancels the global minus (from i^2) in front. Like in the previous diagram, we proceed with the integrals,

$$\begin{aligned} I(\epsilon, d) := & \int d[\dots] V(q) V(Q) \\ & \times \exp[i(p_\epsilon + p_{\epsilon-\omega} + q)x_1 + i(-p_{\epsilon-\omega} - p_{\epsilon-\omega-\nu} + Q)x_2] \\ & \times \exp[i(-p_{\epsilon-\omega-\nu} + p_{\epsilon-\nu} - q)x_3 + i(-p_{\epsilon-\nu} + p_\epsilon - Q)x_4]. \end{aligned}$$

The integrals over the coordinates (regularizers: $\text{Im}(p_\epsilon - p_{\epsilon-\omega-\nu}) = -\eta$ and $\text{Im}(p_\epsilon - p_{\epsilon-\nu}) = -\eta$) yield

$$I(\epsilon, d) = \int d[\dots] \frac{V(Q)V(q' - Q)}{(p_\epsilon - p_{\epsilon-\omega-\nu} + q')(p_\epsilon - p_{\epsilon-\omega-\nu} - q')} \quad (3.3.2)$$

$$\times \frac{1}{(-p_{\epsilon-\omega} - p_{\epsilon-\omega-\nu} + Q)(p_\epsilon - p_{\epsilon-\nu} - Q)}, \quad (3.3.3)$$

where we changed the variable $q \rightarrow q' = q + Q$. q' and Q integrals are evaluated by pole-integration. Again the integration along the contours yield zero and we are left with

$$I(\epsilon, d) = -\frac{V_0^2 v_F^2}{4} \int_{-\infty}^0 d\nu \int_{\epsilon}^{\epsilon-\nu} d\omega \frac{1}{(\omega + \nu)\nu}.$$

⁹See figure 3.3.4, a hole propagator has a negative energy argument, an electron propagator a positive one.

In the last step, we need to integrate over the internal energies ω and ν ,

$$\begin{aligned} I(\epsilon, d) &= -\frac{V_0^2 v_F^2}{4} \int_0^\Delta d\nu \int_{\epsilon+\nu}^\epsilon d\omega \frac{1}{\nu(\omega-\nu)} \\ &= -\frac{V_0^2 v_F^2}{4} \text{PV} \left[\int_0^\Delta d\nu \frac{\log\left(\frac{|\epsilon-\nu|}{\epsilon}\right)}{\nu} \right] \\ &= -\frac{V_0^2 v_F^2}{8} \log^2\left(\frac{\Delta}{\epsilon}\right). \end{aligned}$$

We took the principal value of the integral in the second line. Combining the result with the prefactor we obtain

$$G_{+-}^{(2)}(x, y, \epsilon)_{1\text{-II-A}} = -\frac{1}{8} r \left[\frac{V_0^2 e^{-ip_\epsilon(x+y)}}{v_F^2 i v_F} \right] \log^2(\Delta/\epsilon). \quad (3.3.4)$$

Note that we can construct a similar diagram by inverting the path of the particle, thus the result should be doubled. For a complete record of all possible diagrams, symmetries play a crucial role in determining the correct prefactors.

Results

The result of these calculations are presented in table 3.1. See section A.3 for additional details on the calculations to all 28 diagrams including their real-space pictorial representation.

Diagram	$\log^2(\Delta/\epsilon)$	Diagram	$\log^2(\Delta/\epsilon)$
1-I-A	$1/4r$	3-I-A	$-1/4r r ^2$
1-I-B	$1/4r t ^2$	3-I-B	$-1/8r r ^2$
1-I-C	$1/8r t ^2$	3-I-C	$-1/8r r ^2 t ^2$
1-I-D	$1/8r t ^2$	3-I-D	$-1/8r t ^2 r ^2$
1-I-E	$1/8r t ^4$	3-I-E	$-1/8r r ^2$
1-I-F	$1/8r$	3-II-A	$1/4r r ^2$
1-II-A	$-1/4r$	3-III-A	$-1/4r r ^2 t ^2$
1-II-B	$-1/4r t ^2$	3-III-B	$-1/4r r ^2$
2-I-A	$-1/2t r ^2$	3-III-C	$-1/2r r ^2 t ^2$
2-I-B	$-1/4t r ^2$	4-I-A	$1/4t r ^4$
2-I-C	$-1/4t r ^2 t ^2$	4-III-A	$1/2t r ^4$
2-II-A	$1/2t r ^2$	4-III-B	$1/4t r ^4$
2-III-A	$-1/4t t ^2 r ^2$	5-I-A	$1/8r r ^4$
2-III-B	$-1/4t r ^2$	5-III-A	$1/4r r ^4$

Table 3.1: Second order corrections in interaction to the S-matrix of a featureless scatterer.

3.3.3 Corrections to transmission, reflection and checking of unitarity

Diagrams with one, three and five reflections at the impurity contribute to the total correction to the reflection coefficient,¹⁰

$$r^{(2)} = r \left[1 + \frac{V}{2} \log\left(\frac{v_F}{d\epsilon}\right) [1 + (|t|^2 - |r|^2)] \right] \quad (3.3.5)$$

$$+ \frac{V^2}{8} \log^2\left(\frac{v_F}{d\epsilon}\right) [1 + |t|^4 + 2|t|^2 - 4|r|^2 - 8|t|^2|r|^2 + 3|r|^4] \quad (3.3.6)$$

$$= r \left[1 + V \log\left(\frac{v_F}{d\epsilon}\right) |t|^2 + \frac{V^2}{2} \log^2\left(\frac{v_F}{d\epsilon}\right) [|t|^2 (|t|^2 - 2|r|^2)] \right], \quad (3.3.7)$$

whereas the remaining diagrams with two and four reflections sum up to give the correction to the transmission amplitude,

$$t^{(2)} = t \left[1 - V \log\left(\frac{v_F}{d\epsilon}\right) |r|^2 + \frac{V^2}{2} \log^2\left(\frac{v_F}{d\epsilon}\right) [2|r|^4 - |t|^2|r|^2 - |r|^2] \right] \quad (3.3.8)$$

$$= t \left[1 - V \log\left(\frac{v_F}{d\epsilon}\right) |r|^2 + \frac{V^2}{2} \log^2\left(\frac{v_F}{d\epsilon}\right) [|r|^2 (|r|^2 - 2|t|^2)] \right]. \quad (3.3.9)$$

As can easily be checked, these expression are identical to those calculated by expanding the RG result in section 1.2.3 up to the second order.

Unitarity

The coefficients can both be decomposed into a real prefactor (R_r and R_t) and r or t . Thus, the first unitarity condition,

$$(r^{(2)})^* t^{(2)} - (t^{(2)})^* r^{(2)} = r^* R_r t R_t - t^* R_t r R_r = 0, \quad (3.3.10)$$

is fulfilled just as the second condition, namely

$$|r^{(2)}|^2 + |t^{(2)}|^2 = |r|^2 R_r^2 + (1 - |r|^2) R_t^2 = 1 + O(V^4). \quad (3.3.11)$$

We conclude that the results of the second order perturbation theory are valid corrections in the S-matrix language and coincide with the results from the RG analysis. We will stop our perturbative expansion at second order in interaction and use the framework established in this and the previous sections to look for traces of inelastic scattering in more complex systems, where additional energy scales enter the system. Namely we have to take into account the Thouless energy E_{th} when we confine the interaction to an arbitrary region around the origin in the next section.

3.4 A second scale

3.4.1 Interaction in a box

In this second step we will introduce an additional lengthscale L to confine the interaction to a finite region (see figure 3.4.1). This picture corresponds to a

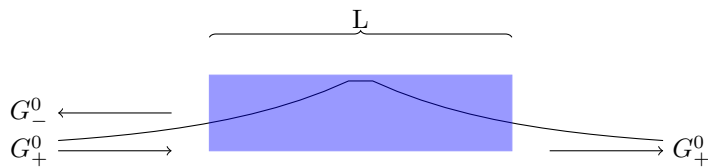


Figure 3.4.1: Interaction over a finite range

single channel 1d wire which is connected to reservoirs by smooth (reflectionless) contacts. Not only is this model a more realistic description of a possible experimental setup, it also justifies the use of free electron propagators in the asymptotic states. In the preceding section the length of the box was infinite and therefore the notion of *asymptotic Green's* was not well defined.

Together with the new lengthscale there comes an energy scale $E_{Th} = \frac{v_F}{L}$, the Thouless energy of the system with a finite interaction range. Depending on the size of the box this energy can be bigger or smaller than the particle energy, temperature or bias. In the latter case the lower cutoff for the logarithmic integrals will still be ϵ , the particle energy, and in the limit of infinitely large systems we expect to restore the results of the previous chapters. In the case $E_{Th} > \epsilon$, the new energy scale will enter most of the logs, replacing ϵ . There are two possible outcomes of this analysis:

- E_{Th} can be found in all logarithmic contributions replacing ϵ as the infrared cutoff. The basic structure of the second order calculation is not changed and the unitarity of the S-matrix is conserved.
- Different combinations of logarithmic contributions arise in second order. If the contributions do not cancel, unitarity can not be restored. This can be understood, for example, as a failure of the method.

Center of mass dependent interaction

The potential used in the following captures all essential features of the system. For simplicity, the (short-ranged) interaction is replaced by a point-like interaction

$$V(x_1, x_2) = V_0 \delta(x_1 - x_2) e^{-|x_1 + x_2|/L}. \quad (3.4.1)$$

This analysis can equally be done with a potential with sharp cutoff or a finite range of interaction (see section A.4) but since it is rather lengthy and does not bring any new physics we use this simple potential.

3.4.2 First order in interaction

Let us see how the additional scale enters the calculations. For example, we consider diagram 2-I-A in the first order in interactions. The expression reads

$$\begin{aligned} G_{++}^{(1)}(x, y, \epsilon)_{\text{2-I-A}} = i \int_0^\infty d\omega \int_0^\infty dx_1 \int_0^\infty dx_2 & G_{++}^0(x, x_1, \epsilon) \\ & \times G_{+-}^0(x_1, x_2, \omega) G_{-+}^0(x_2, y, \epsilon) V(x_1, x_2). \end{aligned}$$

¹⁰The first label of a diagram counts the number of reflections.

We extract the prefactor

$$it|r|^2 A(x, y, \epsilon),$$

where we can identify A from equation (3.2.1), put $v_F = 1$ and proceed with the integrals,

$$I(\epsilon, \Delta, E_{\text{Th}}) := \int_0^\infty d\omega \int_0^\infty dx_1 2i(p_\epsilon + p_\omega + iE_{\text{Th}})x_1,$$

where we used $\delta(x_1 - x_2)$ to calculate the integral over x_2 . After x_1 integration, we get (omitting the prefactor)

$$\begin{aligned} I(\epsilon, \Delta, E_{\text{Th}}) &= \int_0^\Delta d\omega \frac{-1}{2i(\epsilon + \omega + iE_{\text{Th}})} = -\frac{v_F}{2i} \log\left(\frac{\Delta}{\epsilon + iE_{\text{Th}}}\right) \\ &= -\frac{1}{2i} \log\left(\frac{\Delta}{\sqrt{\epsilon^2 + E_{\text{Th}}^2}}\right), \end{aligned}$$

where we neglected a subleading phase factor. We analyze this integral in two different regimes, namely a very large system, $E_{\text{Th}} \ll \epsilon$ and a small one, $\Delta \gg E_{\text{Th}} \gg \epsilon$. As expected, in the limit of infinite system size, we restore our previous result

$$I(\epsilon, \Delta) = -\frac{1}{2i} \log(\Delta/\epsilon),$$

while in the opposite limit, the Thouless energy provides the infrared cutoff:

$$I(E_{\text{th}}, \Delta) = -\frac{1}{2i} \log\left(\frac{\Delta}{E_{\text{th}}}\right).$$

The total contribution due to this diagram reads

$$G_{++}^{(1)}(x, y, \epsilon)_{2\text{-I-A}} = -\frac{V_0}{2v_F} t|r|^2 \log\left(\frac{\Delta}{\max(E_{\text{th}}, \epsilon)}\right) G_{++}^0(x, y, \epsilon).$$

Since all diagrams in the first order share the same essentials, we do not expect the logarithmic structure to change for other diagrams.

3.4.3 Second order in interaction for a finite system

In the following we analyze both “rainbow” and “crossed-lines” diagrams to see if a change in the logarithmic structure appears. “Double Fock” diagrams can be directly deduced from the first order calculus.

“Rainbow” diagrams

We follow the same step-by-step procedure in calculating the Diagram 1-I-B (second order in interaction) as in section 3.3. The complete expression for the

propagator reads

$$\begin{aligned}
G_{+-}^{(2)}(x, y, \epsilon)_{\text{I-I-B}} &= - \int_0^\Delta d\omega \int_0^\Delta d\nu \int_0^L dx_1 \int_0^{x_1} dx_2 \int_0^L dx_4 \int_0^{x_4} dx_3 G_{++}^0(x, x_1, \epsilon) \\
&\quad \times G_{++}^0(x_1, x_2, -\omega) G_{+-}^0(x_2, x_3, -\nu) G_{--}^0(x_3, x_4, -\omega) \\
&\quad \times G_{--}^0(x_4, y, \epsilon) V(x_1, x_4) V(x_2, x_3) \\
&= - \frac{V_0^2}{v_F^4} r |t|^2 G_{+-}^0(x, y, \epsilon) \int_0^\Delta d\omega \int_0^\Delta d\nu \int_0^L dx_1 \int_0^{x_1} dx_2 \\
&\quad \times \exp(2i(\epsilon + \omega + iv_F/L)x_1/v_F + 2i(\nu - \omega + iv_F/L)x_2/v_F).
\end{aligned}$$

We put the prefactor aside and calculate the integrals over the coordinates x_2 and x_1 :

$$\begin{aligned}
I(\epsilon, \Delta, E_{\text{Th}}) &:= \int_0^\Delta d\omega \int_0^\Delta d\nu \left[\frac{1}{4(\nu - \omega + iE_{\text{Th}})(\epsilon + \nu + 2iE_{\text{Th}})} \right. \\
&\quad \left. - \frac{1}{4(\epsilon + \omega + iE_{\text{Th}})(\nu - \omega + iE_{\text{Th}})} \right] \\
&= v_F^2 \int_0^\Delta d\omega \int_0^\Delta d\nu \frac{-1}{4(\epsilon + \omega + iE_{\text{Th}})(\epsilon + \nu + 2iE_{\text{Th}})}.
\end{aligned}$$

Like in the previous section, the integrals are computed in the two regimes of infinitely large and small system size.

$\epsilon \gg v_F/L$ (**The limit of the infinite system**): In the leading logarithmic approximation we neglect the Thouless energy and arrive at

$$I(\epsilon, \Delta) = -\frac{1}{4} \int_0^\Delta d\omega \int_0^\Delta d\nu \frac{1}{(\epsilon + \nu)(\epsilon + \omega)} = -\frac{1}{4} \log^2(\Delta/\epsilon).$$

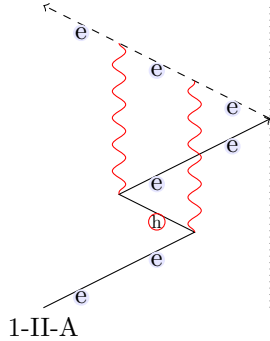
$\epsilon \ll v_F/L$ (**Small system**): Following the same arguments as before we identify the integral in the regime $\epsilon < \nu, \omega < v_F/L$ as small correction and only account for contributions $\omega, \omega \gg v_F/L$. In doing so, we obtain

$$I(\Delta, E_{\text{Th}}) = -\frac{1}{4} \log^2\left(\frac{\Delta}{E_{\text{Th}}}\right).$$

Finally, we account for both parameter ranges in the single expression

$$G_{+-}^{(2)}(x, y, \epsilon)_{\text{I-I-B}} = \frac{V_0^2}{4v_F^2} r |t|^2 \log^2\left(\frac{\Delta}{\max(\epsilon, E_{\text{Th}})}\right) G_{+-}^0(x, y, \epsilon).$$

We conclude that we can't expect any non-trivial behavior from the "rainbow" diagrams. The infrared cutoff of the corrections is replaced by $\max(\epsilon, E_{\text{Th}})$.



“Crossed-lines” diagrams

In this section we discuss the influence of a finite system size on the diagram 1-II-A with crossed interaction lines. This diagram has an entangled structure with electrons and holes, providing the most non-trivial structure at second order. We proceed in the same manner as in the previous section. The full expression for this diagram reads (compare section A.3.1),

$$\begin{aligned}
G_{+-}^{(2)}(x, y, \epsilon)_{1\text{-II-B}} &= - \int_{-\Delta}^0 d\nu \int_{\epsilon}^{\epsilon-\nu} d\omega \int_{-\infty}^0 dx_2 \int_{x_2}^0 dx_1 \int_{-\infty}^0 dx_4 \int_{x_4}^0 dx_3 G_{++}^0(x, x_1, \epsilon) \\
&\quad \times G_{++}^0(x_1, x_2, \epsilon - \omega) G_{+-}^0(x_2, x_3, \epsilon - \omega - \nu) G_{--}^0(x_3, x_4, \epsilon - \nu) \\
&\quad \times G_{--}^0(x_4, y, \epsilon) V(x_1, x_4) V(x_2, x_3) \\
&= r \frac{V_F^2}{v_F^4} G_{+-}^0(x, y, \epsilon) \int_{-\Delta}^0 d\nu \int_{\epsilon}^{\epsilon-\nu} d\omega \int_{-\infty}^0 dx_2 \int_{x_2}^0 dx_1 \\
&\quad \times \exp(2i(\nu - iv_F/L)x_1/v_F + 2i(\omega - iv_F/L)x_2/v_F),
\end{aligned}$$

is first integrated over x_1 and x_2 (we put the prefactor aside):

$$\begin{aligned}
I(\epsilon, \Delta, E_{Th}) &:= \int_{-\Delta}^0 d\nu \int_{\epsilon}^{\epsilon-\nu} d\omega \frac{-1}{4(\nu - iE_{Th})(\omega + \nu - 2iE_{Th})} \\
&= \int_{-\Delta}^0 d\nu \frac{1}{4(\nu - iE_{Th})} \log\left(\frac{|\epsilon + \nu| - 2iE_{Th}}{\epsilon - 2iE_{Th}}\right).
\end{aligned}$$

$\epsilon \gg E_{Th}$ (**Large system**): In this limit,

$$I(\epsilon, \Delta, E_{Th}) = - \int_0^\Delta d\nu \frac{1}{4(\nu + iE_{Th})} \log\left(\frac{\epsilon + \nu}{\epsilon}\right).$$

As long as $\nu < \epsilon$ the contribution is not \log^2 (the logarithm in the integral behaves like $\log(1)$). As soon as we replace the infrared cutoff in the integral by ϵ , v_F/L in the denominator inside the integral can be neglected and we restore

the previous result (compare equation (A.3.8))

$$I(\epsilon, \Delta) = -\frac{1}{8} \log^2\left(\frac{\Delta}{\epsilon}\right).$$

$\epsilon \ll E_{Th}$ (**Small system**): With logarithmic accuracy, we can write

$$I(\epsilon, \Delta, E_{Th}) = - \int_0^\Delta d\nu \frac{1}{4(\nu + iE_{Th})} \log\left(\frac{E_{Th} + \nu}{E_{Th}}\right).$$

Again, the leading \log^2 contribution can be found for $\nu > E_{Th}$ (for $0 < \nu < E_{Th}$ there is only a single log). Finally, we restore the same result as in the previous calculations with the infrared cutoff replaced by E_{Th} , namely

$$I(\Delta, E_{Th}) = -\frac{1}{8} \log^2\left(\frac{\Delta}{E_{Th}}\right).$$

Accounting for both regimes and reinserting the prefactor we get

$$G_{+-}^{(2)}(x, y, \epsilon)_{1-II-A} = -\frac{1}{8} r \log^2\left(\frac{\Delta}{\max(E_{Th}, \epsilon)}\right) C_{+-}(x, y, \epsilon). \quad (3.4.2)$$

When we compare this result to equation (3.3.4) we see that we can expect that the infrared cutoff is replaced in all diagrams with crossed interaction lines as soon as the system size is reduced sufficiently. Ultimately we state that in all three different types of diagrams, the finite size does not change the logarithmic structure of the perturbative corrections in the second order. According to the calculations in section 3.3, the S-matrix, apart from a replacement in the UV cutoff, remains unchanged.

3.5 Energy dependent scattering matrix

We replace the simple structureless scatterer of the previous sections by a scattering structure with a resonant level.

3.5.1 Resonant scattering in a one-dimensional system at first order in interaction

We model the resonance by a compound scatterer made of two tunnel barriers with equal tunnel amplitudes t separated by a distance $\pi v_F/\delta$. This gives rise to a system of resonances separated by energy δ . The magnitude of δ is of the order of the cutoff Δ , so that the distance between the barriers is small (of the order of d , the range of interaction). In this limit the model of a single resonant level of the Breit-Wigner type is valid [62] (see also section 1.4.1). We start with the bare amplitudes of the Breit-Wigner type,

$$t(\epsilon) = \frac{\Gamma}{\Gamma - i(\epsilon - \epsilon_R)} = \frac{i\Gamma}{(\epsilon - \epsilon_R) + i\Gamma} = \frac{i}{\xi + i}, \quad (3.5.1)$$

$$r(\epsilon) = \frac{i(\epsilon - \epsilon_R)}{\Gamma - i(\epsilon - \epsilon_R)} = \frac{-(\epsilon - \epsilon_R)}{(\epsilon - \epsilon_R) + i\Gamma} = \frac{-\xi}{\xi + i}, \quad (3.5.2)$$

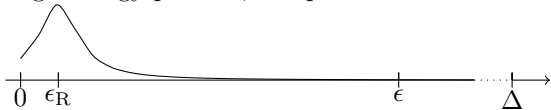
where ϵ_R is the position of the resonant level measured from the Fermi surface, Γ denotes the width of the resonance and $\xi = \frac{\epsilon - \epsilon_R}{\Gamma}$. In this limit, we can safely neglect the renormalization of amplitudes *between* the barriers (see section 1.4.1), and treat the whole structure as a point-like scatterer with energy dependent scattering matrix S . The width Γ is related to the strength of the barriers by $\Gamma = |t|^2 \delta / 2\pi$. Furthermore, we assume that the interaction corrections to both quantities are included in the definition, i.e., changes to those parameters come from energy scales of the order of the Fermi energy. The bare scattering amplitudes given above obey the unitarity conditions $|t|^2 + |r|^2 = 1$ and $tr^* + t^*r = 0$, and the special relation for a delta-function type impurity $r = t - 1$.

3.5.2 Relations of the energy scales

Before we start calculating, it is useful to discuss the possible relations of the energy scales that will appear in the course of calculus. Two of them have been introduced in previous sections, namely the particle energy ϵ , which is of the order of the applied bias or the temperature, and the cutoff Δ , the smaller of either the Fermi energy or the inverse interaction length. With the addition of a resonant scatterer, we have to introduce two new energy scales: The width of the resonant level Γ and the position ϵ_R . We will label the different situations so that we can easily refer to them in the discussion of the results.

a: Off resonance The resonant level is either far above or below the particle energy and the width is small on the scale of the difference of ϵ and ϵ_R .

1. High energy particle, sharp resonance close to Fermi energy.



- $\Delta \gg \epsilon \gg \epsilon_R, \Gamma$
- $t \ll r$

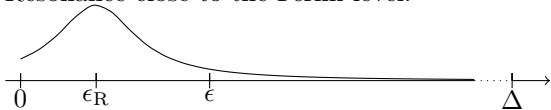
2. Resonance at high energies.



- $\Delta \gg \epsilon_R \gg \Gamma, \epsilon$
- $t \ll r$

b: In the vicinity of the resonant level

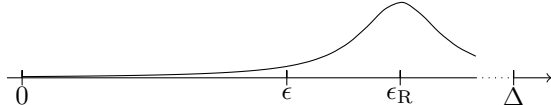
1. Resonance close to the Fermi level.



- $\Delta \gg \epsilon$

- $\epsilon \sim \epsilon_R \sim \Gamma$
- $r \sim t$

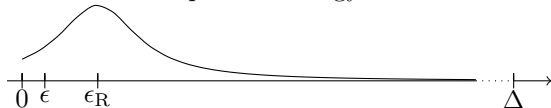
2. Resonance at high energies.



- $\Delta \gg \epsilon_R, \epsilon \gg \Gamma$
- $r \sim t$

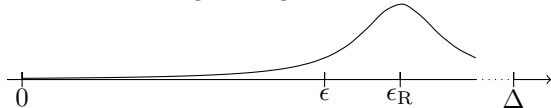
c: Inside the resonant level

1. Resonance and particle energy close to the Fermi level.



- $\Gamma \gg \epsilon$
- $\epsilon - \epsilon_R \ll 1$
- $t \gg r$

2. Resonance at high energies.



- $\epsilon_R, \epsilon \gg \Gamma$
- $\epsilon - \epsilon_R \ll 1$
- $t \gg r$

A Broad resonant level with a width orders of magnitude larger than the particle energy is not validly described by a Breit-Wigner type resonance.

3.5.3 First order in interactions

To demonstrate the influence of energy dependent scattering on the calculations we start with the first order diagram 2-I-A. The prefactor of this process reads

$$it(\epsilon)r(\epsilon),$$

where in contrast to case of a structureless impurity the reflection of the hole is energy dependent and can *not* be added to the prefactor. The integration of the coordinates and Fourier components of the interaction are untouched by this

modification. The energy integrals calculate as follows (see equation (3.2.2) on page 58):

$$\begin{aligned}
I(\epsilon, \Delta, \epsilon_R, \Gamma) &:= \int_0^\Delta d\omega \frac{r^*(-\omega)}{\epsilon + \omega} = - \int_0^\Delta d\omega \frac{(\omega + \epsilon_R)}{(\epsilon + \omega)(i\Gamma + (\omega + \epsilon_R))} \\
&= - \int_{\frac{\epsilon_R}{\Gamma}}^{\frac{\Delta}{\Gamma}} dy \frac{y}{(\xi_\epsilon + y)(y + i)} \\
&= \frac{-\xi}{\xi - i} \int_{\frac{\epsilon_R}{\Gamma}}^{\frac{\Delta}{\Gamma}} dy \frac{1}{\xi + y} + \frac{i}{\xi - i} \int_{\frac{\epsilon_R}{\Gamma}}^{\frac{\Delta}{\Gamma}} dy \frac{1}{i + y} \\
&= r^*(\epsilon) \log\left(\frac{\Delta}{\epsilon}\right) - t^*(\epsilon) \log\left(\frac{\frac{\Delta}{\Gamma} + i}{\frac{\epsilon_R}{\Gamma} + i}\right) \\
&= r^*(\epsilon) \log\left(\frac{\Delta}{\epsilon}\right) - t^*(\epsilon) \left[\log\left(\frac{\Delta}{\sqrt{\epsilon_R^2 + \Gamma^2}}\right) \right. \\
&\quad \left. + i \arctan(\Gamma/\epsilon_R) \right].
\end{aligned}$$

The phase factor does not affect the unitarity of the S-matrix since it is not of leading logarithmic order. This is important because the calculation for the electron reflection in 1-I-B yields a different sign, namely

$$\begin{aligned}
G_{+-}^{(1)}(x, y, \epsilon)_{1-\text{I-B}} &\propto \int_0^\Delta d\omega \frac{r(\omega)}{\omega - \epsilon} = r(\epsilon) \log\left(\frac{\Delta}{\epsilon}\right) - t(\epsilon) \left[\log\left(\frac{\Delta}{\sqrt{\epsilon_R^2 + \Gamma^2}}\right) \right. \\
&\quad \left. - i \arctan(\Gamma/\epsilon_R) \right].
\end{aligned}$$

We will neglect this correction in the following and define

$$L_1 := \log\left(\frac{\Delta}{\epsilon}\right) \quad \text{and} \quad L_2 := \log\left(\frac{\Delta}{\sqrt{\epsilon_R^2 + \Gamma^2}}\right). \quad (3.5.3)$$

Other first order diagrams

In an analogous manner, the other diagrams of first order (see section 3.2.1) can be calculated. The results are presented in table 3.2.

Unitarity of the resonant transmission amplitudes in first order

The perturbative corrections read

$$\delta t(\epsilon) = \frac{V_0}{v_F} [-t(\epsilon)|r(\epsilon)|^2 L_1 + r(\epsilon)|t(\epsilon)|^2 L_2], \quad (3.5.4)$$

$$\delta r(\epsilon) = \frac{V_0}{v_F} \left[r(\epsilon)|t(\epsilon)|^2 L_1 - \frac{t(\epsilon)}{2} (|r(\epsilon)|^2 - |t(\epsilon)|^2 + 1) L_2 \right]. \quad (3.5.5)$$

diagram	correction
1-I-A	$\frac{V_0}{2v_F} (r t ^2 L_1 + t t ^2 L_2)$
1-I-B	$\frac{V_0}{2v_F} (r(\epsilon)L_1 - t(\epsilon)L_2)$
2-I-(A+B)	$\frac{V_0}{v_F} (-t(\epsilon) r(\epsilon) ^2 L_1 + r(\epsilon) t(\epsilon) ^2 L_2)$
3-I-A	$-\frac{V_0}{2v_F} (r(\epsilon) r(\epsilon) ^2 L_1 + t(\epsilon) r(\epsilon) ^2 L_2)$

Table 3.2: First order diagrams in interaction and the logarithmic corrections. The definition of L_1 and L_2 can be found in equation (3.5.3).

The first contribution reproduces the results for the structure-less impurity (see section 3.2.3). This is what we expect far from the resonance. It can be verified that the unitarity conditions for $L_2 \sim L_1$ (the resonant case) are met in the first order (compare with section 3.2.3).

Anti-resonant scattering

Alternatively to the resonant scattering discussed above we can model an anti-resonant level as in section 1.4.2(for example an occupied quantum dot) by exchanging the expressions for t and r in equation (3.5.1) and changing the sign of the nominators (so that $r = t - 1$). This results in a change of the logarithmic cutoff in both the resonant and the off-resonant case. To see this, we analyze an electron (e.g., diagram 1-I-B) and a hole (e.g., diagram 1-I-A) reflection and compute the integral over the internal energy ω ,

$$\begin{aligned}
I_1(\epsilon, \Delta, \epsilon_R, \Gamma) &:= \int_0^\Delta d\omega \frac{r(\omega)}{\omega - \epsilon} = \int_0^\Delta d\omega \frac{-i\Gamma}{(\omega - \epsilon)[\omega + i\Gamma - \epsilon_R]} \\
&= r(\epsilon) \left[\log\left(\frac{\Delta}{\epsilon}\right) - \log\left(\frac{\Delta}{|i\Gamma - \epsilon_R|}\right) \right] \\
&= r(\epsilon) \log\left(\frac{|i\Gamma - \epsilon_R|}{\epsilon}\right) \\
&= r(\epsilon) \log\left(\frac{\sqrt{\Gamma^2 + \epsilon_R^2}}{\epsilon}\right) \\
I_2(\epsilon, \Delta, \epsilon_R, \Gamma) &:= \int_0^\Delta d\omega \frac{r^*(-\omega)}{\epsilon + \omega} = r^*(\epsilon) \log\left(\frac{\sqrt{\Gamma^2 + \epsilon_R^2}}{\epsilon}\right)
\end{aligned}$$

We see that $\max(\Gamma, \epsilon_R)$ replaces the infrared cutoff in the logarithm. This result coincides with Ref. [47]. The unitarity of the S-matrix is not violated in first order because there are no additional logarithms, i.e., the structure remains unaltered.

Resonant scattering at a non-symmetric impurity

In the general case, a resonant scatterer set up by two barriers is not symmetric in space. In section 3.1.1 we derived scattering amplitudes for a small asymmetric

scatterer without a resonant level. In this section, we consider the case presented in section 1.4.1, namely using the same amplitudes as in Ref. [57]:

$$t(\epsilon) = \frac{\sqrt{\Gamma_L \Gamma_R}}{(\Gamma_L + \Gamma_R)/2 - i(\epsilon - \epsilon_R)} \quad (3.5.6)$$

$$r_L(\epsilon) = \frac{(\Gamma_R - \Gamma_L)/2 + i(\epsilon - \epsilon_R)}{(\Gamma_L + \Gamma_R)/2 - i(\epsilon - \epsilon_R)}. \quad (3.5.7)$$

The amplitude r_R can be derived from the unitarity condition for the asymmetric system $tr_R^* + r_L t^* = 0$. The second condition $|r_L|^2 = |r_R|^2 = 1 - |t|^2$ holds true, too, and the unitarity of the initial scattering matrix is ensured. We use equation (3.5.6) and equation (3.5.7) to calculate the corrections to transmission and reflection on the left and right,

$$\begin{aligned} \delta t(\epsilon) &= -t(\epsilon)|r_L(\epsilon)|^2 \log\left(\frac{\Delta}{\epsilon}\right) + \frac{|t(\epsilon)|^2}{2\sqrt{\Gamma_R \Gamma_L}} (\Gamma_L r_R(\epsilon) + \Gamma_R r_L(\epsilon)) \log\left(\frac{\Delta}{\Gamma_m}\right) \\ &= (\dots) \log\left(\frac{\Delta}{\Gamma_m}\right) - t(\epsilon)|r_L(\epsilon)|^2 \log\left(\frac{\Gamma_m}{\epsilon}\right), \end{aligned} \quad (3.5.8)$$

$$\begin{aligned} \delta r_L(\epsilon) &= r_L(\epsilon)|t(\epsilon)|^2 \log(\Delta/\epsilon) - \frac{t(\epsilon)}{2\sqrt{\Gamma_R \Gamma_L}} (\Gamma_R(1 + r_L r_R^*) - \Gamma_L|t|^2) \log\left(\frac{\Delta}{\Gamma_m}\right) \\ &= (\dots) \log\left(\frac{\Delta}{\Gamma_m}\right) + r_L(\epsilon)|t(\epsilon)|^2 \log\left(\frac{\Gamma_m}{\epsilon}\right), \end{aligned} \quad (3.5.9)$$

where $\Gamma_m = \max(\Gamma_R, \Gamma_L, \epsilon_R)$. The two logarithms belong to the different regimes of ϵ on $(\Delta/\Gamma_m \gg \Gamma_m/\epsilon)$ and off-resonance. It is straightforward to prove unitarity in both the resonant and the off-resonant regime. For details please refer to section A.5.2 of the appendix.

3.5.4 Second order for a symmetric resonant scatterer

In the first order in interaction, unitarity is a property of the S-matrix in all regimes. In this section, the second order correction are evaluated in the different regimes in section 3.5.2. To this end, we repeat all calculations for the second order with an energy dependent scattering matrix. Examples for calculations of this type can be found in section A.3.

Let us briefly motivate our calculations before presenting the results. In the second order diagrams, e.g., in 1-I-C in figure 3.3.4 on page 63, we also find transmission amplitudes depending on the internal energy variables. We note that the integrals over internal energy variables yield different cutoffs in the logarithms for reflection and transmission, namely

$$\int_0^\Delta d\omega \frac{r(\omega)}{\omega - \epsilon} \propto \log\left(\frac{\Delta}{\bar{\Gamma}}\right), \quad (3.5.10)$$

$$\int_0^\Delta d\omega \frac{t(\omega)}{\omega - \epsilon} \propto \log\left(\frac{\bar{\Gamma}}{\epsilon}\right), \quad (3.5.11)$$

where $\bar{\Gamma} = \sqrt{\Gamma^2 + \epsilon_R^2}$.¹¹ We can therefore expect a non-trivial interplay of the different cutoffs in the system.

The results of our calculation is presented in table 3.3. Note that the first

Diagr.	L_1^2	L_2^2	$L_2(L_1 - L_2)$	L_1L_2	P
1-I-A	$2r$				$-2t$
1-I-B	$2r t ^2$				$2t t ^2$
1-I-C	$r t ^2$	$-r t ^2$	$2t t ^2$		
1-I-D	$r t ^2$	$t t ^2$			
1-I-E	$r t ^4$	$-r t ^4$		$-2t t ^4$	
1-I-F	r	$-t$			
1-II-A	$-2r$	$2t$			
1-II-B	$-2r t ^2$	$-2t t ^2$			$-4t t ^2$
2-I-A	$-4t r ^2$			$4r t ^2$	
2-I-B	$-2t r ^2$	$2r t ^2$			
2-I-C	$-2t r ^2 t ^2$	$2t r ^2 t ^2$	$-4r t ^4$		
2-II-A	$4t r ^2$	$-4r t ^2$			$-8r t ^2$
2-III-A	$-2t t ^2 r ^2$	$2t t ^4$		$4r t ^4$	
2-III-B	$-2t r ^2$	$-2t t ^2$	$-4r t ^2$		
3-I-A	$-2r r ^2$			$-2t r ^2$	
3-I-B	$-r r ^2$	$-t r ^2$			
3-I-C	$-r r ^2 t ^2$	$r r ^2 t ^2$	$2t r ^2 t ^2$		
3-I-D	$-r t ^2 r ^2$	$[r r ^2 t ^2 - t^2]$	$2t t ^2 r ^2$		
3-I-E	$-r r ^2$	$[r r ^2 + 1]$	$-2t r ^2$		
3-II-A	$2r r ^2$	$2t r ^2$			$4t r ^2$
3-III-A	$-2r r ^2 t ^2$	$2r t ^4$		$-4t t ^2 r ^2$	
3-III-B	$-2r r ^2$	$-2r t ^2$	$4t r ^2$		
3-III-C	$-4r r ^2 t ^2$	$4r t ^4$		$-8t t ^2 r ^2$	
4-I-A	$2t r ^4$	$-2[t r ^4 + rt]$	$4r t ^2 r ^2$		
4-III-A	$4t r ^4$	$-4t r ^2 t ^2$		$-8r r ^2 t ^2$	
4-III-B	$2t r ^4$	$-2t r ^2 t ^2$		$-4r r ^2 t ^2$	
5-I-A	$r r ^4$	$[-r r ^4 + r^2]$	$-2t r ^4$		
5-III-A	$2r r ^4$	$-2r t ^2 r ^2$		$4t r ^4$	

Table 3.3: Corrections to an energy dependent S-matrix in second order in interaction where $L_1 = \log(\Delta/\epsilon)/8$, $L_2 = \log(\Delta/\bar{\Gamma})/8$ and $P = \text{Li}_2(-\epsilon/\bar{\Gamma})/8$.

column correctly reproduces the results for the featureless scatterer. Additionally to combinations of the logarithmic contributions L_1 and L_2 known from first order, a third, poly-logarithmic, correction P appears in table 3.3. It is defined as follows:

$$P = \text{Li}_2(-\epsilon/\bar{\Gamma}) = \begin{cases} \text{const.} & \text{when } \bar{\Gamma} \geq \epsilon, \\ -\frac{1}{2} \log^2\left(\frac{\epsilon}{\bar{\Gamma}}\right) & \text{when } \epsilon \gg \bar{\Gamma}. \end{cases} \quad (3.5.12)$$

For convenience, we sum up the different logarithmic contributions to reflection and transmission in another table, table 3.4. We proceed by an analysis of the

¹¹See section 3.5.3 for the second integral over $t(\omega)$ (the expressions for t and r are exchanged in the anti-resonant case).

	Reflection	Transmission
L_1	$r t ^2$	$-t r ^2$
L_2	$-t r ^2$	$r t ^2$
L_1^2	$1/2r[t ^2(t ^2 - 2 r ^2)]$	$1/2t[r ^2(r ^2 - 2 t ^2)]$
L_2^2	$1/4(t r ^2 - r[t + t ^2(1 - 2 t ^2)])$	$-1/4(r t ^2 + t[t + t ^2(1 - 2 t ^2)])$
$L_2(L_1 - L_2)$	$t r ^2 t ^2$	$-r t ^4$
L_1L_2	$-2t r ^2 t ^2$	$-r t ^2(1 - 2 t ^2)$
P	$1/2t(1 - 2 t ^2)$	$-r t ^2$

Table 3.4: Logarithmic corrections to the S-matrix in the second order in interaction. The variable L_1 and L_2 are defined in equation (3.5.3).

corrections. The unitarity conditions up to second order in interaction read

$$|t|^2 + |r|^2 = 1 + t_0^* \delta t^{(1)} + \text{c.c.} + |\delta t^{(1)}|^2 + t_0^* \delta t^{(2)} + \text{c.c.} + r_0^* \delta r^{(1)} + \text{c.c.} + |\delta r^{(1)}|^2 + r_0^* \delta r^{(2)} + \text{c.c.} + O(\alpha^3), \quad (3.5.13)$$

$$t^*r - r^*t = t_0^* \delta r^{(1)} - \text{c.c.} + r_0(\delta t^{(1)})^* - \text{c.c.} + (\delta t^{(1)})^* \delta r^{(1)} - \text{c.c.} + t_0^* \delta r^{(2)} - \text{c.c.} + (\delta t^{(2)})^* r_0 - \text{c.c.} + O(\alpha^3), \quad (3.5.14)$$

where $\alpha = V_0/v_F$. The calculation is straightforward using table 3.4. We present the result with leading logarithmic accuracy, namely

$$|t|^2 + |r|^2 = 1 + O(\alpha^3), \quad (3.5.15)$$

$$t^*r - r^*t = -\alpha^2|t|^2P. \quad (3.5.16)$$

In the cases a.2, b and c in section 3.5.2, equation (3.5.16) is reduced to the unitary result,

$$t^*r - r^*t = 0,$$

with logarithmic accuracy.

In case a.1, the contribution P is of order \log^2 and equation (3.5.16) yields

$$tr^* - rt^* = -\alpha^2|t|^2P = \alpha^2|t|^2 \log\left(\frac{\epsilon}{\Gamma}\right) \neq 0.$$

The unitarity of the scattering matrix is violated and points towards dephasing in the system. However, this contribution is small due to the prefactor: The logarithmic contribution grows as $\epsilon/\max(\epsilon_R, \Gamma)$ but at the same time the prefactor is of the order $\Gamma/\max(\epsilon - \epsilon_R, \Gamma) \ll 1$. These non-unitary corrections are small with respect to the leading contributions. Nevertheless, this last result shows a trace of dephasing in the system.

Chapter 4

Conclusions

We have studied transport of weakly interacting electrons in a one-dimensional system with a scatterer. The strength of the scatterer in the wire is arbitrary whereas the weak repulsive interaction in the system is treated perturbatively using $T = 0$ Green's functions and a real-space diagrammatic technique. The perturbative corrections modify the two-by-two scattering (S -)matrix of the system connecting asymptotically free incoming and outgoing electrons of right- or left-moving chirality.

The main focus of our analysis was on processes violating the unitarity of the scattering matrix. Such processes, if present, can reflect dephasing or a deviation from the particle conservation for a given energy and can lead to a failure of the RG approach for the system.

We calculated the second order in interaction for a system of infinite and finite size with a simple structureless and a resonant scatterer. In the former case, the infrared energy cutoff is replaced by the Thouless energy of the system in the limit of a small system, but no traces of unitarity-violating processes could be found. In our analysis of the resonant scatterer we saw traces of dephasing in second order in the resonant case. The deviations are of order $\log^2(\epsilon/\bar{T})$ but with a small prefactor. Thus we have found only a small dephasing and the RG procedure is valid for a compound scatterer in the case of finite and infinite systems. The other leading logarithmic corrections coincide with those found in the literature for the different regimes.

Possible continuations of the project could involve an analysis of the sub-leading logarithmic or non-logarithmic corrections, the second RG loop or the third order in interaction at a finite temperature. This will allow to perform a systematic study of dephasing in such systems. Phonons can also contribute to the RG [26] and dephasing.

Alternatively, the diagrammatic approach we used can be applied straightforwardly to the investigation of various other cases, e.g., Junctions of four wires, disorder or extended scattering structures. The investigation of the latter would be an promising project better understand the recent results by Altland and Gefen [3]. For this task, the diagrammatic language can be used with other Green's function techniques, such as the Matsubara or Keldysh technique.

Appendix A

Details of calculations

A.1 The scattering matrix

The scattering matrix relates initial and final states of a scattering event [65]. Let a_o^j and a_i^j be final and initial states of N different kinds (i.e. particle nature or chirality): $j \in \{1, \dots, N\}$. Then we define:

$$\vec{a}_o = S \cdot \vec{a}_i$$

In order to conserve the probability measure we require the matrix to be unitary:

$$SS^\dagger = 1$$

The S-matrix is therefore a member of the *special unitary group* of degree N , $SU(N)$.

A.1.1 Application to the one-dimensional wire with an arbitrary impurity

For the Luttinger liquid model, we distinguish particles of different chirality: Right- and left-moving fermions. The asymptotic initial (i) and final (f) states are “free” states, since they are taken long before the scattering event ($t \rightarrow -\infty$) and far away from the interacting region ($x_{i/f} \rightarrow -\infty$). Thus we can write down the scattering matrix for our purpose in terms of Green’s functions:

$$\begin{pmatrix} G_0^+(x, x_f \rightarrow +\infty, \epsilon) \\ G_0^-(x, x_f \rightarrow -\infty, \epsilon) \end{pmatrix} = \begin{pmatrix} t_{lr}(\epsilon) & r_{ll}(\epsilon) \\ r_{rr}(\epsilon) & t_{rl}(\epsilon) \end{pmatrix} \begin{pmatrix} G_0^+(x_i \rightarrow -\infty, x, \epsilon) \\ G_0^-(x_i \rightarrow +\infty, x, \epsilon) \end{pmatrix}$$

The unitarity condition for such a matrix can be reformulated in terms of the matrix elements, namely

$$|t_{lr}|^2 + |r_{ll}|^2 = |t_{rl}|^2 + |r_{rr}|^2 = 1 \quad \text{and} \quad t_{lr}r_{rr}^* + r_{ll}t_{rl}^* = r_{rr}t_{lr}^* + t_{rl}r_{ll}^* = 0.$$

Note that we can use the two conditions to choose one of the elements. Throughout this thesis, t_{rl} is always chosen equal to t_{lr} .

A.2 Chiral Green's functions in coordinate and energy representation

Below we give expressions for the chiral Green's functions for all different cases:

$$G_{++}^0(x, y, \epsilon) = \begin{cases} \frac{t_R}{iv_F} \exp\{ip_\epsilon(y - x)\} & x < 0 \wedge y > 0 \wedge \epsilon > 0 \text{ (electron transmission)} \\ \frac{1}{iv_F} \exp\{ip_\epsilon(y - x)\} & xy > 0 \wedge y > x \wedge \epsilon > 0 \text{ (electron propagation)} \\ \frac{-t_L^*}{iv_F} \exp\{ip_\epsilon(x - y)\} & y < 0 \wedge x > 0 \wedge \epsilon < 0 \text{ (hole transmission)} \\ \frac{-1}{iv_F} \exp\{ip_\epsilon(x - y)\} & xy > 0 \wedge x > y \wedge \epsilon < 0 \text{ (hole propagation)} \end{cases} \quad (\text{A.2.1})$$

$$G_{--}^0(x, y, \epsilon) = \begin{cases} \frac{t_L}{iv_F} \exp\{ip_\epsilon(x - y)\} & y < 0 \wedge x > 0 \wedge \epsilon > 0 \text{ (electron transmission)} \\ \frac{1}{iv_F} \exp\{ip_\epsilon(x - y)\} & xy > 0 \wedge x > y \wedge \epsilon > 0 \text{ (electron propagation)} \\ \frac{-t_R^*}{iv_F} \exp\{ip_\epsilon(y - x)\} & y < 0 \wedge x > 0 \wedge \epsilon < 0 \text{ (hole transmission)} \\ \frac{-1}{iv_F} \exp\{ip_\epsilon(y - x)\} & xy > 0 \wedge y > x \wedge \epsilon < 0 \text{ (hole propagation)} \end{cases} \quad (\text{A.2.2})$$

$$G_{-+}^0(x, y, \epsilon) = \begin{cases} \frac{r_R}{iv_F} \exp\{ip_\epsilon(x + y)\} & y > 0 \wedge x > 0 \wedge \epsilon > 0 \text{ (electron reflection)} \\ \frac{-r_L^*}{iv_F} \exp\{-ip_\epsilon(x + y)\} & y < 0 \wedge x < 0 \wedge \epsilon < 0 \text{ (hole reflection)} \end{cases} \quad (\text{A.2.3})$$

$$G_{+-}^0(x, y, \epsilon) = \begin{cases} \frac{r_L}{iv_F} \exp\{-ip_\epsilon(x + y)\} & y < 0 \wedge x < 0 \wedge \epsilon > 0 \text{ (electron reflection)} \\ \frac{-r_R^*}{iv_F} \exp\{ip_\epsilon(x + y)\} & y > 0 \wedge x > 0 \wedge \epsilon < 0 \text{ (hole reflection)} \end{cases} \quad (\text{A.2.4})$$

where we used the following abbreviations:

$$p_\epsilon = \frac{|\epsilon|}{v_F} + i\eta.$$

A.3 Detailed calculation of the S-matrix in second order in interaction

We present the calculations for second order in interaction in a one-dimensional system with a structureless impurity in detail. Throughout the calculations, $\hbar = 1$ and factors of v_F are only mentioned in the final answers. The calculation is sorted by ascending number of impurity reflections. We further define

$$C_{+-}(x, y, \epsilon) = \frac{V_0^2}{v_F^2} \frac{1}{iv_F} e^{-ip_\epsilon(x+y)}, \quad (\text{A.3.1})$$

$$C_{++}(x, y, \epsilon) = \frac{V_0^2}{v_F^2} \frac{1}{iv_F} e^{ip_\epsilon(y-x)}. \quad (\text{A.3.2})$$

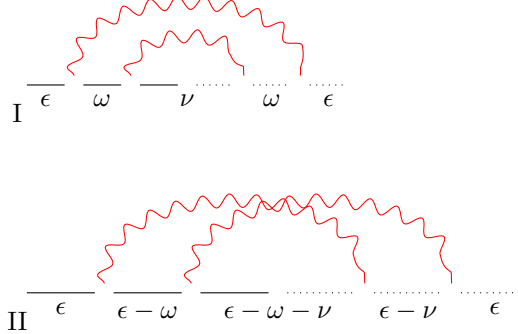


Figure A.3.1: Structure of first order diagrams

and

$$L_1 := \log^2 \left(\frac{\Delta}{\epsilon} \right). \quad (\text{A.3.3})$$

A.3.1 1 impurity reflection

The basic structure of all leading logarithmic diagrams with a single impurity reflection is shown in figure A.3.1. In figure A.3.2 all real-space scattering events of the first (“Rainbow”) type are shown.

“Rainbow diagrams”

1-I-A The first diagram in figure A.3.2 is calculated in the following. The complete expression for the correction is

$$\begin{aligned} G_{+-}^{(2)}(x, y, \epsilon)_{1-I-A} = & - \int_0^\Delta d\omega \int_0^\Delta d\nu \int_{-\infty}^0 dx_1 \int_{x_1}^0 dx_2 \int_{-\infty}^0 dx_4 \int_{x_4}^0 dx_3 \\ & \times G_{++}^0(x, x_1, \epsilon) G_{++}^0(x_1, x_2, \omega) G_{+-}^0(x_2, x_3, \nu) G_{--}^0(x_3, x_4, \omega) \\ & \times G_{--}^0(x_4, y, \epsilon) \int_{-\infty}^\infty dq \int_{-\infty}^\infty dQ \frac{V(q)}{2\pi} e^{i(x_1-x_4)q} \frac{V(Q)}{2\pi} e^{i(x_2-x_3)Q} \end{aligned}$$

Let us start with the prefactor. There is one reflection in this case so we get

$$-r$$

Then we collect all exponentials,

$$\begin{aligned} I(\epsilon, \Delta) := & \int d[\dots] \exp(i(p_\epsilon - p_\omega + q)x_1 + i(p_\omega - p_\nu + Q)x_2) \\ & \times \exp(i(-p_\nu + p_\omega - Q)x_3 + i(p_\epsilon - p_\omega - q)x_4), \end{aligned}$$

wherein every p depends on the absolute value of the energy and contains a regularizer $\pm i\eta$. After integrating over all x_i , $i \in \{1, \dots, 4\}$ (which are convergent

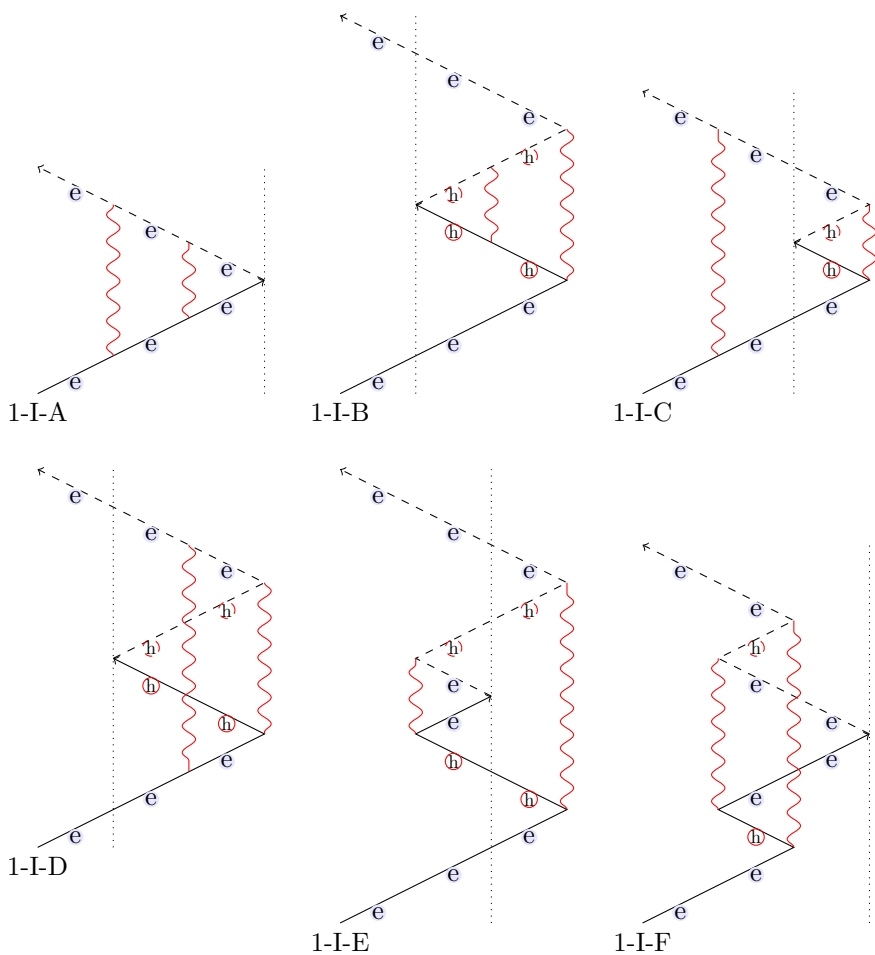


Figure A.3.2: Real-space “rainbow” diagrams with a single reflection dressed by two interactions.

integrals due to the afore mentioned regularizers) we arrive at

$$I(\epsilon, \Delta) = \int d[\dots] [(p_\epsilon - p_\omega + q)(p_\epsilon - p_\nu + q + Q)]^{-1} \\ \times [(p_\epsilon - p_\omega - q)(p_\epsilon - p_\nu - q - Q)]^{-1}.$$

We change the variable Q to $Q' = Q + q$. The interaction $V(Q)$ now depends on $V(Q' - q)$. The contour over the upper half plane is zero, because $1/q^2 \rightarrow 0$ at infinity, and we end up with

$$I(\epsilon, \Delta) = \iint d\omega d\nu \frac{-V(p_\omega - p_\epsilon)V(p_\nu - p_\omega)}{4(p_\epsilon - p_\omega)(p_\epsilon - p_\nu)}.$$

Energy integration in accordance with the first order calculations leads to the \log^2 result,

$$G_{+-}^{(2)}(x, y, \epsilon)_{1-I-A} = \frac{1}{4} r L_1 C_{+-}(x, y, \epsilon). \quad (\text{A.3.4})$$

The label of the Green's function identifies the corresponding diagram. The calculation for diagram B in figure A.3.2 is equal to diagram A.

1-I-C Let's proceed to diagram 1-I-C. We take into account two electron transmissions and one hole reflection processes. Hence the prefactor reads

$$-t(-r^*)t = -|t|^2 r.$$

The exponentials sum up to

$$I(\epsilon, \Delta) := \int d[\dots] \exp(i(p_\epsilon - p_\omega + q)x_1 + i(p_\omega + p_\nu + Q)x_2) \\ \times \exp(i(p_\nu + p_\omega - Q)x_3 + i(p_\epsilon - p_\omega - q)x_4)$$

The regularizers cut the infinities ($\text{Im}(p_\epsilon - p_\omega) = -\eta$ and $\text{Im}(p_\omega + p_\nu) = \eta$). Thus the coordinate integrals are written down at once,

$$I(\epsilon, \Delta) = \int d[\dots] [(p_\epsilon - p_\omega + q)(p_\epsilon - p_\omega - q)(p_\nu + p_\omega + Q)(p_\nu + p_\omega - Q)]^{-1}.$$

The q integration over the upper half-plane gives a prefactor i . Integrating Q yields $-i$ and there are only the energy integrals remaining, namely

$$I(\epsilon, \Delta) = \frac{1}{4} \int_0^\Delta d\omega \int_0^\Delta d\nu \frac{1}{(p_\epsilon - p_\omega)(p_\omega + p_\nu)}$$

Both fractions contain ω , the integrals are entangled. After computing the inner integral we get

$$I(\epsilon, \Delta) = \frac{1}{4} \text{PV} \int_0^\Delta d\omega \frac{1}{(\omega - \epsilon)} \log\left(\frac{\omega}{\omega + \Delta}\right) \\ = \frac{1}{4} \text{PV} \int_{-\epsilon}^\Delta d\omega' \frac{1}{\omega'} \log\left(\frac{\omega' + \epsilon}{\omega' + \Delta}\right) \\ = -\frac{1}{8} \log^2\left(\frac{\Delta}{\epsilon}\right).$$

Note that the interaction potentials are not considered explicitly in this calculation. They enter the equations when we identify the upper cutoff Δ with $\frac{v_F}{d}$. As ϵ is the small parameter, the integral behaves like

$$-\frac{1}{8} \frac{1}{v_F^2} L_1.$$

We end up with the result

$$G_{+-}^{(2)}(x, y, \epsilon)_{1\text{-I-C}} = \frac{1}{8} r |t|^2 \log^2 L_1 C_{+-}(x, y, \epsilon). \quad (\text{A.3.5})$$

Note that diagram 1-I-E has a similar structure and a different prefactor.

1-I-D The prefactor reads

$$-t(-r^*)t = -|t|^2 r.$$

The exponentials in this expression are

$$\begin{aligned} I(\epsilon, \Delta) := & \int d[\dots] \exp(i(p_\epsilon - p_\omega + q)x_1 + i(p_\omega + p_\nu + Q)x_2) \\ & \times \exp(i(p_\omega + p_\nu - Q)x_3 + i(p_\epsilon - p_\omega - q)x_4) \end{aligned}$$

Coordinate integration is done in two steps because we need to make sure that $x_2 > x_1$ and $x_3 > x_4$. We end up with

$$I(\epsilon, \Delta) = \int d[\dots] \frac{V(q)V(Q)}{[(p_\omega + p_\nu^2 - Q^2)][(p_\epsilon + p_\nu)^2 - (q + Q)^2]}$$

The integration over Q and $q' = q + Q$ gives

$$I(\epsilon, \Delta) = \int_0^\Delta d\omega d\nu \frac{-1}{4(p_\epsilon + q_\nu)(p_\omega + p_\nu)}$$

The integration over the internal energies ω and ν is similar to 1-I-C, hence

$$G_{+-}^{(2)}(x, y, \epsilon)_{ID} = \frac{1}{8} r |t|^2 L_1 C_{+-}(x, y, \epsilon). \quad (\text{A.3.6})$$

Diagram 1-I-F is similar to this diagram and the calculation is not done explicitly. Summing all rainbow diagrams with a single impurity reflection:

$$G_I = \frac{r}{8} (3 + 4|t|^2 + |t|^4) \log^2(.) C_{+-}(x, y, \epsilon) \quad (\text{A.3.7})$$

“Crossed diagrams”

Let us consider the second group of diagrams (with “crossed lines”) shown in figure A.3.3. The first two diagrams have symmetric counterparts, so their contribution doubles. This time we will outline only the important steps, as the method of choice remains the same. One important thing in this case are the borders of the energy integrals and the signs of the arguments.

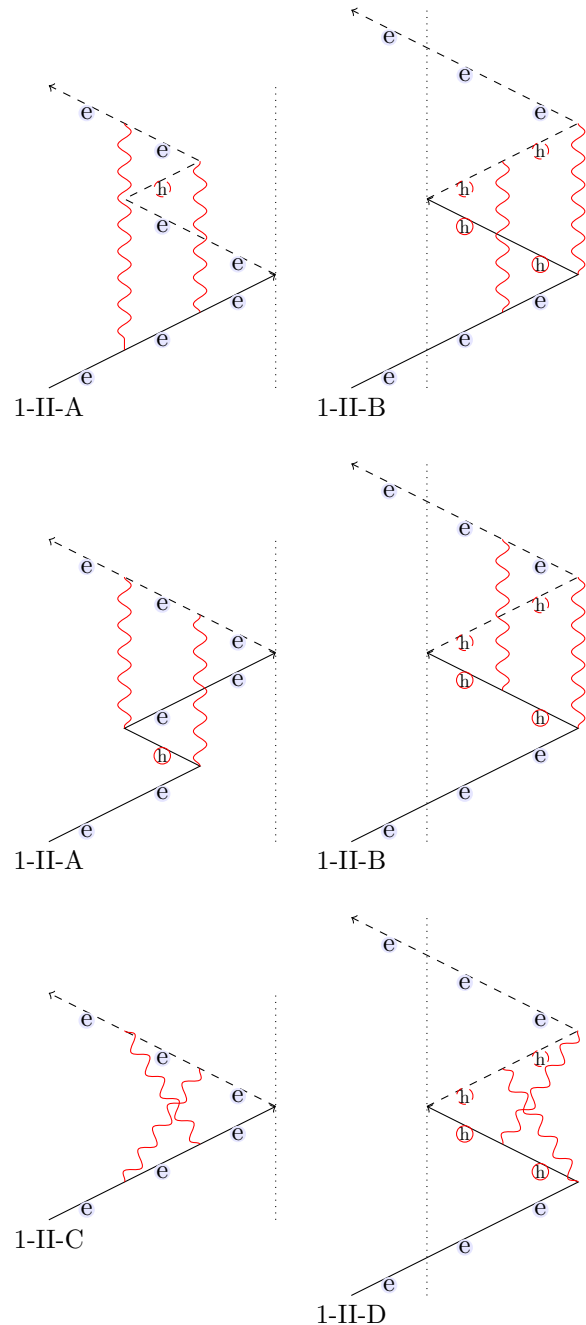


Figure A.3.3: Real-space diagrams of the “crossed lines” type with a single impurity reflection.

1-II-A The prefactor reads

$$r.$$

Note that there is one minus due to the single hole propagation Green which cancels the global minus (from i^2) in front. Diagram 1-II-A is calculated with the following integrals:

$$\begin{aligned} I(\epsilon, \Delta) = & \int_{-\Delta}^0 d\nu \int_{\epsilon}^{\epsilon-\nu} d\omega \int_{-\infty}^0 dx_1 \int_{-\infty}^{x_1} dx_2 \int_{-\infty}^0 dx_3 \int_{-\infty}^{x_3} dx_4 \\ & \times \exp[i(p_\epsilon + p_{\epsilon-\omega} + q)x_1 + i(-p_{\epsilon-\omega} - p_{\epsilon-\omega-\nu} + Q)x_2] \\ & \exp[i(-p_{\epsilon-\omega-\nu} + p_{\epsilon-\nu} - q)x_3 + i(-p_{\epsilon-\nu} + p_\epsilon - Q)x_4] \end{aligned}$$

where the borders are derived from the relations

$$\begin{aligned} \epsilon - \omega < 0 \wedge \epsilon - \omega - \nu > 0 & \implies \epsilon < \omega < \epsilon - \nu \\ \epsilon - \nu > 0 & \implies \epsilon > 0 > \nu \end{aligned}$$

After coordinate integrations we arrive at

$$\begin{aligned} I(\epsilon, \Delta) = & \int d[\dots] [(p_\epsilon - p_{\epsilon-\omega-\nu} + q')(p_\epsilon - p_{\epsilon-\omega-\nu} - q')]^{-1} \\ & \times [(-p_{\epsilon-\omega} - p_{\epsilon-\omega-\nu} + Q)(p_\epsilon - p_{\epsilon-\nu} - Q)]^{-1}, \end{aligned}$$

wherein q' and Q integration yield

$$\begin{aligned} I(\epsilon, \Delta) = & \int_0^\Delta d\nu \int_{\epsilon+\nu}^\epsilon d\omega \frac{1}{\nu(\omega-\nu)} = \int_0^\Delta d\nu \frac{\log\left(\frac{|\epsilon-\nu|}{\epsilon}\right)}{\omega} \\ = & \int_1^{\frac{\Delta}{\epsilon}} dy \frac{\log(1+y)}{y} = \frac{1}{2} \log^2\left(\frac{\Delta}{\epsilon}\right) \end{aligned}$$

We arrive at the following result:

$$G_{+-}^{(2)}(x, y, \epsilon)_{1\text{-II-A}} = -\frac{1}{4} r L_1 C_{+-}(x, y, \epsilon) \quad (\text{A.3.8})$$

We accounted for the second similar diagram in figure A.3.3 with a factor of two.

1-II-B The prefactor reads

$$-t(-1)(-r^*)t = r|t|^2.$$

We evaluate the following integrals:

$$\begin{aligned} I(\epsilon, \Delta) := & \int d[\dots] \exp(i[p_\epsilon + p_{\epsilon-\omega} + q]x_1 + i[-p_{\epsilon-\omega} + p_{\epsilon-\omega-\nu} + Q]x_2) \\ & \times \exp(i[p_{\epsilon-\omega-\nu} + p_{\epsilon-\nu} - q]x_3 + i[-p_{\epsilon-\nu} + p_\epsilon - Q]x_4) \end{aligned}$$

We derive the limits of the energy integration from the relations

$$\begin{aligned} \epsilon - \omega - \nu &< 0 \wedge \epsilon - \nu > 0 & \implies \epsilon - \omega < \nu < \epsilon, \\ \epsilon - \omega &< 0 & \implies \omega > \epsilon. \end{aligned}$$

We integrate over q and Q and end up with

$$I(\epsilon, \Delta) = - \int_{\epsilon}^{\Delta} d\omega \int_{\epsilon-\omega}^{\epsilon} d\nu \frac{1}{4} \frac{1}{\omega(\omega + \nu)}$$

The energy integration is identical to the previous paragraph.

$$G_{+-}^{(2)}(x, y, \epsilon)_{1-II-B} = -\frac{1}{4} r|t|^2 L_1 C_{+-}(x, y, \epsilon) \quad (\text{A.3.9})$$

The factor 2 arises due to the second, similar diagram in figure A.3.3.

1-II-C Diagram 1-II-C in figure A.3.3 is subleading. One can explain this result by the fact that there is no Friedel reflection taking place in this process. The integrals we need to solve read

$$\begin{aligned} I(\epsilon, \Delta) := & \int d[\dots] \exp(i[p_\epsilon - p_{\epsilon-\omega} + q]x_1 + i[p_{\epsilon-\omega} - p_{\epsilon-\omega-\nu} + Q]x_2) \\ & \times \exp(i[-p_{\epsilon-\omega-\nu} + p_{\epsilon-\nu} - q]x_3 + i[-p_{\epsilon-\nu} + p_\epsilon - Q]x_4). \end{aligned}$$

After coordinate integration we get

$$\begin{aligned} I(\epsilon, \Delta) = & \int d[\dots] [(p_\epsilon - p_{\epsilon-\omega} + q)(p_\epsilon - p_{\epsilon-\omega-\nu} + Q + q)]^{-1} \\ & \times [(p_\epsilon - p_{\epsilon-\nu} - Q)(p_\epsilon - p_{\epsilon-\omega-\nu} - Q - q)]^{-1}, \end{aligned}$$

and the integration over $Q' = Q + q$ gives

$$I(\epsilon, \Delta) = i \int d[\dots] [2(p_\epsilon - p_{\epsilon-\omega-\nu})(2p_\epsilon - p_{\epsilon-\omega-\nu} - p_{\epsilon-\nu} + q)(p_\epsilon - p_{\epsilon-\omega} + q)]^{-1}$$

Now all poles are in the lower half plane, so the contour over the upper half-plane contains only the pole i/d originating from the interaction potential V . The result is not double logarithmic. The diagram 1-II-D has a similar structure as 1-II-C.

Summary (1) We sum up all contributions with a single impurity reflection in table A.1

A.3.2 2 reflections

The structure of processes with two impurity reflections is shown in figure A.3.2. Processes of “rainbow” type I are equal to their single reflection counterparts with a slightly modified prefactor: In diagrams 1-I-B, 1-I-D and 1-I-E the last transmission is changed to a reflection. Additionally there is a factor of two because of the time-reversal symmetry. We identify the diagrams as follows:

- 1-I-B is similar to 2-I-A
- 1-I-D is similar to 2-I-B
- 1-I-E is similar to 2-I-C

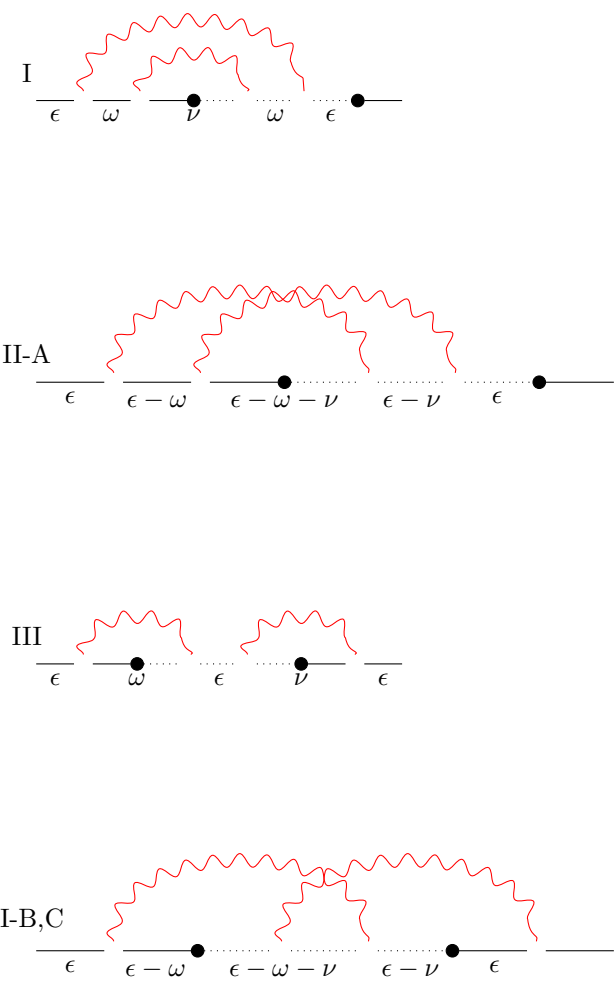


Figure A.3.4: Structure of processes with two impurity reflections.

Diagram	Prefactor	Antisym.	Result
1-I-A	$-r$	no	$\frac{1}{4}r$
1-I-B	$-r t ^2$	no	$\frac{1}{4} t ^2r$
1-I-C	$-r t ^2$	no	$\frac{1}{8}r t ^2$
1-I-D	$-r t ^2$	no	$\frac{1}{8} t ^2r$
1-I-E	$-r t ^4$	no	$\frac{1}{8} t ^4r$
1-I-F	$-r$	no	$\frac{1}{8}r$
1-II-A	r	yes	$-\frac{1}{4}r$
1-II-B	$r t ^2$	yes	$-\frac{1}{4} t ^2r$
1-II-C	—	no	0
1-II-D	—	no	0
Total	$\frac{1}{8}r(t ^4 + 2 t ^2 + 1)$		

Table A.1: Second order perturbative corrections in L_1 . The table contains all processes with a single reflection at the impurity. Antisym. labels diagrams that are not symmetric under time reversal. A second diagram can thus be drawn by inverting the arrows. The resulting diagrams are similar and double the contribution of the original diagram.

2-I Let us examine the prefactor for 2-I diagrams in figure A.3.2, namely

$$\begin{aligned} -t(-r^*)r &= t|r|^2 \\ -t(-t^*)r(-t^*)r &= t|r|^2|t|^2 \end{aligned}$$

The sign of the prefactor is reversed for all geologies in 2-I. Additionally, all second order diagrams have a time-reversed “twin”, thus we multiply these diagrams by a factor of two.

2-II-A This diagram, too, can be derived from first order in reflection (diagram 1-II-B times two) with a different prefactor,

$$-t(-1)(-r^*)r = -t|r|^2.$$

2-II-B The processes shown in figure A.3.5 are not of leading, \log^2 , order. To see this we calculate the integrals for 2-II-B explicitly. The integrals we need to evaluate read

$$\begin{aligned} I(\epsilon, \Delta) := & \int d[\dots] \exp(i(p_\epsilon - p_{\omega'} + q)x_1 + i(-p_{\omega'} + p_\Omega + Q)x_2) \\ & \times \exp(i(-p_\Omega - p_{\nu'} - q)x_3 + i(-p_{\nu'} - p_\epsilon - Q)x_4). \end{aligned}$$

We perform the coordinate integration,

$$I(\epsilon, \Delta) = - \int d[\dots] [(-p_{\omega'} - p_{\nu'} - q + Q)(p_\epsilon - p_\omega + q)]^{-1}.$$

Closing the contours for Q and q in the upper half-plane, we end up with

$$I(\epsilon, \Delta) = - \int_{-\Delta}^0 d\omega \int_{\epsilon}^{\epsilon-\omega} d\nu \frac{1}{4} \frac{1}{\omega(\omega - \nu)},$$

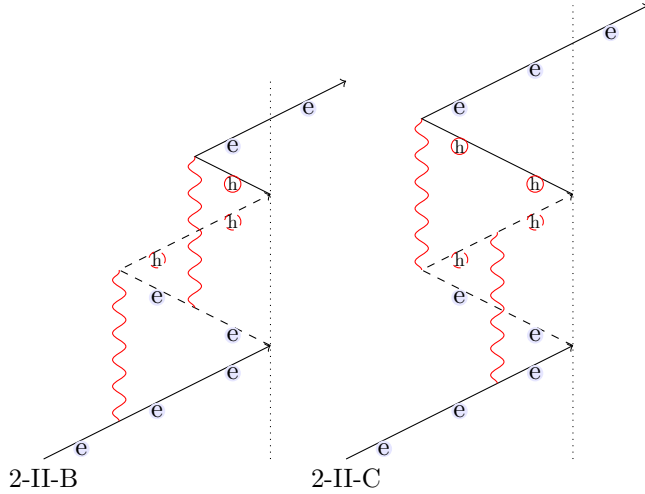


Figure A.3.5: Second order diagrams with crossed interaction lines

where we derived the borders for the energy integration using

$$\begin{aligned} \epsilon - \omega - \nu > 0 \wedge \epsilon - \nu < 0 \wedge \omega < \epsilon &\implies \epsilon < \nu < \epsilon - \omega, \\ &\implies \omega < 0. \end{aligned}$$

Integrating over ν yields

$$I(\epsilon, \Delta) = - \int_0^\Delta d\omega \frac{1}{\omega} \log \left(\frac{\epsilon + 2\omega}{\epsilon + \omega} \right).$$

This contribution is of order $\log(\Delta/\epsilon)$ and not $\log^2(\Delta/\epsilon)$. The calculation for diagram 2-II-C is similar and the result is not double-logarithmic.

2-III There are three possibilities place the two interactions and the two impurity reflections if we allow only diagrams of the “double Fock” type (see figure A.3.6).

2-III-A The prefactor reads

$$-t^3(-r^*)^2 = t|r|^2|t|^2.$$

The two parts of the diagram can be taken from the first order. We split the independent integrals in two parts,

$$G_{++}^{(2)}(x, y, \epsilon)_{2-\text{III-A}} = t|r|^2|t|^2 C_{++}(x, y, \epsilon) I_1(\epsilon, \Delta) I_2(\epsilon, \Delta).$$

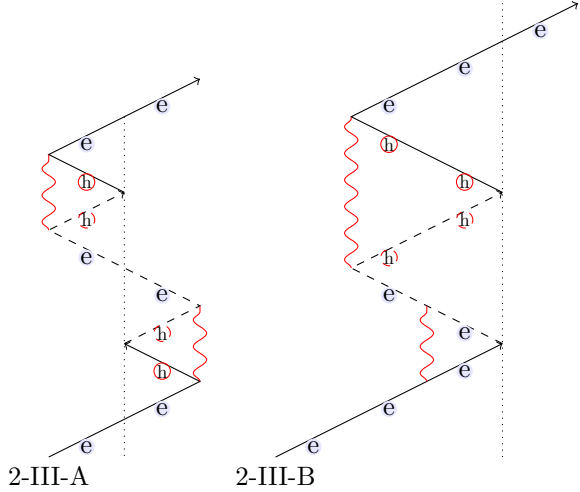


Figure A.3.6: Two interactions in a row dressing two impurity reflections

Compare section 3.2.2 for the detailed calculations. The first part is evaluated as follows:

$$\begin{aligned} I_1(\epsilon, \Delta) &= \int_0^\infty dx_1 \int_0^\infty dx_2 \int_{-\infty}^\infty d\omega \int_{-\infty}^\infty dq \frac{V(q)}{2\pi} \\ &\times \exp[i p_\epsilon(x_1 - x) + i p_\omega(x_1 + x_2) + i p_\epsilon(x_2 - x_3) + i q(x_1 - x_2)] \\ &= i V_0 v_F \frac{1}{2} \log\left(\frac{v_F}{d\epsilon}\right) \frac{e^{-ip_\epsilon(x_3+x)}}{iv_F}, \end{aligned}$$

and the second part reads

$$\begin{aligned} I_2(\epsilon, \Delta) &= \int_{-\infty}^0 dx_3 \int_{-\infty}^0 dx_4 \int_{-\infty}^\infty d\nu \int_{-\infty}^\infty dQ \frac{V(q)}{2\pi} \\ &\times \exp[-i p_\epsilon(x_3 + x) - i p_\nu(x_3 + x_4) + i p_\epsilon(y - x_4) + i q(x_3 - x_4)] \\ &= i V_0 v_F \frac{1}{2} \log\left(\frac{v_F}{d\epsilon}\right) \frac{e^{ip_\epsilon(y-x)}}{iv_F}. \end{aligned}$$

Together with the prefactor, we arrive at the expression

$$G_{++}^{(2)}(x, y, \epsilon)_{2\text{-III-A}} = -\frac{1}{4} t |t|^2 |r|^2 L_1 C_{++}(x, y, \epsilon). \quad (\text{A.3.10})$$

2-III-B The prefactor is evaluated from figure A.3.6:

$$-r(-r^*)t = |r|^2 t.$$

We identify the exponential contributions in the integral, namely

$$\begin{aligned} I(\epsilon, \Delta) &:= \int d[\dots] \exp(i(p_\epsilon - p_\omega + q)x_1 + i(-p_\omega + p_\epsilon - q)x_2) \\ &\times \exp(i(-p_\epsilon - p_\nu + Q)x_3 + i(-p_\nu - p_\epsilon - Q)x_4). \end{aligned}$$

Diagram	similar to	Prefactor	Antisym.	Result
2-I-A	1-I-B	$t r ^2$	yes	$-\frac{1}{2} r ^2t$
2-I-B	1-I-D	$t r ^2$	yes	$-\frac{1}{4} r ^2t$
2-I-C	1-I-E	$t r ^2 t ^2$	yes	$-\frac{1}{4}t r ^2 t ^2$
2-II-A	1-II-B	$-t r ^2$	twice	$\frac{1}{2} r ^2t$
2-II-B	—	—	yes	not \log^2
2-II-C	—	—	yes	not \log^2
2-III-A	—	$t r ^2 t ^2$	no	$-\frac{1}{4} r ^2 t ^2t$
2-III-B	—	$t r ^2$	yes	$-\frac{1}{4} r ^2t$
Total		$-\frac{1}{2}t r ^2(1+ t ^2)$		

Table A.2: Corrections in second order in interaction, L_1 . In the table, processes with two reflections at the impurity are listed.

We integrate over the coordinates x_1 to x_4 ,

$$I(\epsilon, \Delta) = \int d[\dots] [(-p_\epsilon - p_\nu + Q)(-p_\epsilon - p_\nu - Q)]^{-1} \\ \times [(-p_\omega - p_\nu + Q - q)(p_\epsilon - p_\omega + q)]^{-1}.$$

After Q and q integration only the integrals over the energy variables are remaining and we get

$$I(\epsilon, \Delta) = \int_0^\Delta d\omega d\nu \frac{-1}{4(p_\epsilon + p_\nu)(p_\omega + p_\nu)}.$$

The result reads

$$G_{++}^{(2)}(x, y, \epsilon)_{2-III-B} = -\frac{1}{4}t|r|^2 L_1 C_{++}(x, y, \epsilon). \quad (\text{A.3.11})$$

The factor of two is used to account for a second, similar diagram that can be constructed by inverting the direction of the particles and holes.

Summary(2) All contributions of second order in reflection are collected in table A.2.

A.3.3 3 reflections

The processes with 3 reflections have the structure shown in figure A.3.3.

3-I-A,B,C Compared to 2-I-A to C there is just one transmission replaced by a reflection. The diagram is invariant under time-inversion, therefore do not need the factor of two from the previous section.

3-I-D The calculation is very similar to the previous cases. We identify the prefactor from figure A.3.8,

$$-r(r^*)^2 t^2 = r|t|^2|r|^2,$$

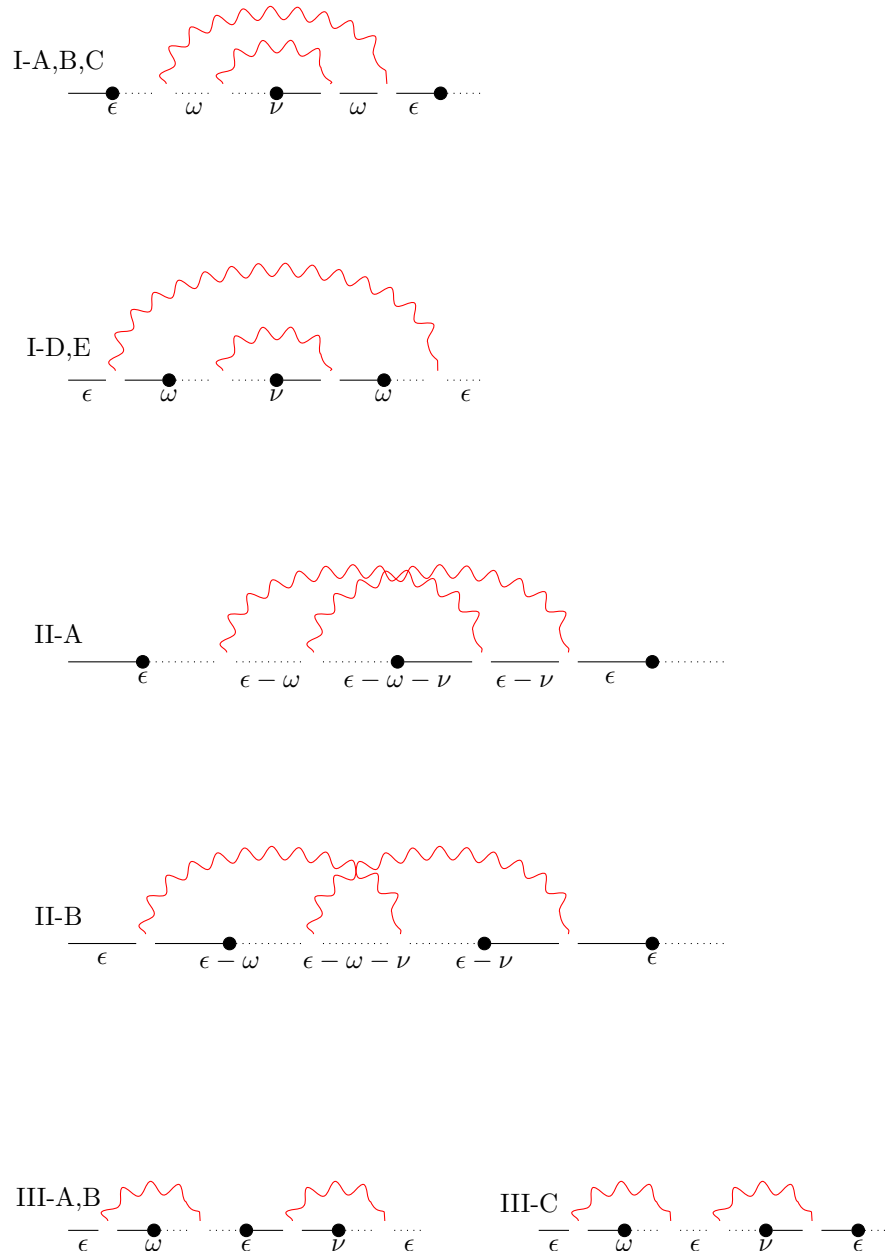


Figure A.3.7: Structure of processes with three impurity reflections.

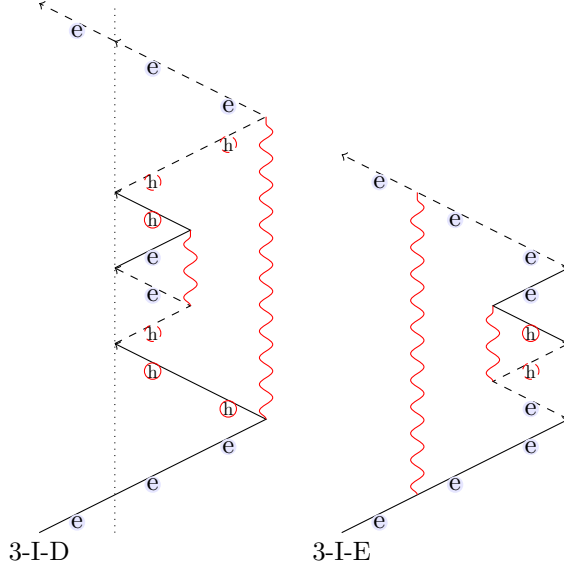


Figure A.3.8: Processes of third order in reflection with parallel interaction lines.

and perform all but the energy integrals at once, being left with

$$\begin{aligned} I(\epsilon, \Delta) &= \int_0^\Delta d\omega \int_0^\Delta d\nu \frac{-1}{4(\epsilon + \omega)(\nu + \omega)} \\ &= -\frac{1}{8} \log^2 \left(\frac{\Delta}{\epsilon} \right). \end{aligned}$$

The result reads

$$G_{+-}^{(2)}(x, y, \epsilon)_{3\text{-I-D}} = -\frac{1}{8} r |t|^2 |r|^2 L_1 C_{+-}(x, y, \epsilon). \quad (\text{A.3.12})$$

Diagram 3-I-E is similar to 3-I-D.

3-II These, too, can be derived from first or second order. See 2-II.

3-III Considering all restrictions, there are three diagrams (figure A.3.9) with the interactions one after another.

3-III All diagrams in 3-III are, except for the prefactor, equal to 2-III.

Summary(3) All contributions of third order in reflection are listed in table A.3.

A.3.4 4 reflections

For the case of four impurity reflections, we can identify all diagram classes from the previous order. Because there is no new calculation involved ¹, we present

¹Note that there is just a reflection added on one of two sides.

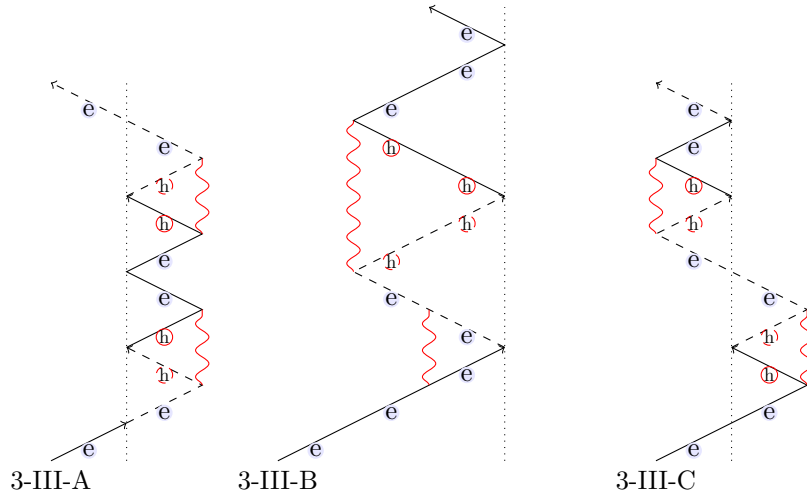


Figure A.3.9: Processes of third order in impurity reflection

Diagram	similar to	Prefactor	Antisym.?	Result
3-I-A	2-I-A	$r r ^2$	no	$-\frac{1}{4} r ^2 r$
3-I-B	2-I-B	$r r ^2$	no	$-\frac{1}{8} r ^2 r$
3-I-C	2-I-C	$r r ^2 t ^2$	no	$-\frac{1}{8}r r ^2 t ^2$
3-I-D	-	$r t ^2 r ^2$	no	$-\frac{1}{8}r t ^2 r ^2$
3-I-E	-	$r r ^2$	no	$-\frac{1}{8}r r ^2$
3-II-A	1-II-B	$-r r ^2$	no	$\frac{1}{4} r ^2 r$
3-II-B	-	-	no	not \log^2
3-III-A	2-III-A	$r r ^2 t ^2$	no	$-\frac{1}{4} r ^2 t ^2 r$
3-III-B	2-III-B	$r r ^2$	yes	$-\frac{1}{4} r ^2 r$
3-III-C	2-III-A	$r r ^2 t ^2$	yes	$-\frac{1}{2} r ^2 t ^2 r$
Total		$-\frac{1}{2}r r ^2(1 + 2 t ^2)$		

Table A.3: Diagrams in the second order (L_1) with three reflections at the impurity.

Diagram	similar to	Prefactor	Antisym.?	Result
4-I-A	3-I-D	$-t r ^4$	yes	$\frac{1}{4} r ^4 t$
4-III-A	3-III-A	$-t r ^4$	yes	$\frac{1}{2} r ^4 t$
4-III-B	3-III-C	$-t r ^4$	no	$\frac{1}{4} r ^4$
Total		$ r ^4 t$		

Table A.4: Results for diagrams in L_1 with four impurity reflections.

Diagram	similar to	Prefactor	Antisym.?	Result
5-I-A	3-I-D	$-r r ^4$	no	$\frac{1}{8} r ^4 r$
5-II-A	3-II-B	—	—	no \log^2
5-III-A	3-III-A	$-r r ^4$	no	$\frac{1}{4} r ^4 r$
Total		$\frac{3}{8} r ^4 r$		

Table A.5: Results for diagrams in L_1 with five impurity reflections.

the contribution of the fourth order in table A.4. There is no diagram with crossed interaction lines and four reflections.

A.3.5 5 reflections

The results for the perturbative corrections in interaction with five reflections at the impurity are presented in table A.5.

A.4 Second scale calculation using pole integrations methods

In this section we revisit the case of a finite interacting region of width L in an one-dimensional wire with a single pointlike scatterer.

Center of mass dependent interaction with smooth cutoff

The potential used in the following depends on both the difference and the sum of the coordinates. The potential reads

$$V(x_1, x_2) = \frac{V_0}{4dL} e^{-\frac{|x_1-x_2|}{d}} e^{-\frac{|x_1+x_2|}{L}}, \quad (\text{A.4.1})$$

$$V(q, q') = \frac{V_0}{L^2 d^2} \frac{1}{(q'^2 + 1/L^2)(q^2 + 1/d^2)}, \quad (\text{A.4.2})$$

$$V(x_2, x_2) = \int_{-\infty}^{\infty} dq \int_{-\infty}^{\infty} dq' \frac{1}{4\pi^2} V(q, q') e^{iq(x_1-x_2)} e^{iq'(x_1+x_2)}, \quad (\text{A.4.3})$$

where we use the latter in the calculations. $V(q, q')$ has two poles in each half-plane and for $q, q' \rightarrow \infty$ it behaves like $q^{-2} q'^{-2} \rightarrow 0$.

A.4.1 First order in interaction

Let's see how the additional scale enters the calculations. For diagram 2-I-A (see figure 3.2.3 on page 57) we evaluate,

$$G_{++}^{(1)}(x, y, \epsilon)_{\text{2-I-A}} = i \int_0^\infty d\omega \int_0^\infty dx_1 \int_0^\infty dx_2 G_{++}^0(x, x_1, \epsilon) \\ \times G_{+-}^0(x_1, x_2, \omega) G_{-+}^0(x_2, y, \epsilon) V(x_1, x_2),$$

where the prefactors

$$it|r|^2 A(x, y, \epsilon),$$

remain unaltered (compare with section 3.2.1) and

$$A(x, y, \epsilon) = \frac{V_0}{v_F} \frac{1}{iv_F} e^{ip_\epsilon(y-x)},$$

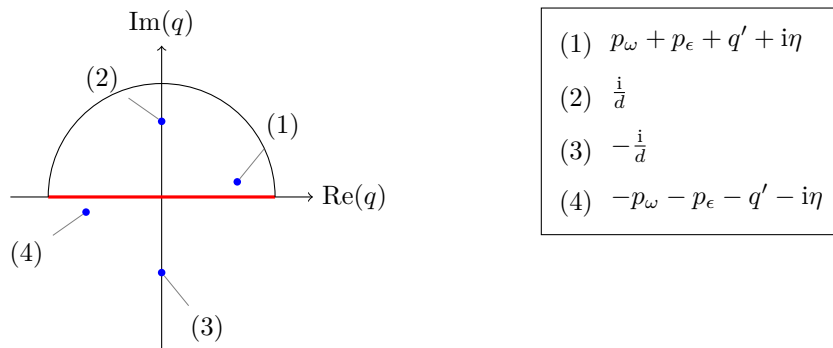
as defined previously. The integrals become

$$I(\epsilon, \Delta, E_{\text{Th}}) := \int d[\dots] \exp[i(p_\epsilon + p_\omega + q + q')x_1 + i(p_\epsilon + p_\omega - q + q')x_2].$$

Thus we get after coordinate integration

$$I(\epsilon, \Delta, E_{\text{Th}}) = \int_0^\Delta d\omega \int_{-\infty}^\infty dq \int_{-\infty}^\infty dq' \frac{-V(q, q')}{(p_\epsilon + p_\omega + q + q')(p_\epsilon + p_\omega - q + q')}.$$

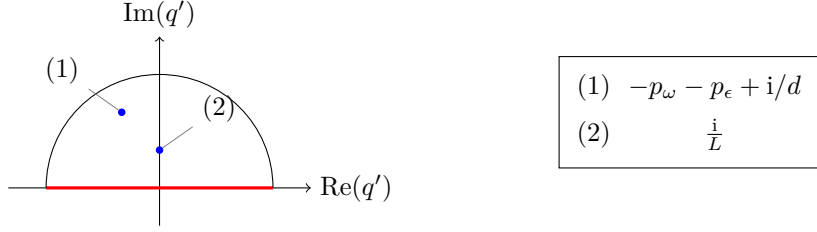
We encounter the following pole structure for q :



Closing the contour over the upper half q -plane yields

$$I(\epsilon, \Delta, E_{\text{Th}}) = \int_0^\Delta d\omega \int_{-\infty}^\infty dq' \frac{i}{2(p_\omega + p_\epsilon + q')} \frac{1}{[(p_\epsilon + p_\omega + q')^2 + 1/d^2]} \frac{1}{[q'^2 + 1/L^2]} \\ - \frac{i}{[(p_\epsilon + p_\omega + q')^2 + 1/d^2]} \frac{1}{2i/d[q'^2 + 1/L^2]}$$

The terms in the sum have the following pole structure in the upper half q' -plane:



We have to discuss each resulting integral concerning its log behavior. Inserting the $-p_\epsilon - p_\omega + i/d$ pole in the first term the length scale of the interaction will cut the integral from below because $\frac{1}{d} \gg \frac{1}{L}$. The same situation occurs for the contributions coming from both the $-p_\epsilon - p_\omega + i/d$ and the i/L pole of the second term. The i/L pole of the first term yields

$$\begin{aligned} I(\epsilon, \Delta, E_{\text{Th}}) &= \int_0^\Delta d\omega \frac{-L}{4i(p_\omega + p_\epsilon + i/L)[(p_\omega + p_\epsilon + i/L)^2 + 1/d^2]} \\ &= \int_0^\Delta d\omega \frac{-L^4}{4i(\frac{L\omega}{v_F} + \frac{L\epsilon}{v_F} + i)[(\frac{L\omega}{v_F} + \frac{L\epsilon}{v_F} + i)^2 + L^2/d^2]}. \end{aligned}$$

After a substitution the integral reads

$$\begin{aligned} I(\epsilon, \Delta, E_{\text{Th}}) &= \frac{-L^4}{4i} \int_{\frac{L\epsilon}{v_F}}^{\frac{L\Delta}{v_F}} d\Omega \frac{1}{(\Omega + i)^2 + \frac{L^2}{d^2}(\Omega + i)} \\ &\approx \frac{-L^4}{4i} \int_{\frac{L\epsilon}{v_F}}^{\frac{L\Delta}{v_F}} d\Omega \frac{1}{\frac{L^2}{d^2}(\Omega + i)} \\ &= \begin{cases} \frac{i}{4} \log\left(\frac{\Delta}{E_{\text{Th}}}\right) & \text{if } \frac{L\epsilon}{v_F} \ll 1 \\ \frac{i}{4} \log\left(\frac{\Delta}{\epsilon}\right) & \text{if } \frac{L\epsilon}{v_F} \gg 1 \end{cases}. \end{aligned}$$

Including the prefactor we get for 2-I-A

$$G_{++}^{(1)}(x, y, \epsilon)_{\text{2-I-A}} = -t|r|^2 \frac{1}{4} A(x, y, \epsilon) \log\left(\frac{\Delta}{E_{\text{Th}}, \epsilon}\right)$$

The same procedure can be repeated for all first order calculations.

A.4.2 Second order

Calculations for the second order get much more involved due to the greater number of poles in the propagators. Nevertheless the same techniques can be applied to single out the logarithmic contributions. We define

$$C_{+-}(x, y, \epsilon) = \frac{1}{v_F^4} e^{ip_\epsilon(x+y)} \frac{V_0^2}{d^4 L^4}. \quad (\text{A.4.4})$$

Example: Diagram 1-I-B

We follow the same step-by-step procedure in calculating the Diagram 1-I-B (compare section A.3). The complete expression for the propagator reads

$$G_{+-}^{(2)}(x, y, \epsilon)_{1-I-B} = - \int_0^\infty d\omega \int_0^\infty d\nu \int_0^\infty dx_1 \int_0^\infty dx_2 \int_0^\infty dx_3 \int_0^\infty dx_4 G_{++}^0(x, x_1, \epsilon) \\ \times G_{++}^0(x_1, x_2, \omega) G_{+-}^0(x_2, x_3, \nu) G_{--}^0(x_3, x_4, \omega) G_{--}^0(x_4, y, \epsilon) \\ \times V(x_1, x_4) V(x_2, x_3),$$

where the momentum representations for the interaction potentials V are not yet included. Note furthermore that there is an overall minus in front due to the expansion of the S-Matrix (see [2]). The prefactor

$$-t^2(-r^*) C_{+-}(x, y, \epsilon)$$

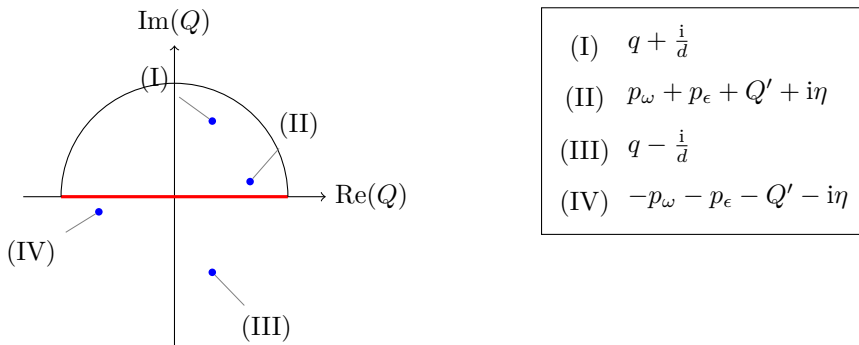
is kept aside and added to the final expression. The argument of the exponential reads

$$I(\epsilon, \Delta, E_{\text{Th}}) := \int d[\dots] \exp[i(p_\epsilon + p_\omega + q + q')x_1 + i(-p_\omega + p_\nu + Q + Q')x_2] \\ \times \exp[i(p_\nu - p_\omega + Q' - Q)x_3 + i(p_\epsilon + p_\omega + q' - q)x_4]$$

We have chosen q, q' as arguments of the first potential and Q, Q' of the second respectively. The coordinate integration is straightforward and we are left with:

$$I(\epsilon, \Delta, E_{\text{Th}}) = \int_{-\infty}^\infty dq' \int_{-\infty}^\infty dq \int_{-\infty}^\infty dQ' \int_{-\infty}^\infty dQ \\ \times \frac{V(q, q')V(Q - q, Q' - q')}{[(p_\epsilon + p_\nu + Q')^2 - Q^2][(p_\epsilon + p_\omega + q')^2 - q^2]}$$

without the energy integrals and with Q shifted to $Q + q$ and Q' to $Q' + q'$. The integrals will be computed in the given order. The pole structure with respect to Q reads:

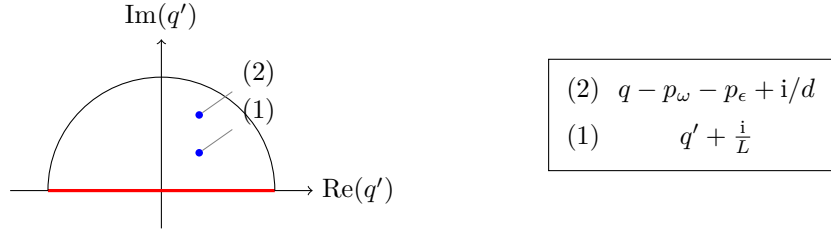


Integrating over Q and closing the contour in the upper half plane leads to two terms I_I and I_{II} , one for each pole.

(I): $Q = q + i/d$

$$I_I := \int d[\dots] \frac{iV(q, q')}{[(p_\epsilon + p_\omega + Q')^2 - (q + i/d)^2]2(q + i/d)[(Q' - q')^2 + 1/L^2]}$$

In the following, integration will be done always over the upper half-plane, therefore the poles in the lower plane will not be mentioned explicitly. Integrating over Q' will involve the following poles:



Pole (1) yields

$$I_{I.1} = \int d[\dots] \frac{-V(q, q')}{[(p_\epsilon + p_\nu + q' + i/L)^2 + (q + i/d)^2]2(q + i/d)2(q' + i/L)}.$$

The only upper half-plane pole for q of this term is i/d . If we perform this integration, the result is clearly non-logarithmic because every term in the denominator contains i/d with the only exception of the denominator of the interaction potential $V(q, q')$ for q' . But inserting the i/L pole for q' we are left with terms all containing i/d . Pole (2) yields

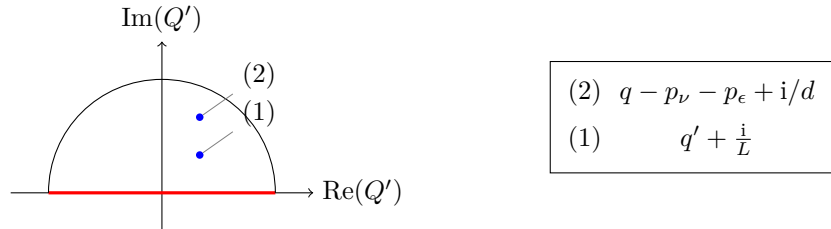
$$I_{I.2} = \int d[\dots] \frac{-V(q, q')}{4(q + i/d)^2[(q - q' - p_\epsilon - p_\nu + i/d)^2 + 1/L^2]}.$$

There is only one pole in the upper half-plane for q : $q = i/d$. The argument is the same as in the previous case: The resulting energy integral is not logarithmic, because every term in the denominator contains the inverse interaction length d which is related to an energy exceeding the integration variables ν and ω by far.

(II): $Q = p_\epsilon + p_\nu + Q'$ The second pole in the Q plane is evaluated as

$$I_{II.1} = - \int [\dots] iV(q, q') [2(p_\epsilon + p_\nu + Q')[(p_\epsilon + p_\omega + q')^2 - q^2]^{-1} \\ \times [(p_\epsilon + p_\nu + Q' - q)^2 + 1/d^2][(Q' - q')^2 + 1/L^2]^{-1}$$

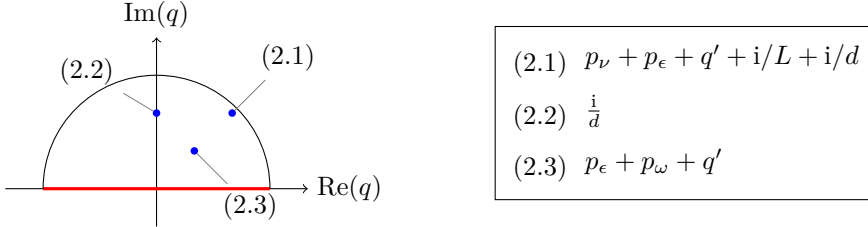
We encounter the following pole structure for Q' in the upper half-plane:



We can now repeat the arguments used above and find that pole (1) yields only contributions of sub-leading order. Let us have a look at the (2) pole in the $Q' = q' + i/L$ plane. We end up with the following expression

$$I_{II.2} = \int [\dots] \frac{V(q, q')}{2(p_\epsilon + p_\nu + q' + i/L)[(p_\epsilon + p_\nu + q' - q + i/L)^2 + 1/d^2]} \\ \times \frac{1}{2i/L[(p_\epsilon + p_\omega + q')^2 - q^2]}.$$

This results in three poles in the upper q half-plane:



The first two poles (2.1) and (2.2) are not of leading logarithmic order while the third one yields

$$I_{II.2.3} = \int d[\dots] \frac{-i}{8i/L(p_\epsilon + p_\nu + q' + i/L)[(p_\nu - p_\omega + i/L)^2 + 1/d^2]} \\ \times \frac{1}{(p_\epsilon + p_\omega + q') \underbrace{[(p_\epsilon + p_\omega + q')^2 + 1/d^2]}_{q' = -p_\epsilon - p_\omega + i/d} \underbrace{(q'^2 + 1/L^2)}_{q' = i/L}}$$

The first pole is not logarithmic. The second pole in the upper half-plane ($q' = i/L$) yields:

$$I_{\text{lead.}} = - \iint d\omega d\nu [16/L^2(p_\epsilon + p_\nu + 2i/L)(p_\epsilon + p_\omega + i/L) \\ \times [(p_\epsilon - p_\omega + i/L)^2 + 1/d^2][(p_\epsilon + p_\omega + i/L)^2 + 1/d^2]^{-1} \\ \approx \iint d\omega d\nu \frac{-d^4 L^4}{16[\frac{L}{v_F}(\epsilon + \nu) + 2i][\frac{L}{v_F}(\epsilon + \omega) + i]}$$

The last result is clearly of order \log^2 and repeating the reasoning for the first order we arrive at

$$G_{+-}^{(2)}(x, y, \epsilon)_{2\text{-I-B}} = \frac{r|t|^2}{16} C_{+-} \log^2 \left(\frac{\Delta}{\max(E_{Th}, \epsilon)} \right) \quad (\text{A.4.5})$$

Comparing this result to the calculation done before with infinite range of interaction, we see that apart from the prefactor the result is the same.

A.5 Check of the unitarity of the S-matrix in various cases

A.5.1 Inside a symmetric resonant level

The perturbative corrections read

$$\delta t(\epsilon) = \frac{V_0}{v_F} [-t(\epsilon)|r(\epsilon)|^2 + r(\epsilon)|t(\epsilon)|^2] \log\left(\frac{\Delta}{\max(\Gamma, \epsilon_R)}\right) \quad (\text{A.5.1})$$

$$\delta r(\epsilon) = \frac{V_0}{v_F} [r(\epsilon)|t(\epsilon)|^2 - t(\epsilon)|r(\epsilon)|^2] \log\left(\frac{\Delta}{\max(\Gamma, \epsilon_R)}\right) \quad (\text{A.5.2})$$

We already calculated the transmission probability $|t^{(1)}|^2$:

$$\begin{aligned} |t^{(1)}(\epsilon)|^2 &= |t|^2 + t^*(\epsilon)\delta t + t(\epsilon)\delta t^* \\ &= |t|^2 - 2|t|^2|r|^2 + 2|t|^2\Re(r^*t) \end{aligned}$$

The absolute value of the reflection amplitude reads:

$$\begin{aligned} |r^{(1)}(\epsilon)|^2 &= |r|^2 + r^*(\epsilon)\delta r + r(\epsilon)\delta r^* \\ &= |r|^2 + 2|t|^2|r|^2 - 2|r|^2\Re(r^*t) \end{aligned}$$

where

$$\Re(r^*t) = \Re\left(\frac{-i\Gamma(\epsilon - \epsilon_R)}{\Gamma^2 + (\epsilon - \epsilon_R)^2}\right) = 0$$

We conclude that the condition

$$|t^{(1)}|^2 + |r^{(1)}|^2 = 1$$

is satisfied.

The second condition reads

$$t^{(1)}(r^{(1)})^* + (t^{(1)})^*r^{(1)} = tr^* + rt^* + \Re(t\delta r^*) + \Re(r\delta t^*) = 0$$

The first two summands cancel by construction. The remainings yield:

$$\Re(t\delta r^*) + \Re(r\delta t^*) = \Re(-|t|^2|r|^2 + tr^*|t|^2) + \Re(|t|^2|r|^2 - rt^*|r|^2) = 0$$

A.5.2 Resonant scatterer with broken spacial symmetry

In this section we consider the more complex case where the energy of the external particle is in the range of the resonant level ($\log(\Delta/\Gamma) \gg \log(\Gamma/\epsilon)$). The corrections due to interaction read:

$$\begin{aligned} \delta t(\epsilon) &= -t(\epsilon)|r_L(\epsilon)|^2 + \frac{|t(\epsilon)|^2}{2\sqrt{\Gamma_R\Gamma_L}} (\Gamma_L r_R(\epsilon) + \Gamma_R r_L(\epsilon)) \log\left(\frac{\Delta}{\Gamma_m}\right) \\ \delta r_L(\epsilon) &= \left[r_L(\epsilon)|t(\epsilon)|^2 - \frac{t(\epsilon)}{2\sqrt{\Gamma_R\Gamma_L}} (\Gamma_R(1 + r_L r_R^*) - \Gamma_L|t|^2) \right] \log\left(\frac{\Delta}{\Gamma_m}\right) \\ \delta r_R(\epsilon) &= \left[r_R(\epsilon)|t(\epsilon)|^2 - \frac{t(\epsilon)}{2\sqrt{\Gamma_R\Gamma_L}} (\Gamma_L(1 + r_R r_L^*) - \Gamma_R|t|^2) \right] \log\left(\frac{\Delta}{\Gamma_m}\right) \end{aligned}$$

We start with the condition $|t|^2 + |r_L|^2 = 1$. In the following we write all amplitudes without the explicit energy dependence:

$$\begin{aligned}
 |t^{(1)}|^2 &= |t|^2 + \delta t^* t + \delta t t^* \\
 &= |t|^2 + \left(-2|t|^2 |r_L|^2 + \frac{|t|^2}{\sqrt{\Gamma_L \Gamma_R}} [\Gamma_L \operatorname{Re}(r_R^* t) + \Gamma_R \operatorname{Re}(r_L^* t)] \right) \\
 |r_L^{(1)}|^2 &= |r_L|^2 + \delta r_L r_L^* + \delta r_L^* r_L \\
 &= |r_L|^2 + 2|t|^2 |r_L|^2 \\
 &\quad + \frac{1}{\sqrt{\Gamma_L \Gamma_R}} (\Gamma_L |t|^2 \operatorname{Re}(r_L^* t) - \Gamma_R (|r_L|^2 \operatorname{Re}(t r_L^*) + \operatorname{Re}(t r_L^*)))
 \end{aligned}$$

One can show that $\operatorname{Re}(r_L^* t) = -\operatorname{Re}(r_R^* t)$. Using this property we can rewrite $|r_L^{(1)}|^2$:

$$\begin{aligned}
 &= |r_L|^2 + 2|t|^2 |r_L|^2 + \frac{1}{\sqrt{\Gamma_L \Gamma_R}} (-\Gamma_L |t|^2 \operatorname{Re}(r_R^* t) + \Gamma_R ((|r_L|^2 - 1) \operatorname{Re}(t r_L^*))) \\
 &= |r_L|^2 + 2|t|^2 |r_L|^2 + \frac{|t|^2}{\sqrt{\Gamma_L \Gamma_R}} (-\Gamma_L \operatorname{Re}(r_R^* t) - \Gamma_R \operatorname{Re}(t r_L^*)) \quad \text{q.e.d}
 \end{aligned}$$

The second condition reads:

$$t^{(1)}(r_L^{(1)})^* + r_R^{(1)}(t^{(1)})^* = \underbrace{tr_L^* + t^* r_R + t \delta r_L^* + r_L^* \delta t + r_R \delta t^* + \delta r_R t^*}_0 = 0$$

$$\begin{aligned}
 t \delta r_L^* + r_L^* \delta t &= \left(tr_L^* |t|^2 - \frac{|t|^2}{\sqrt{\Gamma_R \Gamma_L}} (\Gamma_R (1 + r_L^* r_R) - \Gamma_L |t|^2) \right) \\
 &\quad + \left(-tr_L^* |r_L|^2 + \frac{|t|^2}{\sqrt{\Gamma_R \Gamma_L}} (\Gamma_R |r_L|^2 + \Gamma_L r_L^* r_R) \right) \\
 &= tr_L^* (|t|^2 - |r_L|^2) + \frac{|t|^2}{\sqrt{\Gamma_R \Gamma_L}} (\Gamma_R (-|t|^2 - r_L^* r_R) + \Gamma_L (r_L^* r_R + |t|^2))
 \end{aligned}$$

$$\begin{aligned}
 t^* \delta r_R + r_R \delta t^* &= \left(-t^* r_R |r_L|^2 + \frac{|t|^2}{\sqrt{\Gamma_R \Gamma_L}} (\Gamma_L |r_R|^2 + \Gamma_R r_R r_L^*) \right) \\
 &\quad + \left(t^* r_R |t|^2 - \frac{|t|^2}{\sqrt{\Gamma_R \Gamma_L}} (\Gamma_L (1 + r_R r_L^*) - \Gamma_R |t|^2) \right) \\
 &= t^* r_R (|t|^2 - |r_L|^2) \\
 &\quad + \frac{|t|^2}{\sqrt{\Gamma_R \Gamma_L}} (\Gamma_R (|t|^2 + r_L^* r_R) + \Gamma_L (-r_L^* r_R - |t|^2))
 \end{aligned}$$

Thus we see that in the first order in interaction for a asymmetric close-to-resonance setting, the unitarity of the S-matrix is conserved.

A.6 Example calculations for an energy-dependent S-matrix in second order

We show exemplary calculations for rainbow diagrams and such with crossed lines. The integration over the internal coordinates remains unaffected by the modification and we can start directly by calculating the integrals over the internal energies.

A.6.1 Rainbow diagram: 1-I-E

1-I-E We separate the signs and constants in front,

$$t^2(\epsilon) \frac{C_{+-}(x, y, \epsilon)}{4},$$

The energy integrals derived from the diagram in figure A.3.2 are combined with the internal, energy-dependent S-matrix elements.

$$I(\epsilon, \Delta, \epsilon_R, \Gamma) := \int_0^\Delta d\omega \int_0^\Delta d\nu \frac{[t^*(-\omega)]^2 r(\nu)}{(\omega + \nu)(\epsilon + \omega)}$$

We integrate first over ν :

$$\begin{aligned} I(\epsilon, \Delta, \epsilon_R, \Gamma) &= \int_0^\Delta d\omega \int_0^\Delta d\nu \frac{[t^*(-\omega)]^2 r(\nu)}{(\omega + \nu)(\epsilon + \omega)} \\ &= \frac{[t^*(-\omega)]^2}{(\epsilon + \omega)} (r(-\omega) \log(\Delta/\omega) - t(-\omega) \log(\Delta/\bar{\Gamma})) \end{aligned}$$

where we used the results of our previous calculations in section 3.5.3. The integration over the second internal energy variable yields

$$\begin{aligned} I(\epsilon, \Delta, \epsilon_R, \Gamma) &= \int_0^\Delta d\omega \frac{[t^*(-\omega)]^2}{(\epsilon + \omega)} (r(-\omega) \log(\Delta/\omega) - t(-\omega) \log(\Delta/\bar{\Gamma})) , \\ &:= A - B \end{aligned}$$

whereby we split the calculation in two parts A and B :

$$\begin{aligned} A &= \int_0^\Delta d\omega \frac{[t^*(-\omega)]^2}{(\epsilon + \omega)} r(-\omega) \log(\Delta/\omega) \\ &= \int_0^\Delta d\omega [t^*(-\omega)]^2 \left(\frac{r(\epsilon)}{\epsilon + \omega} - \frac{t(\epsilon)}{\omega + \epsilon_R - i\Gamma} \right) \log(\Delta/\omega) \\ &= \int_0^\Delta d\omega \left[t^*(-\omega) t^*(\epsilon) r(\epsilon) \left(\frac{1}{\omega + \epsilon} - \frac{1}{\omega + \epsilon_R + i\Gamma} \right) \right. \\ &\quad \left. + \frac{\Gamma^2 t(\epsilon)}{(\omega + \epsilon_R - i\Gamma)(\omega + \epsilon_R + i\Gamma)^2} \right] \log(\Delta/\omega). \end{aligned}$$

We analyze the asymptotics of the last fraction: In the range $\omega \gg \epsilon_R, \Gamma$, the integrand clearly behaves as $1/\omega^3 \log(\Delta/\omega)$. Thus, the integral is single logarithmic and small as $(\bar{\Gamma}/\Delta)^2$. On the other hand, if $\omega \ll \epsilon_R, \Gamma$, ω can be neglected in the denominator and the prefactor scales like $1/\bar{\Gamma}$, while the integrand is single logarithmic with $\bar{\Gamma}$ in front.

The comportment is in both ranges therefore small with respect to the leading \log^2 contributions and we can neglect the term. The remaining part reads

$$A = \int_0^\Delta d\omega \left[(t^*(\epsilon))^2 r(\epsilon) \left(\frac{1}{\omega + \epsilon} - \frac{1}{\omega + \epsilon_R + i\Gamma} \right) - \frac{i\Gamma t^*(\epsilon) r(\epsilon)}{(\omega + \epsilon_R + i\Gamma)^2} \right] \log(\Delta/\omega).$$

We can repeat the argument above for the last fraction in the integrand and end up with

$$A = -\frac{r(\epsilon)|t(\epsilon)|^2}{2} (\log^2(\Delta/\epsilon) - \log^2(\Delta/\bar{\Gamma})).$$

There is no essential difference in the arguments for the second part. We cut this part short:

$$\begin{aligned} B &= - \int_0^\Delta d\omega \frac{t(-\omega)(t^*(-\omega))^2}{\omega + \epsilon} \log(\Delta/\bar{\Gamma}) \\ &= - \int_0^\Delta d\omega t(\epsilon)(t^*(\epsilon))^2 \left[\frac{1}{\omega + \epsilon} - \frac{1}{\omega + \epsilon_R - i\Gamma} \right] \log(\Delta/\bar{\Gamma}) \\ &= -t|t|^2 \log(\Delta/\bar{\Gamma}) [\log(\Delta/\epsilon) - \log(\Delta/\bar{\Gamma})]. \end{aligned}$$

We sum up all contributions and collect the prefactor,

$$G_{+-}^{(2)}(x, y, \epsilon)_{1\text{-I-E}} = \left[\frac{r|t|^4}{8} (L_1^2 - L_2^2) - \frac{t|t|^4}{4} \log_2(L_1 - L_2) \right] C_{+-}(x, y, \epsilon).$$

We showed how the different logarithmic scales emerge in a second order perturbative calculation. In the next section, we repeat the exercise for a diagram with crossed interaction lines and generate a poly-logarithmic contribution.

A.6.2 Diagram with crossed interaction lines: 1-II-B

To calculate diagram 1-II-B (shown in figure A.3.3), we proceed in the same fashion as above. We put aside the prefactor,

$$\frac{t^2(\epsilon)}{4} C_{+-}(x, y, \epsilon),$$

and start with the inner energy integrals:

$$\begin{aligned} I(\epsilon, \Delta, \epsilon_R, \Gamma) &:= \int_\epsilon^\Delta d\omega \int_{\epsilon-\omega}^\epsilon d\nu \frac{r^*(\epsilon - \omega - \nu)}{\omega(\omega + \nu)} \\ &= \int_\epsilon^\Delta \frac{d\omega}{\omega} \int_{\epsilon-\omega}^\epsilon d\nu \left[\frac{r^*(\epsilon)}{\omega + \nu} - \frac{t^*(\epsilon)}{\omega + \nu - \epsilon + \epsilon_R + i\Gamma} \right] \\ &= \int_\epsilon^\Delta \frac{d\omega}{\omega} \left[r^*(\epsilon) \log\left(\frac{\epsilon + \omega}{\epsilon}\right) - t^*(\epsilon) \log\left(\frac{\omega + \bar{\Gamma}}{\bar{\Gamma}}\right) \right] \\ &=: A + B \end{aligned}$$

The first of the two integrands can be identified with the off-resonant situation, where the “clean” setup with a structureless impurity is restored,

$$A = \frac{r^*(\epsilon)}{2} \log(\Delta/\epsilon).$$

The second integrand behaves differently, depending whether $\bar{\Gamma} \gg \epsilon$ or vice versa. In the former case, the logarithm in the integrand is cut from below by Γ and the result is of order $\log^2(\Delta/\bar{\Gamma})$. In the complementary case, ϵ/Γ can be found in a second logarithm, coming from the lower limit of the integral. This behaviour can be identified as poly-logarithmic contribution, namely

$$\begin{aligned} B &= -t^*(\epsilon) \left[\frac{\log^2(\Delta/\bar{\Gamma})}{2} + \text{Li}_2(-\epsilon/\bar{\Gamma}) \right] \\ &= -t^*(\epsilon) \left[\frac{\log^2(\Delta/\bar{\Gamma})}{2} - \begin{cases} \text{const.}, & \epsilon \lesssim \bar{\Gamma} \\ \frac{1}{2} \log^2\left(\frac{\epsilon}{\bar{\Gamma}}\right), & \epsilon \gg \bar{\Gamma} \end{cases} \right]. \end{aligned}$$

We put the prefactor back into place and find the term

$$G_{+-}^{(2)}(x, y, \epsilon)_{1\text{-II-B}} = -\frac{|t|^2}{4} \left[\frac{r}{2} \log^2(\Delta/\epsilon) + \frac{t}{2} \log^2(\Delta/\bar{\Gamma}) + t \text{Li}_2(-\epsilon/\bar{\Gamma}) \right],$$

equivalent to the diagram in the leading logarithmic approximation.

Bibliography

- [1] A. A. Abrikosov. Magnetic Impurities in Metals: The sd Exchange Model. *Physics*, 2(5), 1965.
- [2] A. A. Abrikosov. *Methods of Quantum Field Theory in Statistical Physics (Selected Russian Publications in the Mathematical Sciences.)*. Dover Publications, 1975.
- [3] A. Altland, Y. Gefen, and B. Rosenow. Incoherent scatterer in a Luttinger liquid: a new paradigmatic limit. *Arxiv preprint arXiv:1104.3125*, page 4, April 2011.
- [4] P. Anderson. A poor man's derivation of scaling laws for the Kondo problem, 1970.
- [5] W. Apel and T. Rice. Combined effect of disorder and interaction on the conductance of a one-dimensional fermion system. *Physical Review B*, 26(12):7063–7065, December 1982.
- [6] D. Aristov and P. Wölfle. Conductance through a potential barrier embedded in a Luttinger liquid: Nonuniversal scaling at strong coupling. *Physical Review B*, 80(4), July 2009.
- [7] O. M. Auslaender, A. Yacoby, de Picciotto R., K. W. Baldwin, L. N. Pfeiffer, and K. W. West. Experimental evidence for resonant tunneling in a luttinger liquid. *Physical review letters*, 84(8):1764–7, February 2000.
- [8] D. S. Bethune and C. Kiang. The Discovery of Single-Wall Carbon Nanotubes at IBM. *IBM-Research*, February 2001.
- [9] D. S. Bethune, C. H. Klang, M. S. de Vries, G. Gorman, R. Savoy, J. Vazquez, and R. Beyers. Cobalt-catalysed growth of carbon nanotubes with single-atomic-layer walls. *Nature*, 363(6430):605–607, June 1993.
- [10] M. Bockrath. Single-Electron Transport in Ropes of Carbon Nanotubes. *Science*, 275(5308):1922–1925, March 1997.
- [11] M. Bockrath, D. H. Cobden, J. Lu, A. G. Rinzler, R. E. Smalley, L. Balents, and P. L. McEuen. Luttinger-liquid behaviour in carbon nanotubes. *Nature*, 397(6720):598–601, February 1999.
- [12] M. Bockrath, W. Liang, D. Bozovic, J. H. Hafner, C. M. Lieber, M. Tinkham, and H. Park. Resonant electron scattering by defects in single-walled carbon nanotubes. *Science (New York, N.Y.)*, 291(5502):283–5, January 2001.

- [13] Y. Bomze, H. Mebrahtu, I. Borzenets, A. Makarovski, and G. Finkelstein. Resonant tunneling in a dissipative environment. *Physical Review B*, 79(24):5, June 2009.
- [14] D. Bozovic, M. Bockrath, J. H. Hafner, C. M. Lieber, H. Park, and M. Tinkham. Electronic properties of mechanically induced kinks in single-walled carbon nanotubes. *Applied Physics Letters*, 78(23):3693, 2001.
- [15] M. Büttiker, Y. Imry, R. Landauer, and S. Pinhas. Generalized many-channel conductance formula with application to small rings. *Physical Review B*, 31(10):6207–6215, May 1985.
- [16] A. Chubukov and D. Maslov. Nonanalytic corrections to the Fermi-liquid behavior. *Physical Review B*, 68(15), October 2003.
- [17] P. Coleman. *Introduction to Many Body Physics*. Rutgers University, 2004.
- [18] S. Das, S. Rao, and D. Sen. Renormalization group study of the conductances of interacting quantum wire systems with different geometries. *Physical Review B*, 70(8), August 2004.
- [19] S. Datta. *Electronic transport in mesoscopic systems*. Cambridge University Press, 1997.
- [20] M. Dresselhaus, G. Dresselhaus, P. Avouris, Z. Yao, and C. Dekker. *Carbon Nanotubes*, volume 80 of *Topics in Applied Physics*. Springer Berlin Heidelberg, Berlin, Heidelberg, March 2001.
- [21] K. B. Efetov and I. L. Aleiner. Collective mode description for a clean Fermi gas with repulsion in arbitrary dimensions: interaction of spin excitations and its consequences. *Journal of Physics: Condensed Matter*, 19(25):255215, June 2007.
- [22] K. B. Efetov and A. I. Larkin. Correlation functions in one-dimensional systems with strong interaction. *Sov. Phys. JETP*, 42(2):390–396, 1975.
- [23] D. S. Fisher and P. A. Lee. Relation between conductivity and transmission matrix. *Physical Review B*, 23(12):6851–6854, 1981.
- [24] A. Furusaki. Resonant tunneling through a quantum dot weakly coupled to quantum wires or quantum Hall edge states. *Physical Review B*, 57(12):7141–7148, March 1998.
- [25] A. Furusaki and N. Nagaosa. Resonant tunneling in a Luttinger liquid. *Physical Review B*, 47(7):3827–3831, February 1993.
- [26] A. Galda, I. Yurkevich, and I. Lerner. Effect of electron-phonon coupling on transmission through Luttinger liquid hybridized with resonant level. *EPL (Europhysics Letters)*, 93(1):17009, January 2011.
- [27] A. Galda, I. Yurkevich, and I. Lerner. Impurity scattering in a Luttinger liquid with electron-phonon coupling. *Physical Review B*, 83(4), January 2011.

- [28] Y. Gefen and D. Thouless. Zener transitions and energy dissipation in small driven systems. *Physical Review Letters*, 59(15):1752–1755, October 1987.
- [29] T. Giamarchi. *Quantum Physics in One Dimension (International Series of Monographs on Physics)*. Oxford University Press, USA, 2004.
- [30] T. Giamarchi and H. Schulz. Anderson localization and interactions in one-dimensional metals. *Physical Review B*, 37(1):325–340, January 1988.
- [31] I. Gornyi, A. Mirlin, and D. Polyakov. Dephasing and Weak Localization in Disordered Luttinger Liquid. *Physical Review Letters*, 95(4), July 2005.
- [32] I. Gornyi, a. Mirlin, and D. Polyakov. Electron transport in a disordered Luttinger liquid. *Physical Review B*, 75(8), February 2007.
- [33] F. D. M. Haldane. Luttinger liquid theory of one-dimensional quantum fluids. I. Properties of the Luttinger model and their extension to the general 1D interacting spinless Fermi gas. *Journal of Physics C: Solid State Physics*, 2585, 1981.
- [34] S. Iijima. Helical microtubules of graphitic carbon. *Nature*, 354(6348):56–58, November 1991.
- [35] K. I. Imura, K. V. Pham, P. Lederer, and F. Piéchon. Conductance of one-dimensional quantum wires. *Physical Review B*, 66(3), July 2002.
- [36] C. Kane, L. Balents, and M. Fisher. Coulomb Interactions and Mesoscopic Effects in Carbon Nanotubes. *Physical Review Letters*, 79(25):5086–5089, December 1997.
- [37] C. Kane and M. Fisher. Transmission through barriers and resonant tunneling in an interacting one-dimensional electron gas. *Physical Review B*, 46(23):15233–15262, December 1992.
- [38] A. Y. Kasumov. Supercurrents Through Single-Walled Carbon Nanotubes. *Science*, 284(5419):1508–1511, May 1999.
- [39] J. Kong, E. Yenilmez, T. Tombler, W. Kim, H. Dai, R. Laughlin, L. Liu, C. Jayanthi, and S. Wu. Quantum Interference and Ballistic Transmission in Nanotube Electron Waveguides. *Physical Review Letters*, 87(10), August 2001.
- [40] V. Kravtsov, A. Ossipov, and O. Yevtushenko. Return probability and scaling exponents in the critical random matrix ensemble. *Arxiv preprint arXiv:1104.3872*, page 14, April 2011.
- [41] V. Kravtsov, A. Ossipov, O. Yevtushenko, and E. Cuevas. Dynamical scaling for critical states: Validity of Chalker’s ansatz for strong fractality. *Physical Review B*, 82(16), October 2010.
- [42] I. V. Krive, A. Palevski, R. I. Shekhter, and M. Jonson. Resonant tunneling of electrons in quantum wires (Review). *Low Temperature Physics*, 36(2):119, 2010.

- [43] S. Lal, S. Rao, and D. Sen. Junction of several weakly interacting quantum wires: A renormalization group study. *Physical Review B*, 66(16), October 2002.
- [44] L. Landau. Die Theorie der Fermi-Flüssigkeit. *Sov. Phys. JETP*, 1(1058), 1956.
- [45] R. Landauer. Electrical transport in open and closed systems. *Zeitschrift für Physik B Condensed Matter*, 68(2-3):217–228, June 1987.
- [46] A. I. Larkin and I. E. Dzyaloshinskii. Correlation Functions for a One-Dimensional Fermi System with Long-Range Interaction (Tomonaga Model). *Sov. Phys. JETP*, 38(1):202–208, 1974.
- [47] I. Lerner, V. Yudson, and I. Yurkevich. Quantum Wire Hybridized With a Single-Level Impurity. *Physical Review Letters*, 100(25):1–4, June 2008.
- [48] J. M. Luttinger. An Exactly Soluble Model of a Many-Fermion System. *Journal of Mathematical Physics*, 4:1154, 1963.
- [49] D. Maslov. Fundamental aspects of electron correlations and quantum transport in one-dimensional systems. *Arxiv preprint arXiv:cond-mat/0506035*, page 108, June 2005.
- [50] D. Maslov and M. Stone. Landauer conductance of Luttinger liquids with leads. *Physical Review B*, 52(8):R5539–R5542, August 1995.
- [51] D. C. Mattis and E. H. Lieb. Exact Solution of a Many-Fermion System and Its Associated Boson Field. *Journal of Mathematical Physics*, 6(2):304, 1965.
- [52] K. Matveev, D. Yue, and L. Glazman. Tunneling in one-dimensional non-Luttinger electron liquid. *Physical review letters*, 71(20):3351–3354, 1993.
- [53] U. Meirav, M. A. Kastner, M. Heiblum, and S. J. Wind. One-dimensional electron gas in GaAs: Periodic conductance oscillations as a function of density. *Physical Review B*, 40(8):5871–5874, 1989.
- [54] S. Nakaharai, J. R. Williams, and C. M. Marcus. Gate-Defined Graphene Quantum Point Contact in the Quantum Hall Regime. *Arxiv preprint arXiv:1010.1919*, October 2010.
- [55] C. Nayak, M. Fisher, A. Ludwig, and H. Lin. Resonant multilead point-contact tunneling. *Physical Review B*, 59(24):15694–15704, June 1999.
- [56] Y. Nazarov. Coulomb Blockade without Tunnel Junctions. *Physical Review Letters*, 82(6):1245–1248, February 1999.
- [57] Y. Nazarov and L. Glazman. Resonant Tunneling of Interacting Electrons in a One-Dimensional Wire. *Physical Review Letters*, 91(12), September 2003.
- [58] H. Niedoba, H. Launois, D. Brinkmann, R. Brugger, and H. R. Zeller. NMR Study of the Low-Temperature Insulating State in the One-Dimensional “Conductor” $K_2Pt(CN)_4Br_0.3 \cdot 3H_2O$. *Physica Status Solidi (b)*, 58(1):309–314, July 1973.

- [59] P. Nozières and C. De Dominicis. Singularities in the X-Ray Absorption and Emission of Metals. III. One-Body Theory Exact Solution. *Physical Review*, 178(3):1097–1107, February 1969.
- [60] Y. Oreg and A. Finkel'stein. dc transport in quantum wires. *Physical Review B*, 54(20):R14265–R14268, November 1996.
- [61] K. V. Pham, F. Piéchon, K. I. Imura, and P. Lederer. Tomonaga-Luttinger liquid with reservoirs in a multiterminal geometry. *Physical Review B*, 68(20), November 2003.
- [62] D. Polyakov and I. Gornyi. Transport of interacting electrons through a double barrier in quantum wires. *Physical Review B*, 68(3), July 2003.
- [63] H. W. Postma, T. Teepen, Z. Yao, M. Grifoni, and C. Dekker. Carbon nanotube single-electron transistors at room temperature. *Science (New York, N.Y.)*, 293(5527):76–9, July 2001.
- [64] Stefano Roddaro, Vittorio Pellegrini, Fabio Beltram, Loren Pfeiffer, and Ken West. Particle-Hole Symmetric Luttinger Liquids in a Quantum Hall Circuit. *Physical Review Letters*, 95(15), October 2005.
- [65] D. Saxon. Tensor Scattering Matrix for the Electromagnetic Field. *Physical Review*, 100(6):1771–1775, December 1955.
- [66] H. Schulz, G. Cuniberti, and P. Pieri. Fermi liquids and Luttinger liquids. *Arxiv preprint arXiv:cond-mat/9807366*, page 62, July 1998.
- [67] J. Sólyom. The Fermi gas model of one-dimensional conductors. *Advances in Physics*, 28(2):201–303, April 1979.
- [68] S. Tarucha, T. Honda, and T. Saku. Reduction of quantized conductance at low temperatures observed in 2 to 10 [μ m] m-long quantum wires. *Solid state communications*, 94(6):413–418, 1995.
- [69] S. I. Tomonaga. Remarks on Bloch's method of sound waves applied to many-fermion problems. *Progress of Theoretical Physics*, 5:544–569, 1950.
- [70] J. von Delft and H. Schoeller. Bosonization for Beginners — Refermionization for Experts. *Annalen der Physik*, 4(3):1–71, 1998.
- [71] A. Yacoby, H. L. Stormer, N. S. Wingreen, L. N. Pfeiffer, K. W. Baldwin, and K. W. West. Nonuniversal Conductance Quantization in Quantum Wires. *Physical review letters*, 77(22):4612–4615, November 1996.
- [72] Z. Yao, C. Kane, and C. Dekker. High-Field Electrical Transport in Single-Wall Carbon Nanotubes. *Physical Review Letters*, 84(13):2941–2944, March 2000.
- [73] Z. Yao, H. W. Postma, L. Balents, and C. Dekker. Carbon nanotube intramolecular junctions. *Nature*, 402(6759):273–276, November 1999.
- [74] D. Yue, L. Glazman, and K. Matveev. Conduction of a weakly interacting one-dimensional electron gas through a single barrier. *Physical Review B*, 49(3):1966–1975, January 1994.

- [75] H. R. Zeller and A. Beck. Anisotropy of the electrical conductivity in the one-dimensional conductor [K₂ Pt (CN)₄ Br_{0.30.3}] (H₂O). *Journal of Physics and Chemistry of Solids*, 35(1):77–80, 1974.

Hiermit versichere ich, dass ich die vorliegende Arbeit selbständig und ohne Benutzung anderer als der angegebenen Hilfsmittel angefertigt, noch nicht einer anderen Prüfungsbehörde vorgelegt und noch nicht veröffentlicht habe.

Datum / Unterschrift